Planar Robotic Mechanisms: Analysis and Configuration Comparison

by

Robert L. Williams II

Dissertation submitted to the Faculty of the

Virginia Polytechnic Institute and State University

in partial fulfillment of the requirements for the degree of

Doctor of Philosophy

in

Mechanical Engineering

APPROVED:

Dr. Charles Reinholtz, Chairman

Dr. Arvid Myklebust

Dr. Robert Fries

Dr. Harry Robertshaw

Dr. Michael Deisenroth

August 5, 1988

Blacksburg, Virginia

Planar Robotic Mechanisms: Analysis and Configuration Comparison

by

Robert L. Williams II

Dr. Charles Reinholtz, Chairman

Mechanical Engineering

(ABSTRACT)

Robotic mechanisms are defined in this dissertation to be closed-loop, in-parallel actuated mechanical devices possessing several degrees-of-freedom. Parallel robotic mechanisms have recently received attention in the robotics literature as a potential alternative to the existing serial industrial robot. Serial robots are in a cantilever configuration which makes them relatively compliant and leads to poor accuracy. Many serial manipulators have motors that are carried on moving links which limits dynamic performance. Robotic mechanisms are in a parallel configuration which provides excellent stiffness, load bearing, and accuracy. Robotic mechanisms combine the advantages of serial robots and closed-loop single degree-of-freedom mechanisms to form a versatile new robotic tool.

This dissertation presents theoretical kinematic analysis and design of planar robotic mechanisms. The topics covered are type and number synthesis, kinematic position solution, velocity and acceleration analysis, kinetostatic analysis, workspace optimization, and link interference avoidance. Throughout this work comparisons are made among three general manipulator configurations: serial, parallel-serial, and fully parallel. Strengths and limitations are discussed for each configuration type.

This investigation provides the analytical foundation for implementation of planar robotic mechanisms. Closed-form solutions to the kinematic position, velocity, and acceleration problems are presented. Manipulator reachable hand areas are maximized. An underlying theme of this work is tradeoffs between competing factors relating to various configurations of parallel robotic mechanisms; these tradeoffs are important design considerations. The recommendation of this dissertation is to pursue practical development of robotic mechanisms for general industrial manipulation tasks.

Acknowledgements

I would foremost like to thank Dr. Charles F. Reinholtz, who served as my advisor during my MS and PhD degrees. He has always given a proper balance of freedom and guidance. Dr. Reinholtz' contribution to my professional development is truly inestimable. Over the course of four years, in his own gentle manner, he has been advisor, teacher, co-author, and friend to me, for which I am grateful.

I would also like to acknowledge Dr. Arvid Myklebust, Dr. Robert Fries, Dr. Harry Robertshaw, and Dr. Michael Deisenroth for their service on my advisory committee.

I would like to acknowledge the National Science Foundation for the partial financial support of this dissertation, through Grant DMC 8657828.

I would also like to recognize and thank my parents from the bottom of my heart. Without them, this dissertation would not exist, for many reasons. Thanks and love also to my wife for living the fine life of a graduate student for three years. Someday, our collective families hope that she will produce a dissertation in her own field.

Table of Contents

Figure List

Table List

Chapter 1 Introduction and Literature Review

1.1 Introduction

Kinematic mechanisms and robots are the primary movers of industry and industrial automation. These devices play a large role in increasing the productivity of industry and thus the economy. Current industrial robots are open-loop devices with many degrees-of-freedom, programmable for a variety of tasks. Mechanisms are closed-loop, one degree-of-freedom devices which are not programmable to accomplish different tasks. The purpose of this dissertation is to study devices which combine the advantages of robots and mechanisms to produce a versatile new breed of manipulator, hereafter referred to as robotic mechanisms. Robotic mechanisms have more than one degree-of-freedom, and thus are re-programmable for a variety of motions. In addition, this new type of device is relatively rigid due to the closed-loop geometry.

Industrial robots currently in use are almost exclusively of the open-loop, serial configuration. The advantages of serial robot topology are long reach, ability to reach into a small space, and large overall workspace. The kinematic motion description is straightforward because the serial arm geometry is relatively simple. There are also several disadvantages, however, which limit potential industrial applications for the serial robot arm. An extended

serial arm acts as a cantilever beam, which is a poor structure for resisting loads and deflections. The actuators are driven in series so errors are additive. Positioning accuracy is reduced and a complicated robot controller is necessary. Except for the base driving motor, all motors are moving, which accounts for a major portion of the arm inertia. Therefore, high speeds are a problem for the serial robot configuration. Certain serial robots are designed such that the motors are fixed to ground and the serial links are driven through differentials. This design is a dynamic improvement, but still has extra mass compared to a fully parallel manipulator. These characteristics prevent the serial robot from being effective for high speed, precision assembly such as in the electronic industry.

Due to the above disadvantages, a research effort is being undertaken to develop an alternative to the serial robot topology. Robotic mechanisms are closed-loop mechanical linkages with multiple freedoms, actuated in a parallel fashion. In general, a robotic mechanism has better positioning accuracies, faster running speeds, and greater load bearing characteristics than its serial counterpart. Parallel robotic mechanisms inherently are much stiffer against deflections compared to a serial manipulator. Therefore, robotic mechanism links may be constructed with less material to achieve the same stiffness characteristics. Due to the improved positioning accuracy in a parallel robot configuration, a simpler controller may be used. It is envisioned that robotic mechanisms may be built economically in-house using off-the-shelf parts.

The thrust of this research is to explore possibilities and develop design theories for planar robotic mechanisms in general. Throughout this work, the theory is applied to specific manipulators. Closed-form mathematical solutions independent of manipulator position information are presented, where possible.

1.2 Literature Review

The field of robotic mechanisms is relatively new, and the literature is somewhat sparse compared to the wealth of information available regarding serial robots. However, there are several useful papers concerning parallel robots which serve as a springboard for further investigations. The papers discussed in this literature review are grouped into six general categories: 1) Survey Papers; 2) Type and Number Synthesis; 3) Forward and Inverse Kinematic Simulation; 4) Dynamics; 5) Workspace Considerations; and 6) Link Interference.

The first work in the area of robotic mechanisms is in the form of general survey papers. These introduce the alternative of parallel topology robots and discuss general areas where research effort must be concentrated. Two papers by Hunt (1982, 1983) provide an introduction to robotic mechanisms, plus a preliminary study of various parallel robot structures and their associated mobility. Hunt emphasizes that research in robot geometries is necessary to de-emphasize the current need for the development of sophisticated electronics and robot "intelligence". Earl and Rooney (1983) explore existing and future possibilities for serial and parallel robot configurations. Djoldasbekov and Slutskii (1983) propose a mechanism with variable link lengths. This device is a compromise between a fixed automation mechanism with one degree-of-freedom and a multi-degree-of-freedom robotic mechanism. Sandor et. al. (1986) study a similar adaptive hard automation module, a spatial RS-SRR-SS motion generator with adjustable links.

Cox and Tesar (1981) present a comprehensive comparison of the relative merits of serial and parallel robots. The factors studied are range of motion, rigidity, computability of inverse kinematics and dynamics, precision positioning, load bearing, economics, and compactness. The parallel configuration is reported to be favorable for rigidity, inverse kinematics, precision positioning, load bearing, and velocity and acceleration characteristics.

Type and number synthesis determines the number of links and the specific robot configuration. As the number of links increases, the number of configuration possibilities for

a given number of freedoms becomes quite large. Several authors have dealt with this subject. Waldron (1966) uses the theory of screws to determine relative mobility between two links in a kinematic chain. Mruthyunjaya (1984) presents a computer-automated method for enumerating the large number of configuration possibilities of kinematic structures. Examples for zero, one, two, and three degrees-of-freedom are presented. For ten link, three degree-of-freedom chains, ninety-seven distinct connectivity alternatives exist. Freudenstein and Mayourian (1984) use graph theory to tabulate one degree-of-freedom planar and spatial mechanism configurations. Baker (1981) studies the mobility of multi-loop linkages and relates structures to mechanisms in this light. Yan and Chen (1985) present all ninety-eight possibilities from a parent wheel-damping mechanism.

A promising configuration combines elements of parallel and serial robots to achieve advantages of both types. Some existing serial robots use parallel linkages such as four-bar linkages to strengthen the serial components. Mohamed (1987) explores this idea and presents a number and type synthesis for these parallel-serial robots.

To date, the robotic mechanism example cited most often is the spatial, six degree-of-freedom Stewart's platform. This device was originally developed as a flight simulator by Stewart (1965). Several authors have explored the use of Stewart's platform as a parallel robot manipulator. Fichter and McDowell (1980) present a study on this subject and point out that such a manipulator may be fabricated in-house using commercially available parts. Yang and Lee (1984) deal with Stewart's platform, including physical joint constraints and workspace maneuverability. Powell (1982) derives the basic kinematic control equations for this device.

Forward kinematic simulation involves calculating the robot hand position and orientation given values for the actuators. Inverse kinematics solves for the actuator positions given the position and orientation of the hand. Efficient, closed-form solutions are desirable for forward and inverse kinematics in an attempt to provide real-time control. Aradayfio and Qiao (1985) present closed-form forward and inverse kinematics solutions for three different three degree-of-freedom planar robotic mechanisms. However, due to trigonometric ambiguities the solutions are not applicable to all ranges of robot motion; this problem is not

mentioned in the paper. Sumpter and Soni (1985) present a numerical solution to the forward kinematics problem of a three degree-of-freedom planar robotic mechanism. The numerical method is less efficient than a closed-form solution, and requires an initial guess to start. Mohamed and Duffy (1985) use the theory of screws to solve the forward and inverse kinematics of robotic mechanisms in general. Davies (1981) presents an interesting application of Kirchoff's Circulation Law to multi-loop kinematic chains. Kirchoff's Law is used to produce independent screw motors from which the motion may be solved using existing means.

In addition to position and orientation specification, dynamics is important in the study of parallel manipulators. Sugimoto (1986) presents kinematic and dynamic analysis for general parallel robotic mechanisms. This work uses motor algebra and the Newton-Euler dynamics formulation. Freeman and Tesar (1982) show how to reduce the mathematical complexity in dynamics simulation of one and several degree-of-freedom planar kinematic chains through suitable choice of parameters. Mabie and Reinholtz (1987) present a matrix kinetostatic method for planar mechanisms where all internal joint forces and driving torques are solved simultaneously, from the rigid body dynamics equations. This method is extendable to deal with robotic mechanisms.

The reachable workspace of a parallel robotic mechanism is significantly reduced compared to a serial robot of similar dimensions. Therefore, workspace optimization must be explored in order to make robotic mechanisms competitive with their serial counterparts. Considerable attention has been paid to the workspace of serial robot arms, for example Sugimoto and Duffy, (1981a and 1981b), Kumar and Waldron, (1981), Selfridge, (1983), Tsai and Soni, (1985). Robotic mechanisms are geometrically more complex than serial robots, which compounds the problem of workspace determination. The following papers deal at least partially with parallel manipulator workspace considerations.

Cwiakala (1986) uses the numerical "Optimum Path Search Technique" to calculate the workspace volume of Stewart's platform. Only platforms with complete symmetry are considered. Powell (1982) uses kinematic equations to determine the workspace volume of Stewart's platform given the manipulator parameters. Gosselin and Angeles (1987a) study the

kinematics and workspace of a planar three degree-of-freedom parallel robot. The conditions for the existence of a non-vanishing workspace for every hand orientation are established, and the global workspace is maximized. The same authors extend the previous investigation to a three degree-of-freedom spherical parallel robot in another paper (Gosselin and Angeles, 1987b). Stoughton and Kokkinis (1987) study a three degree-of-freedom spatial extension of the two degree-of-freedom planar five-bar linkage. They generate the workspace volume with special attention to the relationship between singularities of the workspace and the Jacobian matrix. Weng et. al. (1987) present a spatial six degree-of-freedom robotic mechanism actuated by three ground-mounted cylindrical actuators. Various workspace regions are defined and calculated, considering the rotatability of the hand and size of the hand platform. Young and Duffy (1987a) study the workspace of simple planar serial robots in their work on articulating robots.

Along with workspace optimization, the topic of manipulator link interference must be considered. Keil et. al. (1985) develop a position-dependent method for link interference detection. This method is three-dimensional; however, the emphasis of the work is prediction of link interference in planar mechanisms. Ganter and Uicker (1986) present the method of swept solids to detect collisions between two spatial bodies travelling on independent three-dimensional trajectories. This method, using solid modeling techniques, is applied to collision detection in spatial serial robots. Young and Duffy (1987b) present a method for obstacle and link interference avoidance, plus collision detection between two robots, applied to planar serial robots.

Material from this dissertation has been published by Williams and Reinholtz (1988a, 1988b, 1987a, and 1987b).

Chapter 2 Type and Number Synthesis

In this chapter, planar linkage mobility is developed using the Grubler Criterion. From this, it is seen that there are an infinite number of manipulator configurations to produce two or three degrees-of-freedom in the plane. Next, the manipulator naming convention used in this dissertation is presented. Finally, eight potentially useful planar robotic mechanisms are identified for detailed study.

2.1 Planar Linkage Mobility

Three parameters are required to position a body in a general planar location, e.g. x, y, and θ. A general planar manipulator should thus possess three overall degrees-of-freedom. However, in order to increase dexterity, a fourth degree-of-freedom may be added. It is assumed that each of the manipulators studied has as one degree-of-freedom the free rotation of the hand. Two degrees-of-freedom plus the rotation of the hand provides the minimum three degrees-of-freedom required for planar tasks. Ignoring the hand rotation freedom, both two and three degree-of-freedom planar robotic mechanisms are studied in this dissertation.

In addition to the hand rotation, a second extra freedom may be added in the form of Z axis travel (perpendicular to the plane of the robotic mechanism) for the hand. With this condition, the workspace becomes a volume rather than a plane area. However, for a planar manipulator, the stiffness advantage may be lost for loads applied out of the plane of motion.

The Grubler Criterion for gross planar degrees-of-freedom is as follows. This equation ignores the possible extra freedoms added by the manipulator hand rotation and Z-axis motion.

$$F = 3(N-1) - 2J_1 - J_2 \tag{2.1}$$

where:

$F \equiv$ number of freedoms of the device

$N \equiv$ number of links (including ground)

$J_1 \equiv$ number of 1 DOF joints

$J_2 \equiv$ number of 2 DOF joints

In this dissertation, only manipulators with one degree-of-freedom joints (revolute and prismatic) are considered; therefore $J_2 = 0$. From Eq. 2.1 there are an infinite number of (N, J_1) combinations that give integer values for F. When F is specified the above equation may be rearranged to calculate J_1 given N. Equation 2.2a and Table 2.1a summarize the results for F = 2, while Equation 2.2b and Table 2.1b give the results for F = 3. Only integer values for J_1 are reported. For each case, $N \leq 15$.

$$J_1 = \frac{3N-5}{2} \tag{2.2a}$$

$$J_1 = \frac{3N-6}{2} \tag{2.2b}$$

Table 2.1a Planar Mobility for F = 2

	N	J_1
1	3	2
2	5	5
3	7	8
4	9	11
5	11	14
6	13	17
7	15	20

Table 2.1b Planar Mobility for F = 3

	N	J_1
1	2	0
2	4	3
3	6	6
4	8	9
5	10	12
6	12	15
7	14	18

The first entry of Table 2.1b represents a ground link and a free-floating coupler link, which is of no interest in the present dissertation. The first entry of Table 2.1a and the second entry of Table 2.1b are planar serial robots, of two and three degrees-of-freedom, respectively. Entry 3 of Table 2.1b represents a parallel-serial configuration. The remaining entries of Tables 2.1a and 2.1b represent parallel closed loop robotic manipulators. Each (N,J_1) combination may represent several unique manipulators because of multiple connectivity possibilities. For example, For F = 3, N = 8, J_1 = 9, (Table 2.1b, Entry 4) there are six distinct connectivity alternatives, not considering the additional possibilities of using revolute or prismatic joints.

2.2 Manipulator Naming Convention

Due to the large number of (N, J_1) combinations and the large number of potential connectivities within a single (N, J_1) pair, a convention has been adopted for referring to manipulators in this dissertation. All manipulators in this dissertation are named according to the following rule.

$$NnnRrrPpp - qq$$

where:

$nn \equiv$ number of links

$rr \equiv$ number of revolute joints

$pp \equiv$ number of prismatic joints

$qq \equiv$ configuration identification number

If a manipulator has no revolute joints, the R designation is omitted; the P designation is dropped when a manipulator has no prismatic joints. The appendage qq is used only when there are multiple manipulator configurations from a single (N, J_1) pair. For example, there are four distinct three degree-of-freedom manipulators reported in the next section which are derived from (N, J_1) = (8,9).

2.3 Robotic Mechanisms for Consideration

Figure 2.1 shows the serial three degree-of-freedom planar robot. This manipulator is not in a parallel configuration. However, this robot is referred to in this dissertation, and thus is pictured here.

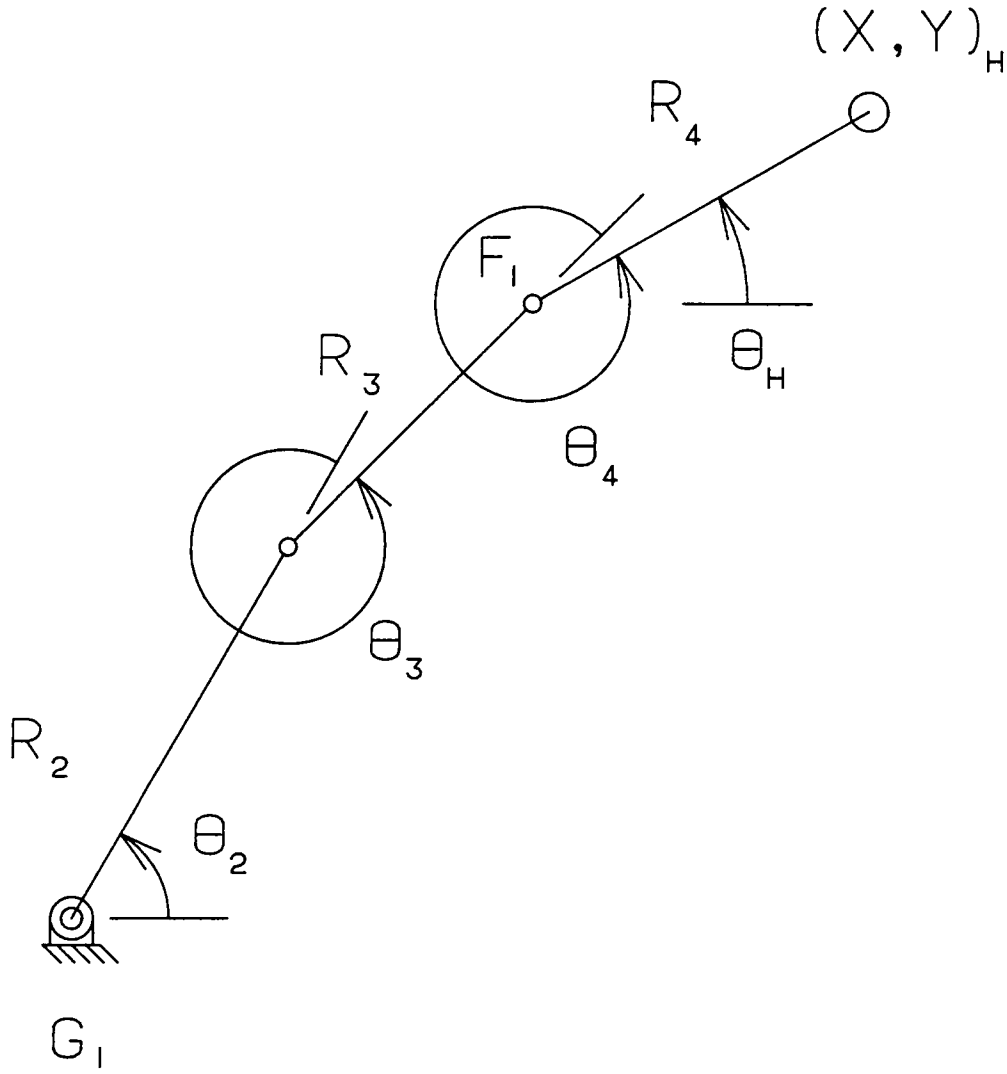

Figure 2.1
"N4R3" Serial Robot

The closed-loop planar robotic mechanisms studied in this dissertation are pictured in Figs. 2.2 through 2.9. These manipulators were chosen as potentially useful planar robotic mechanisms. The number of links are relatively few, and the connectivities represented are relatively simple. The output parameters are denoted by (x_H, y_H), plus θ_H for three degree-of-freedom manipulators. The rotary input actuators are θ_i , while the linear actuators are L_j. The hand fixture is attached to location (x_H, y_H); the nature of the hand fixture is not an issue in this dissertation.

Figures 2.2 and 2.3 present the two degree-of-freedom manipulators studied in this dissertation. Figure 2.2 is a five-bar linkage, and Fig. 2.3 is a five-bar with another dyad attached.

Figures 2.4 through 2.9 present the three degree-of-freedom manipulators under consideration. The "N6R6" (Fig. 2.4) is a five-bar linkage with an arm extending from the coupler triangle. This manipulator is a parallel-serial configuration. Figures 2.5 and 2.6 present robotic mechanisms with all rotary inputs. The "N8R7P2-3" manipulator (Fig. 2.7) is modeled roughly after the human arm (Hunt, 1983), which is serial with parallel components. The two linear actuators of the "N8R7P2-3" represent the expansion and contraction of arm muscles. The "N8R6P3-4" robotic mechanism (Fig. 2.8) is kinematically equivalent to the "N8R9-1", but the actuators are linear rather than rotary. The "N10R12" of Fig. 2.9 is also similar to the "N8R9-1"; another (non-actuated) constraining dyad is added.

Some of these manipulators have been suggested by other authors. Referring to Fig. 2.5, the "N8R9-1" has been proposed by Sumpter and Soni (1985), by Cox and Tesar (1981), and also by Hunt (1983). The "N8R7P2-3" shown in Fig. 2.7 has been pictured by Hunt (1983), and also by Aradayfio and Qiao (1985). Aradayfio and Qiao (1985) have additionally studied the "N6R6" (Fig. 2.4) and the "N8R9-2" (Fig. 2.6) manipulators.

Figure 2.10 is a summary of the planar robotic mechanisms shown in Figs. 2.1 through 2.9. The reader is encouraged to photocopy Fig. 2.10 for manipulator reference while reading this dissertation.

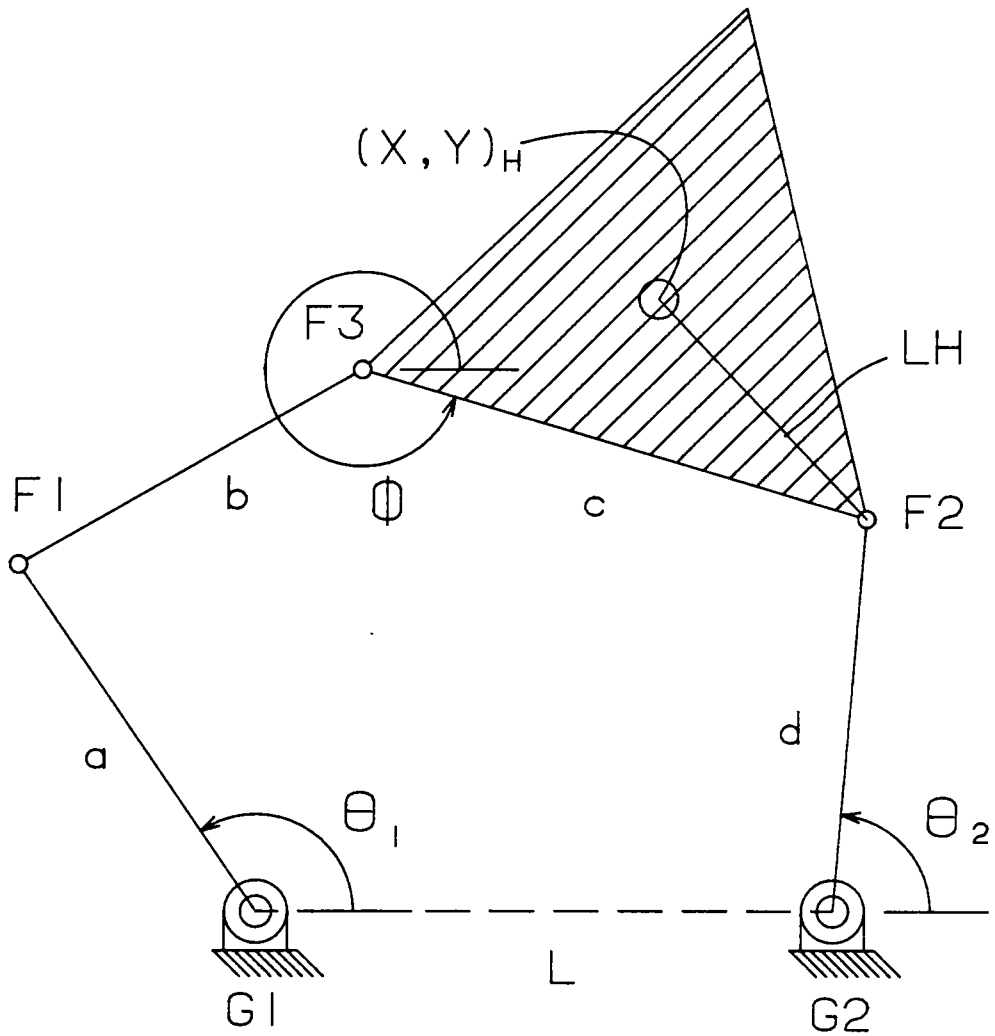

Figure 2.2
"N5R5" Robotic Mechanism

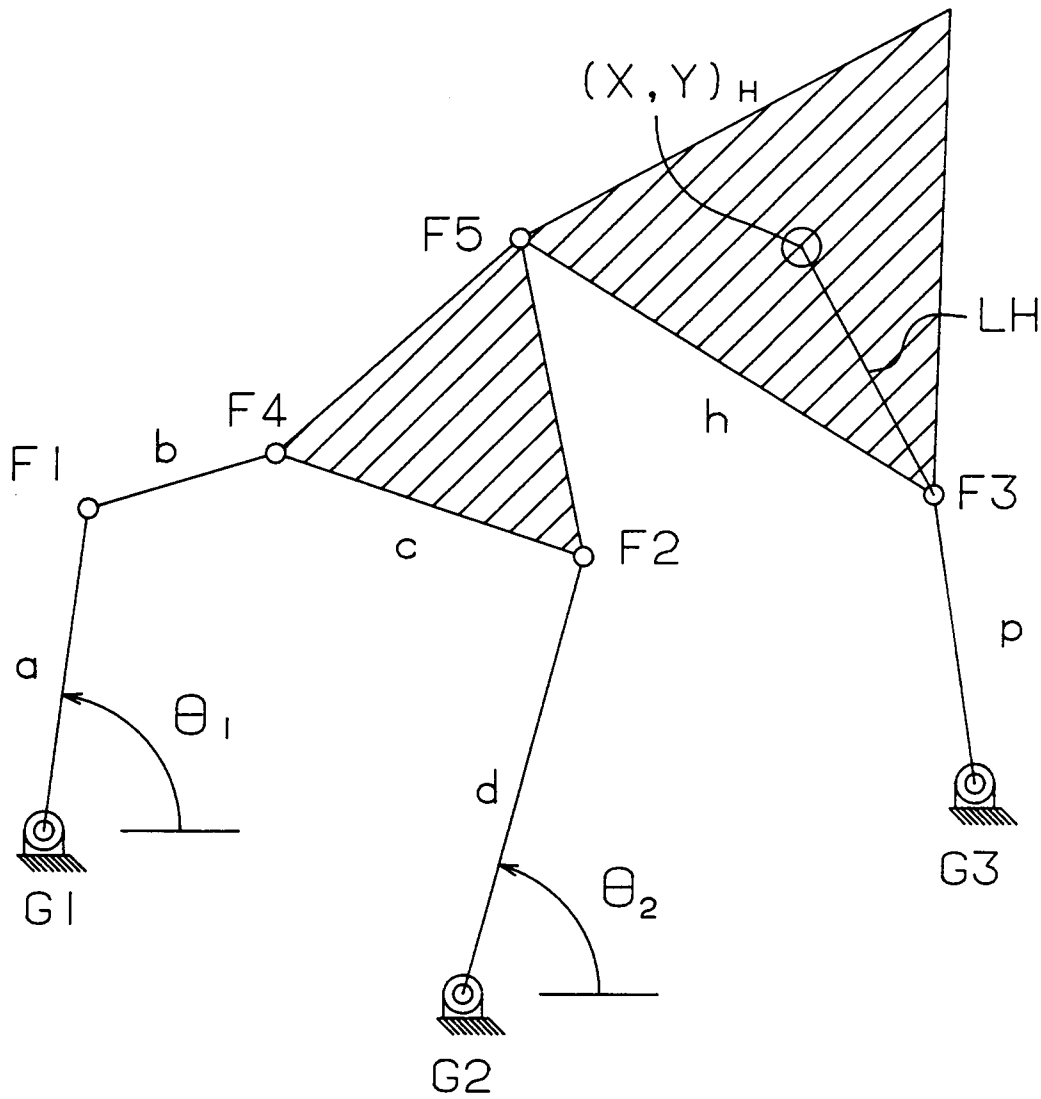

Figure 2.3
"N7R8" Robotic Mechanism

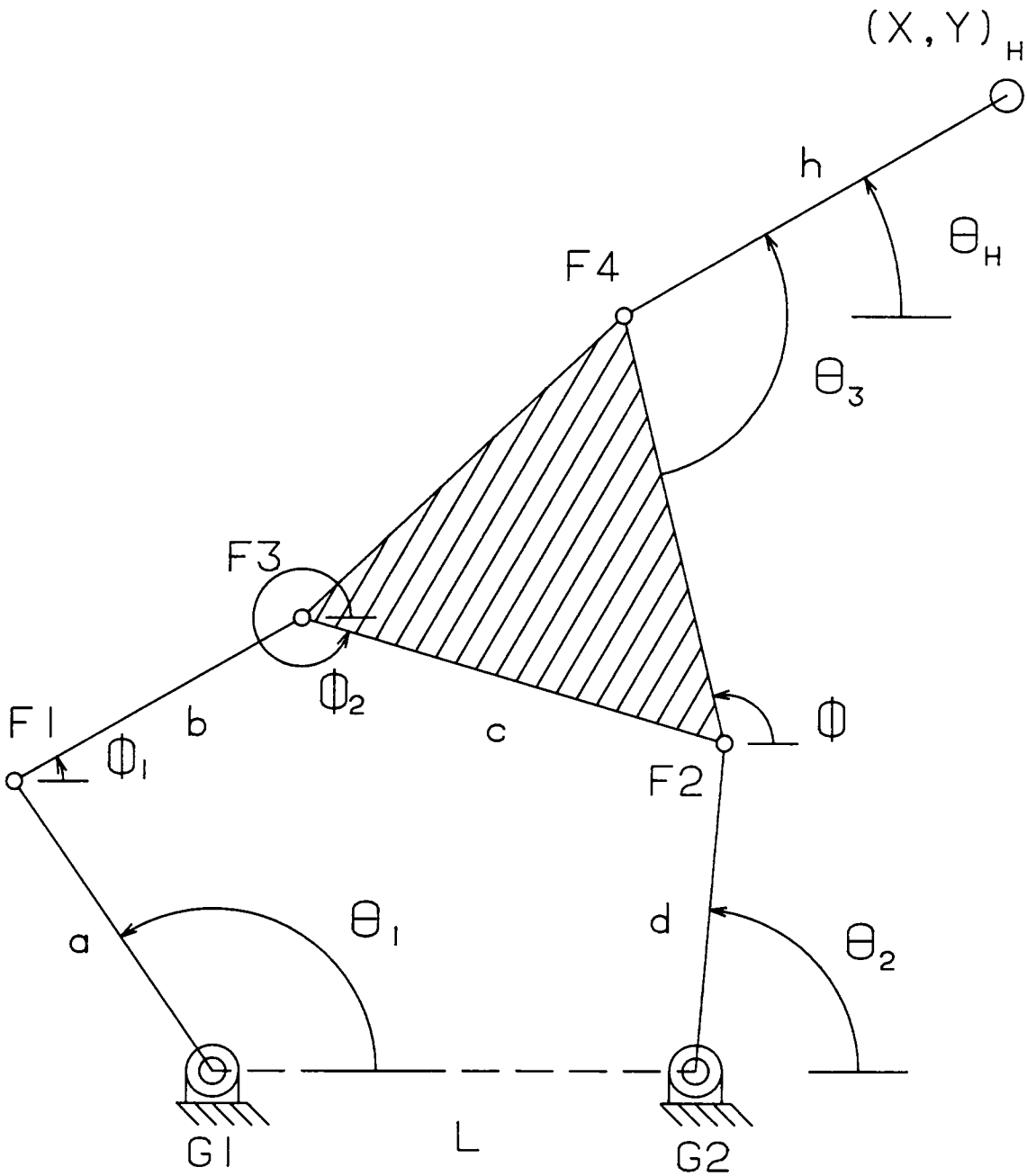

Figure 2.4
"N6R6" Robotic Mechanism

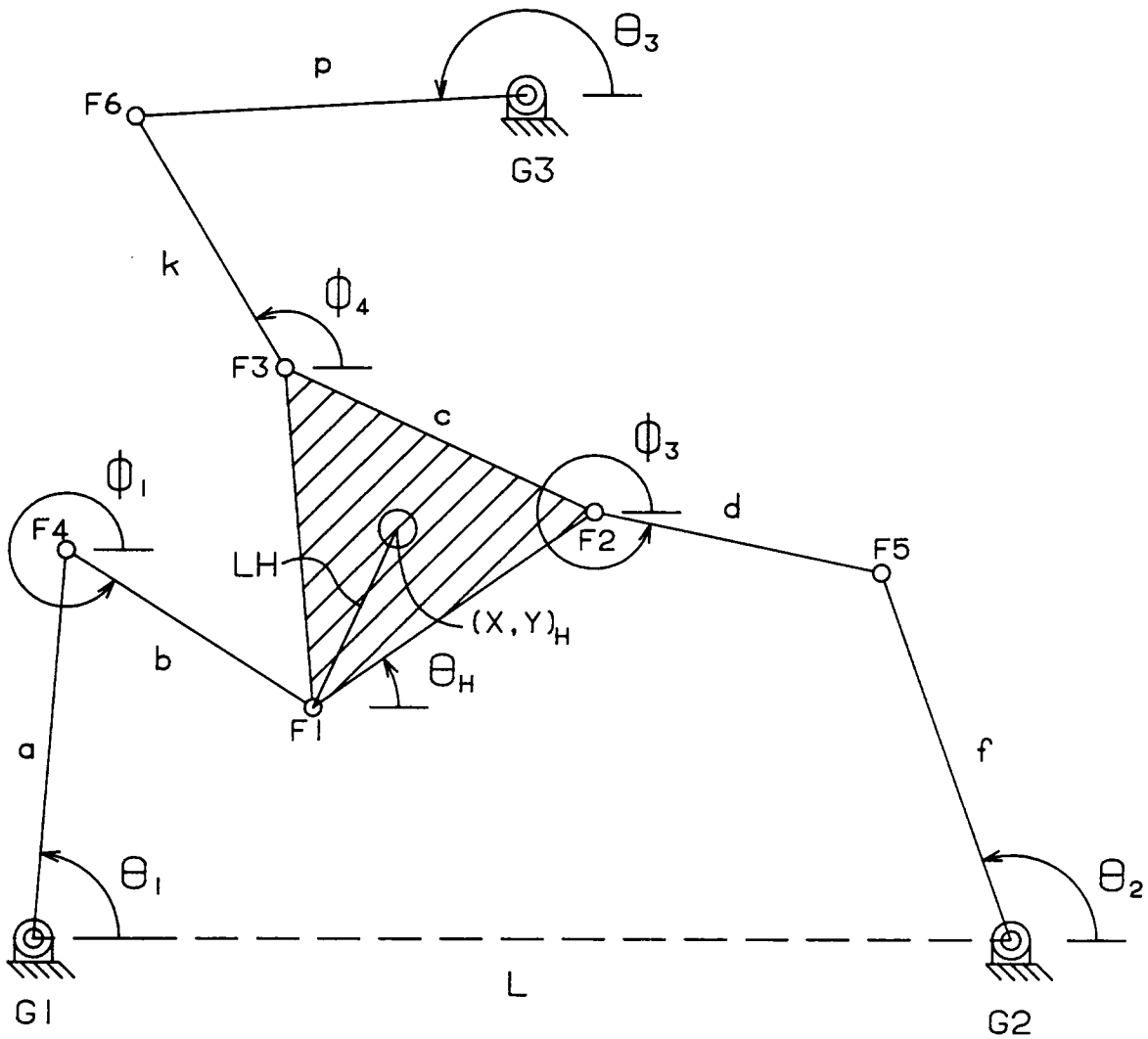

Figure 2.5
"N8R9-1" Robotic Mechanism

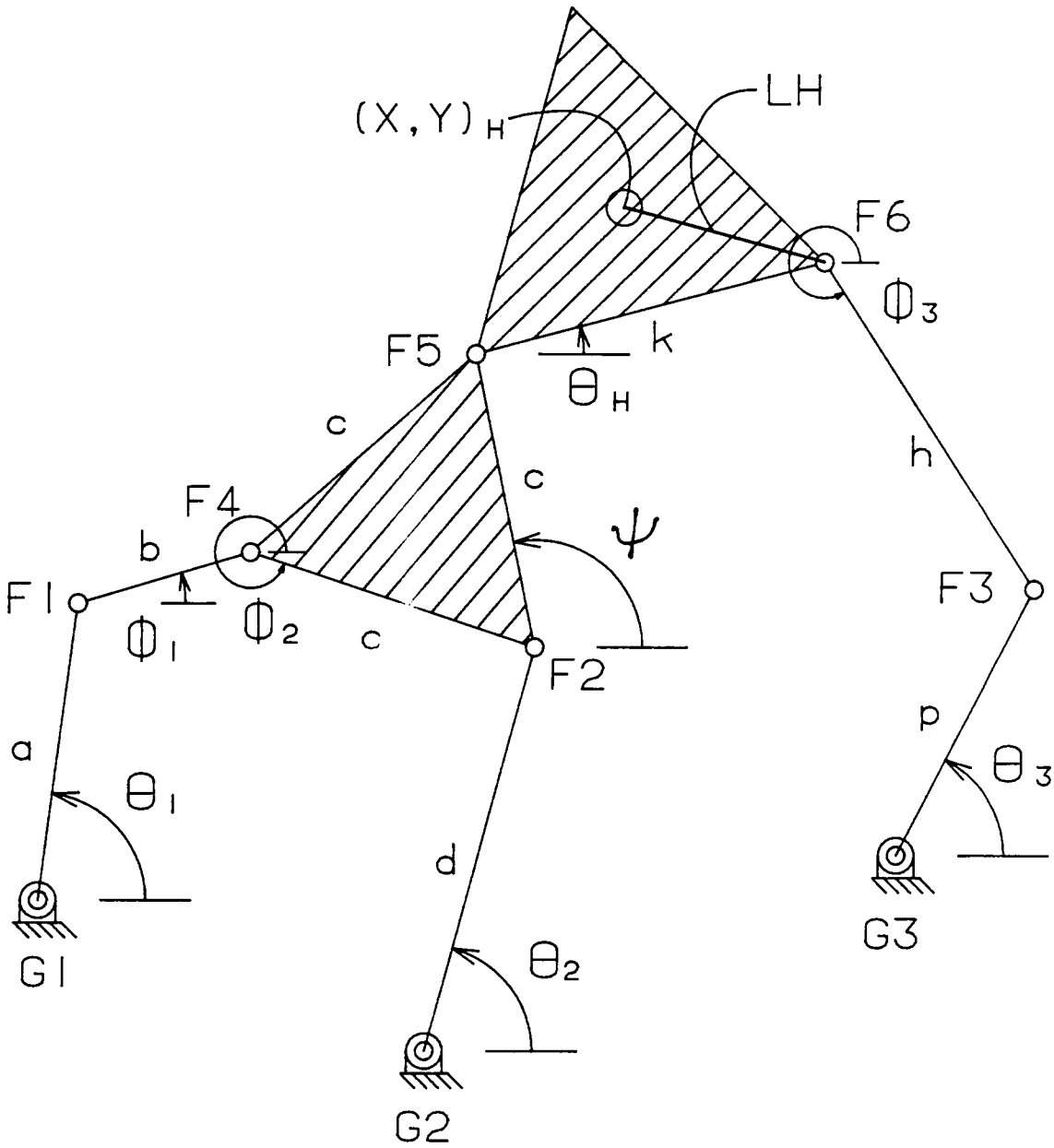

Figure 2.6
"N8R9-2" Robotic Mechanism

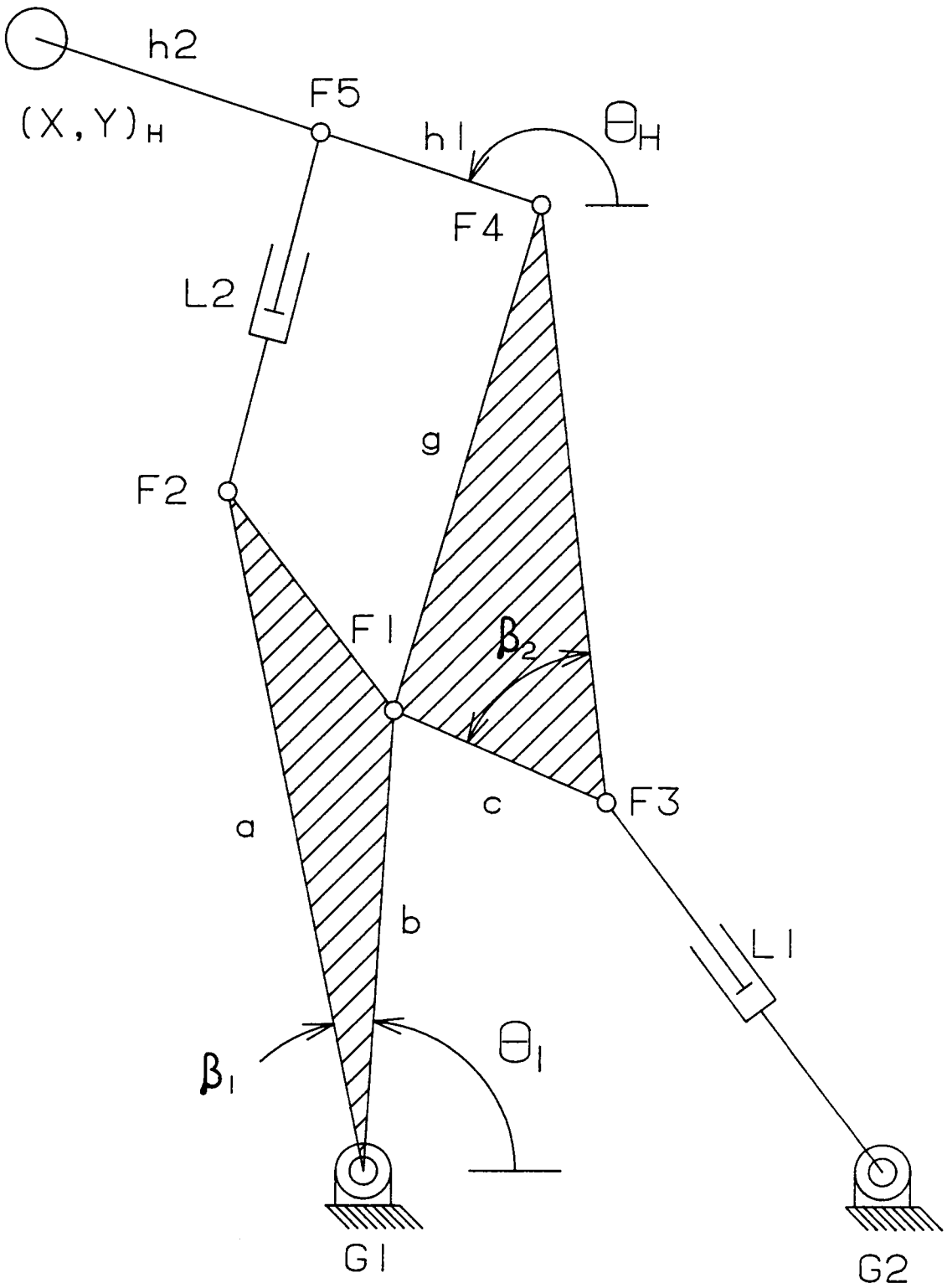

Figure 2.7
"N8R7P2-3" Robotic Mechanism

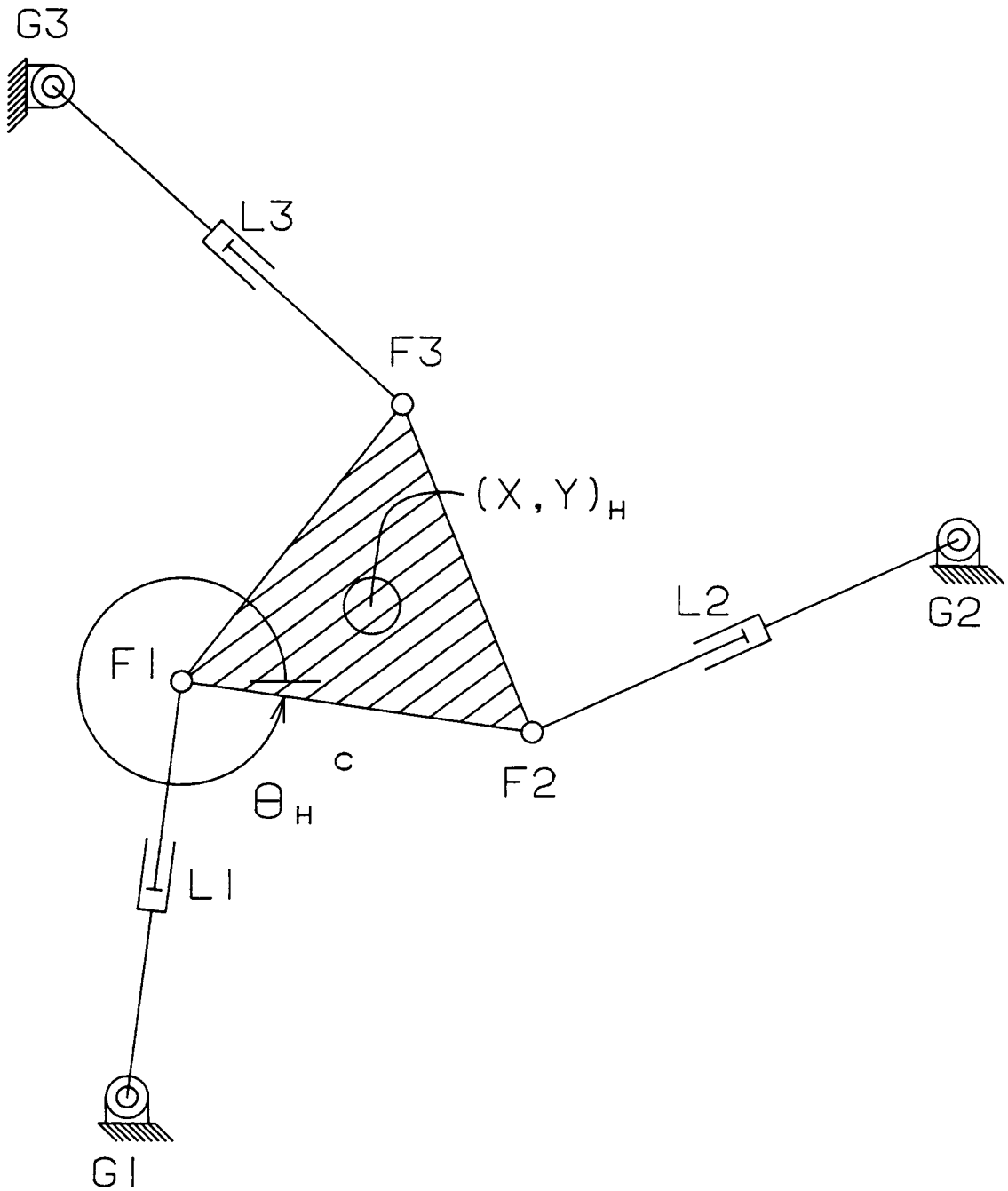

Figure 2.8
"N8R6P3-4" Robotic Mechanism

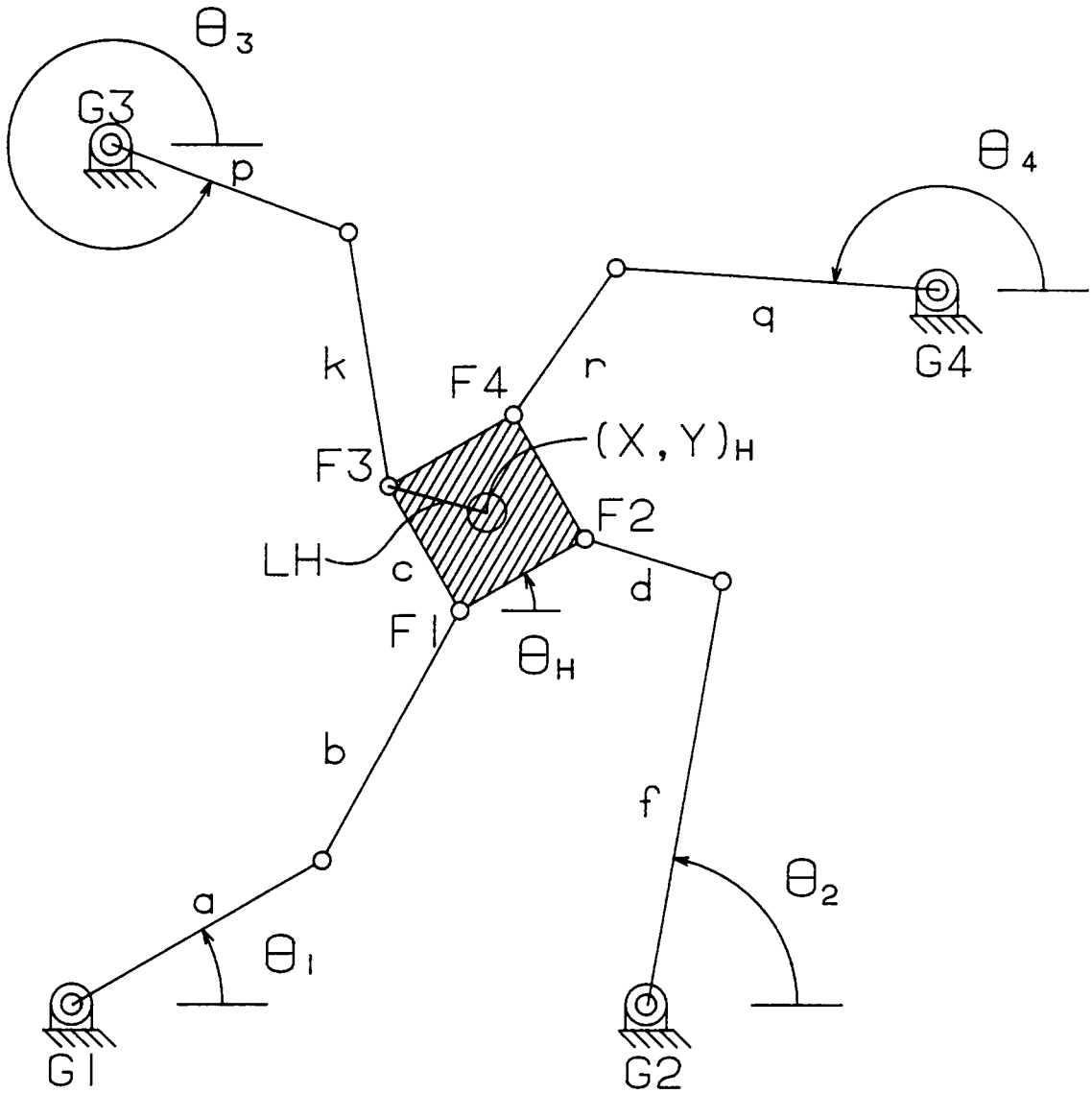

Figure 2.9
"N10R12" Robotic Mechanism

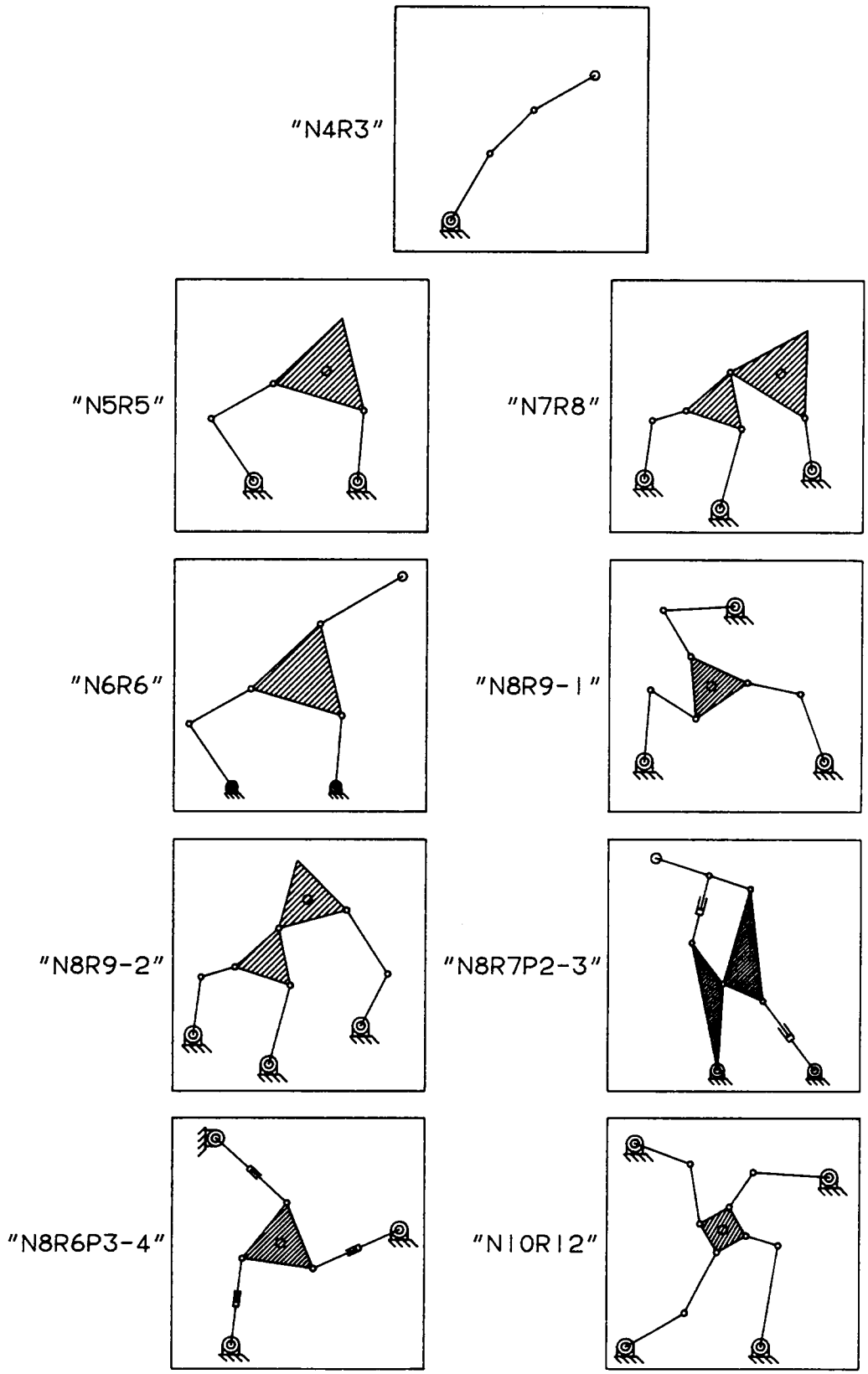

Figure 2.10
Planar Robotic Mechanisms

Chapter 3 Kinematic Position Simulation

This chapter is concerned with kinematic position analysis of planar robotic mechanisms. The goal is to provide solutions to position equations which may be used for computer robot control. Therefore, efficient closed-form solutions are desired.

The forward kinematics problem is: Given values for the input actuators, calculate the position and orientation of the manipulator hand. The inverse kinematics problem is to calculate the required input actuator values given the position and orientation of the manipulator hand. The rotary input actuators are the theta angles while the linear input actuators are represented by the L's in Figs. 2.1 through 2.9. The output parameters are the position and orientation of the hand. The number of input actuators and output parameters are the same; this is the number of manipulator freedoms. The kinematic position problems are solved for all manipulators pictured in Figs. 2.1 through 2.9. The theory of this chapter is adaptable to solve the kinematic position problem of many planar robotic mechanism configurations.

The present chapter deals with finitely separated positions, for both forward and inverse kinematics. The infinitesimally separated problems of velocity and acceleration are addressed in Chapter 4.

In general, there are multiple solutions to the forward and inverse position problems for robotic mechanisms, due to complex kinematic topology. Multiple position solutions lead

to kinematic indeterminancy, a potential problem in the design of robot controllers. Robot control is not a direct issue in this dissertation. All possible position solutions are presented.

Position analysis of a given robotic mechanism is accomplished by writing vector loop closure equations and solving for unknowns. This chapter first presents a closed-form algorithm which facilitates solving loop closure equations through repeated applications. As an alternative to this approach, the numerical Newton-Raphson technique is discussed briefly. This numerical method is presented in detail in Appendix A. Next, the closed-form algorithm is applied to solve the inverse kinematics problem. The "N8R9-2" manipulator is solved in detail, and the results are stated for the remaining manipulators. Following this, the forward kinematics problem is solved. The "N8R9-2" manipulator is again detailed, while results are presented for four additional manipulators. The forward kinematics problem of the remaining three manipulators cannot be solved in closed-form. Therefore, Sylvester's Eliminant method is presented and used to obtain a sixth degree polynomial that must then be rooted. Finally, the forward and inverse kinematic solutions are used in computer graphics animation of various robotic mechanisms.

3.1 Loop Closure Equations

The first step in solving the forward or inverse kinematics problem for a robotic mechanism is to write the loop closure equation(s). Most parallel manipulators require more than one loop equation, and many have different combinations of equations possible, not all independent. A single planar vector equation represents two scalar equations. Therefore, the kinematic position problem of a planar robotic mechanism requires half as many independent vector loop closure equations as there are unknown parameters for solution.

Specific vector loop closure equations depend on the given problem and manipulator; the general method for writing these equations is as follows. Each link of a manipulator may

be represented by a vector, conveniently written in phasor form. For example, the phasor representing a link of length 'a' oriented at angle θ from the horizontal is $ae^{i\theta}$. The vector loop closure equation is obtained by starting from the origin of a fixed reference frame and adding or subtracting phasors around a manipulator loop until the last phasor reaches the origin.

A major difference between serial and parallel manipulator topologies is the existence of intermediate angular unknowns in the parallel configurations. These intermediate unknowns are neither input actuators nor output parameters. The kinematic solutions of parallel manipulators are thus more complicated than those of similar serial manipulators. A general method for solution of planar vector loop closure equations is presented by Shigley and Uicker (Chapter 2, 1980).

3.1.1 "N8R9-2" Manipulator

This section presents loop closure equations for parallel robotic mechanisms. The "N8R9-2" manipulator, pictured in Fig. 2.6, is used as a specific example. The input actuators of this manipulator are θ_1, θ_2, and θ_3 , and the output parameters are x_H, y_H , and θ_H . There are three intermediate angles: ϕ_1, ϕ_2 , and ϕ_3.

In forward kinematics, θ_1, θ_2 , and θ_3 , are given; the output parameters must be calculated. When the three unknown intermediate angles and θ_H have been determined, the forward kinematics problem is solved, because the hand location and orientation may then be determined from the fixed geometry. Therefore, two vector loop closure equations are required in the forward kinematics solution. For the "N8R9-2" manipulator, three loop closure equations are possible; the following two are chosen for use in the solution.

$$ae^{i\theta_1} + be^{i\phi_1} + ce^{i\phi_2} - de^{i\theta_2} = \underline{G}_2 - \underline{G}_1 \qquad (3.1a)$$

$$ae^{i\theta_1} + be^{i\phi_1} + ge^{i(\phi_2 + \frac{\pi}{3})} + ke^{i\theta_H} + he^{i\phi_3} - pe^{i\theta_3} = \underline{G}_3 - \underline{G}_1 \qquad (3.1b)$$

The inverse kinematic solution for the "N8R9-2" manipulator requires different vector equations. The output parameters x_H, y_H , and θ_H. are given, which fixes the position of the triangular hand link in the plane. There are six unknowns: θ_1, θ_2, θ_3, ϕ_1, ϕ_2 , and ϕ_3. Therefore, three vector equations are required. In Eq. 3.2a, $\psi = \phi_2 - \frac{4\pi}{3}$.

$$de^{i\theta_2} + ce^{i\psi} = E_5 - G_2 \tag{3.2a}$$

$$pe^{i\theta_3} - he^{i\phi_3} = E_6 - G_3 \tag{3.2b}$$

$$ae^{i\theta_1} + be^{i\phi_1} + ce^{i(\phi_2 + \frac{\pi}{3})} = E_5 - G_1 \tag{3.2c}$$

Equations 3.2a and 3.2b are independent. Equation 3.2c may be solved only after Eq. 3.2a, because the value of ϕ_2 (obtained through angle ψ) is required.

Additional examples of loop closure equations for robotic mechanisms appear elsewhere in this dissertation: Forward kinematic loop equations are given for the "N6R6" in Eqs. 4.1 and 4.2 and the "N8R9-1" in Eqs. A.1a and A.1b, and inverse kinematic loop equations for the "N6R6" manipulator in Eqs. 4.2 and 4.14. The next section develops an algorithm for solving vector loop closure equations.

3.1.2 CIRCLE Algorithm

A closed-form algorithm is now developed for use as an integral component of the forward and inverse kinematic solution for most planar robotic mechanism topologies. This allows the generality desired when dealing with a large number of manipulators. Application to a certain manipulator configuration involves specifying the unique geometry of that manipulator. This algorithm is generally used repeatedly to solve a single manipulator position problem.

The algorithm mentioned above is the determination of the possible intersections between two circles, referred to as the CIRCLE Algorithm. Figure 3.1 shows the geometry for a

dyad connecting two points in the plane. These locations (X,Y) and (XX,YY) are known points, either from the problem specification, manipulator geometry, or from the results of an intermediate solution step. The manipulator link lengths R_1 and R_2 are known. The unknowns are angles γ_1 and γ_2, plus vector location $\underline{PT}$. The problem of solving for the point $\underline{PT}$ is to find the intersections of two circles: 1) Radius R_1, Center (X,Y); 2) Radius R_2, Center (XX,YY).

The following procedure is used to solve for the unknowns. The values of R and γ are found from known quantities.

$$R = \sqrt{(XX - X)^2 + (YY - Y)^2} \tag{3.3a}$$

$$\gamma = \tan^{-1}\left[\frac{(YY - Y)}{(XX - X)}\right] \tag{3.3b}$$

The following vector loop closure equation is written:

$$R_1 e^{i\gamma_1} + R_2 e^{i\gamma_2} = R e^{i\gamma} \tag{3.4}$$

This loop closure equation is solved by isolating the γ_2 terms, then separating into real and imaginary components. The real and imaginary scalar equations are then squared and added to eliminate γ_2 to yield the following equation.

$$D \cos\gamma_1 + E \sin\gamma_1 + F = 0 \tag{3.5}$$

where:

$$D = 2RR_1 \cos\gamma_1 \tag{3.5a}$$

$$E = 2RR_1 \sin\gamma_1 \tag{3.5b}$$

$$F = R_2^2 - R_1^2 - R^2 \tag{3.5c}$$

This equation may be solved using the tangent half-angle substitution, which follows.

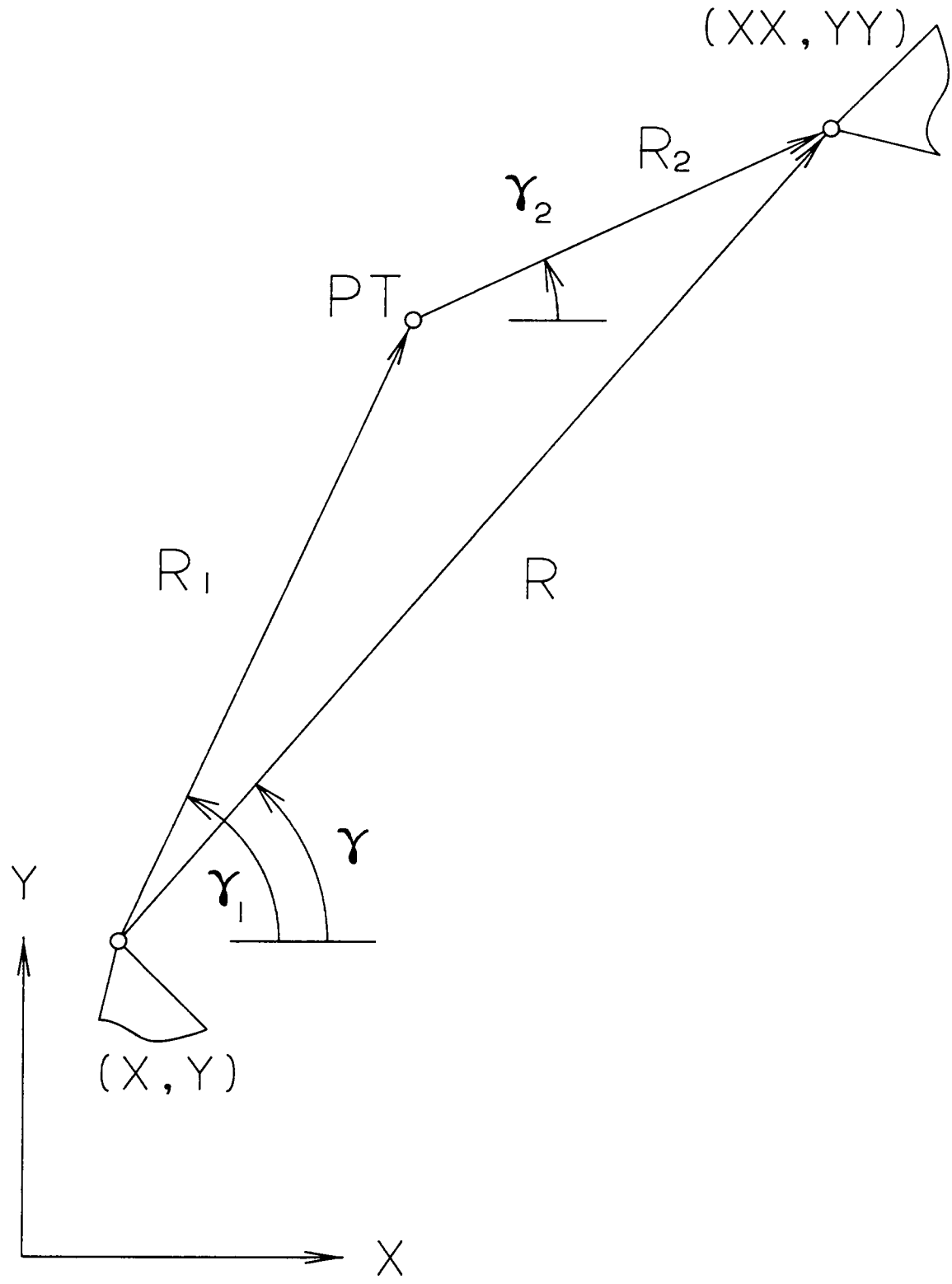

Figure 3.1
CIRCLE Algorithm Geometry

$$t = \tan\left(\frac{\gamma_1}{2}\right) \tag{3.6a}$$

$$\cos\gamma_1 = \frac{(1-t^2)}{(1+t^2)} \tag{3.6b}$$

$$\sin\gamma_1 = \frac{2t}{(1+t^2)} \tag{3.6c}$$

Substituting Eqs. 3.6b and 3.6c into Eq. 3.5, the result is:

$$At^2 + Bt + C = 0 \tag{3.7}$$

where:

$$A = F - D \tag{3.7a}$$

$$B = 2E \tag{3.7b}$$

$$C = F + D \tag{3.7c}$$

From Eq. 3.7, two solutions for t are found using the quadratic formula.

$$t_{1,2} = \frac{-B \pm \sqrt{B^2 - 4AC}}{2A} \tag{3.8}$$

At this point it is evident that if $B^2 - 4AC < 0$, then assembly is not possible; i.e. the circles do not intersect. If the circles do intersect, then the two values for γ_1 are found from Eq. 3.9 below. If $B^2 - 4AC = 0$, then the circles intersect in one point only. The two t roots are equal, which represents a limit of travel.

$$\gamma_{1i} = 2\tan^{-1}(t_i) \qquad i = 1,2 \tag{3.9}$$

For each i, two γ_{1i} values appear to result from Eq. 3.9, because the inverse tangent function is double-valued. However, when the factor two is multiplied, both values for γ_{1i} come to the same physical angle.

If required, the coordinates of the two $\underline{PT}$ locations may be evaluated (i = 1,2).

$$PTX_i = X + R_1 \cos \gamma_{1i} \tag{3.10a}$$

$$PTY_i = Y + R_1 \sin \gamma_{1i} \tag{3.10b}$$

Assembly conditions are given above, based on the tangent half-angle solution. If only assembly information is required (when the values of γ_1 and $\underline{PT}$ are not needed) a simpler assembly criterion may be used. This is used in numerical workspace determination, presented in Chapter 6, Section 6.1. If the following conditions are satisfied, then the manipulator dyad of Fig. 3.1 assembles.

$$R_1 + R_2 \geq R \geq |R_1 - R_2| \tag{3.11}$$

3.1.3 Newton-Raphson Method

This section briefly discusses the Newton-Raphson numerical technique as an alternative for solving kinematic loop closure equations This method may be applied to the position problem of any robotic mechanism. The method is presented in detail in Appendix A, because the emphasis of this dissertation is on closed-form solutions.

The Newton-Raphson technique is a predictor-corrector method. It is based on a first order Taylor series expansion of the vector loop closure equations. An initial guess is required to commence the iterative solution. Each solution step solves a linear system of equations to update the previous solution vector. Convergence is rapid; however, no general guarantee of convergence is possible.

Appendix A presents the Newton-Raphson method applied to the forward kinematics problem of the "N8R9-1" manipulator. The inverse kinematics problem may also be solved using this numerical method.

3.2 *Inverse Kinematics*

The inverse kinematic problem is stated as follows: Given the position of the manipulator hand, plus orientation for three degree-of-freedom manipulators, find the input parameters that produce this hand location. In general, more than one solution results from the inverse kinematics problem. In practice this should not create a problem because the set of input parameters closest to the previous position is usually selected. The inverse kinematic solutions for the manipulators of Figs. 2.1 - 2.9 are accomplished in closed-form in this section. The closed-form solution is an important advantage for real time computer control of a manipulator.

3.2.1 "N8R9-2" Manipulator

The inverse kinematic solution is now demonstrated, spotlighting the "N8R9-2" manipulator. The inverse kinematic solutions for the remaining manipulators are given in outline form. All triangular links are assumed to be equilateral.

In the following the notation CIRCLE(R_1, R_2) indicates application of the CIRCLE algorithm (Section 3.1.2) between two known points connected by a dyad of link lengths R_1 and R_2. As previously mentioned, when assembly occurs there are generally two values for γ and $\underline{PT}$. At any step in the inverse kinematic solution process, if the CIRCLE algorithm fails to assemble, there is no need to continue calculation.

The "N8R9-2" manipulator is shown in Fig. 2.6. Given the output parameters x_H , y_H, and θ_H, the position of the triangular hand link is uniquely determined. From this information, we can calculate the points E_5 and E_6.

$$F5_x = x_H - LH\cos(\theta_H + \frac{\pi}{6}) \tag{3.12a}$$

$$F5_y = y_H - LH\sin(\theta_H + \frac{\pi}{6}) \tag{3.12b}$$

$$F6_x = x_H + LH\cos(\theta_H - \frac{\pi}{6}) \tag{3.13a}$$

$$F6_y = y_H + LH\sin(\theta_H - \frac{\pi}{6}) \tag{3.13b}$$

From the fixed pivot G_3 to the coupler point E_6 the CIRCLE algorithm is applied, and two possible values of the input parameter θ_3 result. The CIRCLE Algorithm is again applied from G_2 to E_5 to yield two values of θ_2 and two corresponding E_2 locations. For each value of E_2, E_4 is calculated from the geometry of the second ternary link. In the following equations, i = 1,2 denotes the two possible values resulting from the CIRCLE Algorithm, for each E_2 value.

$$F4_{xi} = F2_{xi} + c\cos(\psi_i + \frac{\pi}{3}) \tag{3.14a}$$

$$F4_{yi} = F2_{yi} + c\sin(\psi_i + \frac{\pi}{3}) \tag{3.14b}$$

$$\psi_i = \tan^{-1}\left[\frac{F5_y - F2_{yi}}{F5_x - F2_{xi}}\right] \tag{3.14c}$$

With the values for E_4 calculated from above, the CIRCLE Algorithm is again applied to calculate the input angle θ_1. For each of the two θ_2 values, there are two θ_1 values possible; for each of these four combinations there are two θ_3 values. Therefore, a total of eight different solutions exist for the inverse kinematic solution of the "N8R9-2" manipulator.

3.2.2 Remaining Manipulators

The closed-form inverse kinematic solutions for the remaining manipulators will now be outlined. The solution procedures are similar to that of the "N8R9-2"manipulator, presented above. The manipulators are pictured in Figs. 2.1 through 2.9, excluding Fig. 2.6.

"N4R3": 2 solutions

1) Calculate E_1 value
2) CIRCLE(R_2, R_3) - Calculate absolute angles
3) Calculate relative angles θ_2 and θ_3 from geometry

"N5R5": 4 solutions

1) CIRCLE(LH,d) - Calculate θ_2 and E_2 values
2) Calculate E_3 values
3) CIRCLE(a,b) - Calculate θ_1 values

"N7R8": 8 solutions

1) CIRCLE(p,LH) - Calculate E_3 values
2) Calculate E_5 values
3) CIRCLE(d,c) - Calculate θ_2 and E_2 values
4) Calculate E_4 values
5) CIRCLE(a,b) - Calculate θ_1 values

"N6R6": 4 solutions

1) Calculate $\underline{E}_4$ value
2) CIRCLE(d,c) - Calculate θ_2 and $\underline{E}_2$ values
3) Calculate $\underline{E}_3$ values
4) CIRCLE(a,b) - Calculate θ_1 values
5) Calculate θ_3 from θ_H and geometry

"N8R9-1": 8 solutions

1) Calculate $\underline{E}_1, \underline{E}_2, \underline{E}_3$; one value each
2) CIRCLE(a,b) - Calculate θ_1 values
3) CIRCLE(f,d) - Calculate θ_2 values
4) CIRCLE(p,k) - Calculate θ_3 values

"N8R7P2-3": 8 solutions

1) Calculate $\underline{E}_4, \underline{E}_5$; one value each
2) CIRCLE(b,g) - Calculate θ_1 and $\underline{E}_1$ values
3) Calculate $\underline{E}_3$ values
4) Calculate L_1 values using Euclidean length
5) Calculate $\underline{E}_2$ values
6) Calculate L_2 values using Euclidean length

"N8R6P3-4": 1 unique solution

1) Calculate $\underline{E}_1, \underline{E}_2, \underline{E}_3$; one value each
2) Calculate L_1, L_2, L_3 using Euclidean length

"N10R12": 8 solutions

1) Calculate $\underline{E}_1, \underline{E}_2, \underline{E}_3, \underline{E}_4$; one value each
2) CIRCLE(a,b) - Calculate θ_1 values
3) CIRCLE(f,d) - Calculate θ_2 values
4) CIRCLE(p,k) - Calculate θ_3 values
5) CIRCLE(q,r) - Ensure that fourth leg assembles

3.3 *Forward Kinematics*

The forward kinematics problem is the opposite of inverse kinematics: Given values for the input actuators, determine the position and orientation of the hand. Unlike serial manipulators, multiple solutions generally occur in forward kinematic analysis of robotic mech-

anisms. A closed-form solution to the forward kinematics problem has been achieved for all of the manipulators shown in Figs. 2.1 - 2.9. However, three of these manipulators ("N8R9-1", "N8R6P3-4", and "N10R12") have six solutions to the forward kinematic problem. In these cases, the "closed-form" solution is presented via the coefficients of a sixth order polynomial, which are functions of the fixed manipulator parameters. The forward kinematic solution of manipulators with four or less assemblies is based on the CIRCLE algorithm developed in Section 3.1.2. This process is equivalent to writing the vector loop closure equations and solving them in closed form, starting with the loop where sufficient information is known and proceeding to the remaining loops as unknowns are solved. For the "N8R9-1", "N8R6P3-4", and "N10R12" manipulators, a similar closed-form solution is not possible because six solutions exist.

In this section, the closed-form forward kinematic solution for the "N8R9-2" manipulator is presented in detail. The solution outlines for the remaining manipulators with four or less solutions appear next. Then the polynomial method, obtained by using Sylvester's eliminant, is given for the "N8R9-1" manipulator. It is shown that the forward kinematic problems of the "N8R6P3-4" and "N10R12" manipulators are solved using the same polynomial.

3.3.1 "N8R9-2" Manipulator

The "N8R9-2" manipulator is pictured in Fig. 2.6. Given the input angles θ_1, θ_2, and θ_3, the values of points E_1, E_2, and E_3 are uniquely determined. In Eqs. 3.15a and 3.15b, L_j takes the values a, d, and p, for j equal to 1, 2, and 3, respectively.

$$Fj_x = Gj_x + L_j \cos(\theta_j) \tag{3.15a}$$

$$Fj_y = Gj_y + L_j \sin(\theta_j) \tag{3.15b}$$

Using CIRCLE(b,c), two values for the point E_4 are calculated. Corresponding to each E_4 location, the value of point E_5 is obtained from geometry.

$$F5_{xi} = F4_{xi} + ccos(\phi_2 + \frac{\pi}{3}) \tag{3.16a}$$

$$F5_{yi} = F4_{yi} + csin(\phi_2 + \frac{\pi}{3}) \tag{3.16b}$$

$$\phi_2 = \tan^{-1}\left[\frac{F2_{yi} - F4_{yi}}{F2_{xi} - F4_{xi}} \right] \tag{3.16c}$$

For each of the two E_5 values, the CIRCLE algorithm is applied from E_5 to E_3 to calculate values for the second manipulator loop. When using CIRCLE(k,h), the first loop angle is the orientation of the hand, θ_H , from which the hand position may be calculated.

$$x_H = F5_x + LHcos(\theta_H + \frac{\pi}{6}) \tag{3.17a}$$

$$y_H = F5_y + LHsin(\theta_H + \frac{\pi}{6}) \tag{3.17b}$$

Given the unique locations E_1, E_2, and E_3, there are two values for E_4, and E_5. For each value of E_5, there are two values for θ_H . Thus, there are four solutions to the forward kinematics problem of the "N8R9-2" manipulator.

3.3.2 Remaining Closed-Form Solutions

The remaining closed-form forward kinematic solutions are presented below. The manipulators of this section are shown in Figs. 2.1, 2.2, 2.3, 2.4, and 2.7. The CIRCLE Algorithm from Section 3.1.2 is used in the forward kinematic solutions of all manipulators except the "N4R3".

"N4R3": 1 solution

1) $x_H = R_2 \cos\theta_2 + R_3 \cos(\theta_2 + \theta_3) + R_4 \cos(\theta_2 + \theta_3 + \theta_4)$
2) $y_H = R_2 \sin\theta_2 + R_3 \sin(\theta_2 + \theta_3) + R_4 \sin(\theta_2 + \theta_3 + \theta_4)$
3) $\theta_H = \theta_2 + \theta_3 + \theta_4$

"N5R5": 2 solutions

1) Calculate $\underline{E}_1, \underline{E}_2$; one value each
2) CIRCLE(b,c) - Calculate $\underline{E}_3$ values
3) Calculate the (x_H, y_H) values

"N7R8": 4 solutions

1) Calculate $\underline{E}_1, \underline{E}_2$; one value each
2) CIRCLE(b,c) - Calculate $\underline{E}_4$ values
3) Calculate $\underline{E}_5$ values
4) CIRCLE(h,p) - Calculate $\underline{E}_3$ values
5) Calculate the (x_H, y_H) values

"N6R6": 2 solutions

1) Calculate $\underline{E}_1, \underline{E}_2$; one value each
2) CIRCLE(b,c) - Calculate $\underline{E}_3$ values
3) Calculate $\underline{E}_4$ values
4) Calculate the (x_H, y_H, θ_H) values

"N8R7P2-3": 4 solutions

1) Calculate $\underline{E}_1, \underline{E}_2$; one value each
2) CIRCLE(c,L_1) - Calculate $\underline{E}_3$ values
3) Calculate $\underline{E}_4$ values
4) CIRCLE(L_2, h_1) - Calculate $\underline{E}_5$ values
5) Calculate the (x_H, y_H, θ_H) values

3.3.3 "N8R9-1", "N8R6P3-4", "N10R12" Forward Kinematics

The "N8R9-1" manipulator is pictured in Fig. 2.5. The input parameters are θ_1 , θ_2, and θ_3; the output values to be solved for are x_H , y_H, and θ_H. Figure 3.2a presents the same manipulator redrawn for ease of visualization in the ensuing derivation. Given the input angles, the vector locations $\underline{E}_4$, $\underline{E}_5$, and $\underline{E}_6$ are uniquely determined. Figure 3.2b presents a sub-chain of the "N8R9-1" manipulator with these known points as the fixed pivots. This sub-chain is a structure (F = 0).

From Fig. 3.2b, it is evident that the closed-form CIRCLE Algorithm cannot be used to solve the forward kinematic problem of the "N8R9-1" manipulator. The reason for this is that

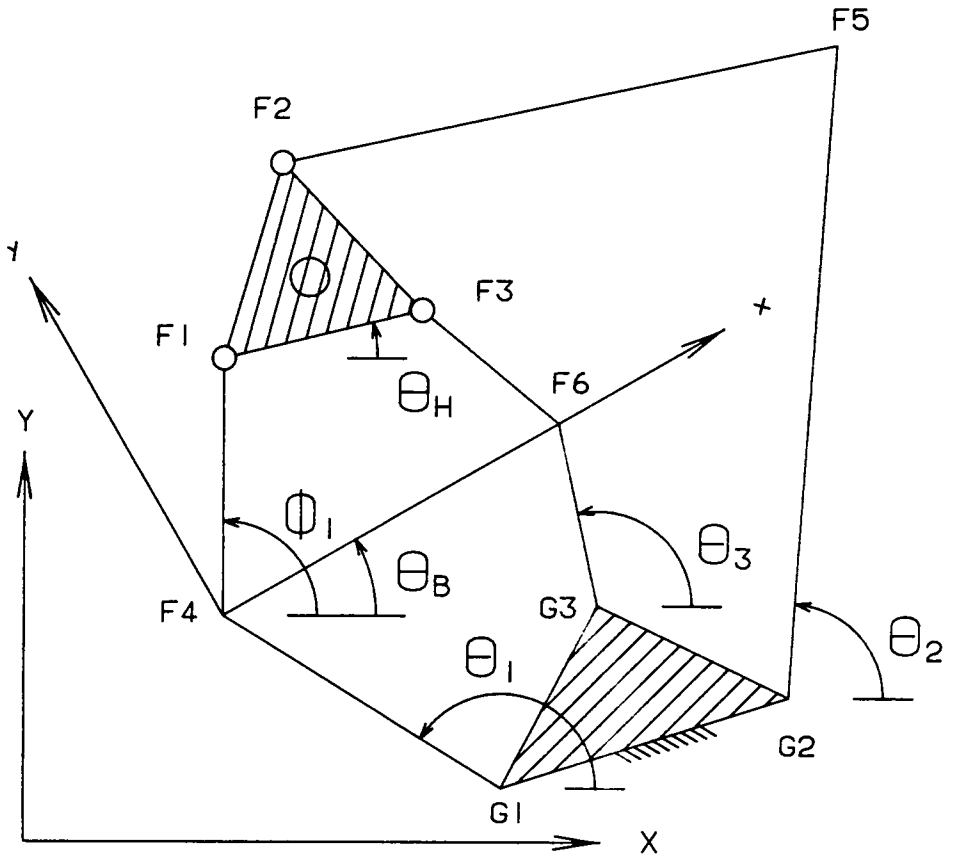

3.2a
"N8R9-1" Geometry Redrawn

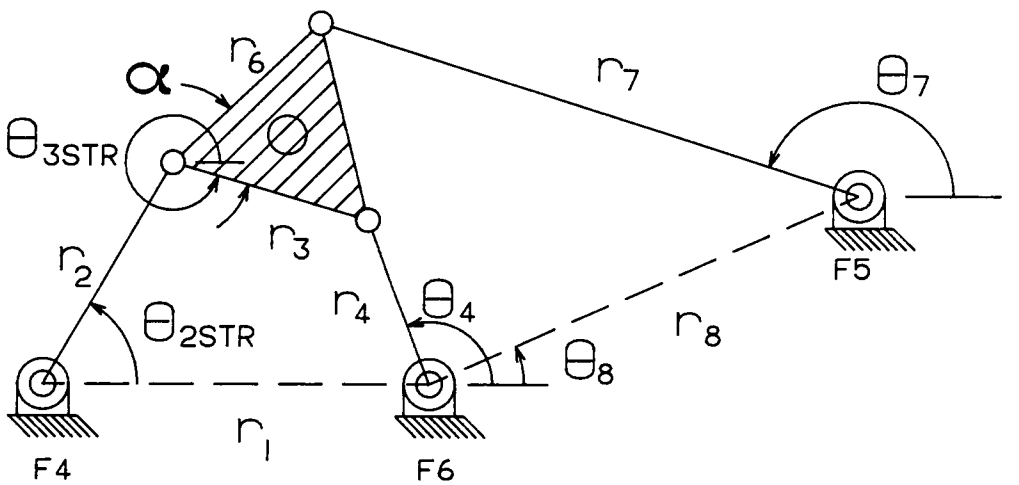

3.2b
"N8R9-1" Sub-Structure

Figure 3.2
"N8R9-1" Forward Kinematics

two unknown points lie between each pair of known points; the CIRCLE Algorithm allows only one unknown point. A completely closed-form solution is not possible. In this section, the forward kinematic problem of the "N8R9-1" robotic mechanism is solved using Sylvester's eliminant (Sandor and Erdman, 1984). Sylvester's eliminant method is used because it allows a coupled non-linear system of equations in several unknowns to be ultimately expressed in terms of a polynomial in one unknown. The same method is extended to solve the forward kinematic problems of the "N8R6P3-4" and "N10R12" manipulators.

In order to apply the forward kinematic solution, the following transformation between the xy and XY coordinate frames of Fig. 3.2a must be used. The subscript STR denotes the structure of Fig. 3.2b. The following derivation refers to Fig. 3.2b.

$$\theta_B = \tan^{-1}\left[\frac{F6_y - F4_y}{F6_x - F4_x}\right] \tag{3.18a}$$

$$\theta_8 = \tan^{-1}\left[\frac{F5_y - F6_y}{F5_x - F6_x}\right] - \theta_B \tag{3.18b}$$

$$\phi_1 = \theta_B + \theta_{2STR} \tag{3.18c}$$

$$\theta_H = \theta_B + \theta_{3STR} \tag{3.18d}$$

The forward kinematic solution for this manipulator amounts to determining the possible ways the structure of Fig. 3.2b can be assembled. There are four unknowns, namely, the angles θ_2, θ_3, θ_4,, and θ_7. The "fixed pivots" and θ_8 plus all link lengths are known from the forward problem specifications. The structure of Fig. 3.2b is comprised of three four-bar linkages, two of which are independent.

The general solution strategy is as follows. Two independent vector loop equations are required, because there are four unknowns. These have the form:

$$f_1 = f_1(\theta_2, \theta_3, \theta_4) = 0 \tag{3.19a}$$

$$f_2 = f_2(\theta_2, \theta_3, \theta_7) = 0 \tag{3.19b}$$

The angle θ_4 is eliminated from Eq. 3.19a, while θ_7 is eliminated from Eq. 3.19b. This yields two equations, coupled and non-linear, in the unknowns θ_2 and θ_3. Sylvester's eliminant is then used to obtain a polynomial in terms of one unknown angle, θ_2.

From Fig. 3.2b, the two vector loop equations are:

$$r_2 e^{i\theta_2} + r_3 e^{i\theta_3} - r_4 e^{i\theta_4} - r_1 = 0 \tag{3.20a}$$

$$r_2 e^{i\theta_2} + r_6 e^{i\theta_3} e^{i\alpha} - r_7 e^{i\theta_7} - r_8 e^{i\theta_8} - r_1 = 0 \tag{3.20b}$$

The θ_4 and θ_7 terms are brought to the right hand sides of Eqs. 3.20a and 3.20b; these equations are multiplied by their respective complex conjugates to eliminate θ_4 and θ_7. The resulting two equations are:

$$A e^{i\theta_3} + \bar{A} e^{-i\theta_3} + C = 0 \tag{3.21a}$$

$$B e^{i\theta_3} + \bar{B} e^{-i\theta_3} + D = 0 \tag{3.21b}$$

The coefficients A, B, C, and D are functions of θ_2.

$$A = r_3(r_2 e^{-i\theta_2} - r_1) \tag{3.22a}$$

$$C = R_1 - r_1 r_2 (e^{i\theta_2} + e^{-i\theta_2}) \tag{3.22b}$$

$$R_1 = r_1^2 + r_2^2 + r_3^2 - r_4^2 \tag{3.22c}$$

$$B = r_6 e^{i\alpha}(r_2 e^{-i\theta_2} - r_8 e^{-i\theta_8} - r_1) \tag{3.23a}$$

$$D = R_2 - \bar{R} e^{i\theta_2} - R e^{-i\theta_2} \tag{3.23b}$$

$$R_2 = r_1^2 + r_2^2 + r_6^2 - r_7^2 + r_8^2 + 2 r_1 r_8 \cos\theta_8 \tag{3.23c}$$

$$R = r_2(r_1 + r_8 e^{i\theta_8}) = RR + iRI \tag{3.23d}$$

$$RR = r_2(r_1 + r_8 \cos\theta_8) \tag{3.23e}$$

$$RI = r_2 r_8 \sin\theta_8 \tag{3.23f}$$

Sylvester's eliminant is now used to obtain a polynomial in terms of θ_2 alone. Equations 3.21a and 3.21b are multiplied by $e^{i\theta_3}$ to yield a total of four equations in the "unknowns" $e^{i2\theta_3}$, $e^{i\theta_3}$, $e^{i0\theta_3}$, and $e^{-i\theta_3}$. The resulting system is homogeneous; for the solution to exist, the determinant must be equal to zero.

$$\begin{vmatrix} 0 & A & C & \overline{A} \\ 0 & B & D & \overline{B} \\ A & C & \overline{A} & 0 \\ B & D & \overline{B} & 0 \end{vmatrix} = 0 \tag{3.24}$$

Expansion of the above determinant yields the following polynomial in terms of $e^{i\theta_2}$:

$$\sum_n K_n e^{in\theta_2} = 0 \tag{3.25}$$

In Eq. 3.25, n = -3, -2, -1, 0, 1, 2, 3. The coefficients K_n and K_{-n} are complex conjugates, while K_0 is real. Therefore, the expression of Eq. 3.25 is real. This determinant may thus be transformed to a trigonometric polynomial of maximum power three using trigonometric identities.

$$X_1 \cos^3\theta_2 + X_2 \cos^2\theta_2 \sin\theta_2 + X_3 \cos\theta_2 \sin^2\theta_2 + X_4 \cos^2\theta_2 + X_5 \sin^2\theta_2 +$$

$$X_6 \cos\theta_2 \sin\theta_2 + X_7 \cos\theta_2 + X_8 \sin\theta_2 + X_9 = 0 \tag{3.26}$$

Using the tangent half-angle substitution from Eqs. 3.6, a sixth-degree polynomial is obtained.

$$S_1 t^6 + S_2 t^5 + S_3 t^4 + S_4 t^3 + S_5 t^2 + S_6 t + S_7 = 0 \tag{3.27}$$

The roots of Eq. 3.27 give the six possible values for θ_2. There may be 0, 2, 4, or 6 real θ_2 values resulting, because the S_i coefficients are real, and thus any imaginary roots must

be complex conjugates. The X_i and S_i coefficients are given in Appendix B, in terms of manipulator parameters.

Given each value of θ_2 , the other unknown angles may be solved for, as needed. In particular, if θ_3 is determined also, the position of the hand is found from the manipulator geometry. The angle θ_4 is eliminated from the four-bar loop equation, Eq. 3.20a, by multiplying the equation with its complex conjugate, after the θ_4 term has been brought to the right hand side. At this point, the tangent half-angle substitution (Eqs. 3.6) is used to solve for the two possible values of θ_3.

$$at^2 + bt + c = 0 \tag{3.28}$$

$$a = r_4^2 - r_1^2 - r_2^2 - r_3^2 + 2r_1r_2\cos\theta_2 - 2r_1r_3 + 2r_2r_3\cos\theta_2 \tag{3.28a}$$

$$b = -4r_2r_3\sin\theta_2 \tag{3.28b}$$

$$c = r_4^2 - r_1^2 - r_2^2 - r_3^2 + 2r_1r_2\cos\theta_2 + 2r_1r_3 - 2r_2r_3\cos\theta_2 \tag{3.28c}$$

The quadratic formula is used to calculate the values for t, from which two values of θ_3 are found. The transformed orientation of the hand is θ_3 (see Eq. 3.18d). For each θ_2, there are generally two values for θ_3 . However, in general only one of these two possible values allows the structure to assemble. Therefore, it is necessary to select the correct θ_3 . This is done by checking the length of r_7 and choosing the θ_3 which gives the proper value for this fixed parameter. In summary, there are six mathematical solutions for the angle θ_2 . In general, there are six solutions for the assembly of the structure given in Fig. 3.2b, some of which may be imaginary. The solution in the original coordinate system is found through reversing the transformation given in Eqs. 3.18.

This completes the forward kinematic solution of the "N8R9-1" manipulator. Due to the six possible solutions, a numerical routine must be employed to calculate the roots. The same polynomial may be used to solve the forward kinematics problem for the "N8R6P3-4" and "N10R12" manipulators, pictured in Figs. 2.8 and 2.9, respectively. For the "N8R6P3-4" manipulator, the variable link lengths L_1 , L_2, and L_3 in Fig. 2.8 are identified with the link lengths

r_2 , r_4, and r_7 in Fig. 3.2b. The "fixed pivots" in Fig. 3.2b (points $\underline{E}_4$, $\underline{E}_6$, and $\underline{E}_5$) are the actual fixed pivots in Fig. 2.7 ($\underline{G}_1$, $\underline{G}_2$, and $\underline{G}_3$).

The vector loop closure equations of the "N10R12" manipulator are identical to those of the "N8R9-1". After solution, the assembly of the fourth manipulator leg (q,r) must be checked. The following condition must hold true:

$$q + r \geq D \geq |q - r| \tag{3.29}$$

where D is the Euclidean distance between $\underline{G}_4$ and $\underline{E}_4$.

The preceding solution of the "N8R9-1" forward kinematic problem may also be applied to the position analysis of the Stephenson III six-bar mechanism, when the input angle is as shown in Fig. 3.3.

3.4 Numerical Examples for Position Analysis

In this section, a kinematic position example is given for each of the manipulators in Figs. 2.1 - 2.9. To save space, only one of the generally multiple solutions is presented. Therefore, these examples apply to either forward or inverse kinematics. The input parameters are θ_i and L_i, while the output parameters are x_H, y_H, and θ_H. The ground pivot $\underline{G}_1$ is assumed to be located at the origin. For inverse kinematics, the output parameters are given and the input parameters calculated and forward kinematics is the reverse of this. Any convenient unit of length may be used; angular units are degrees.

"N4R3" Manipulator

$R_2 = 3.00, R_3 = 2.00, R_4 = 1.00$

$\theta_2 = 60.00, \theta_3 = 345.00, \theta_4 = 335.00;$ $\quad x_H = 3.85, y_H = 4.35, \theta_H = 20.00$

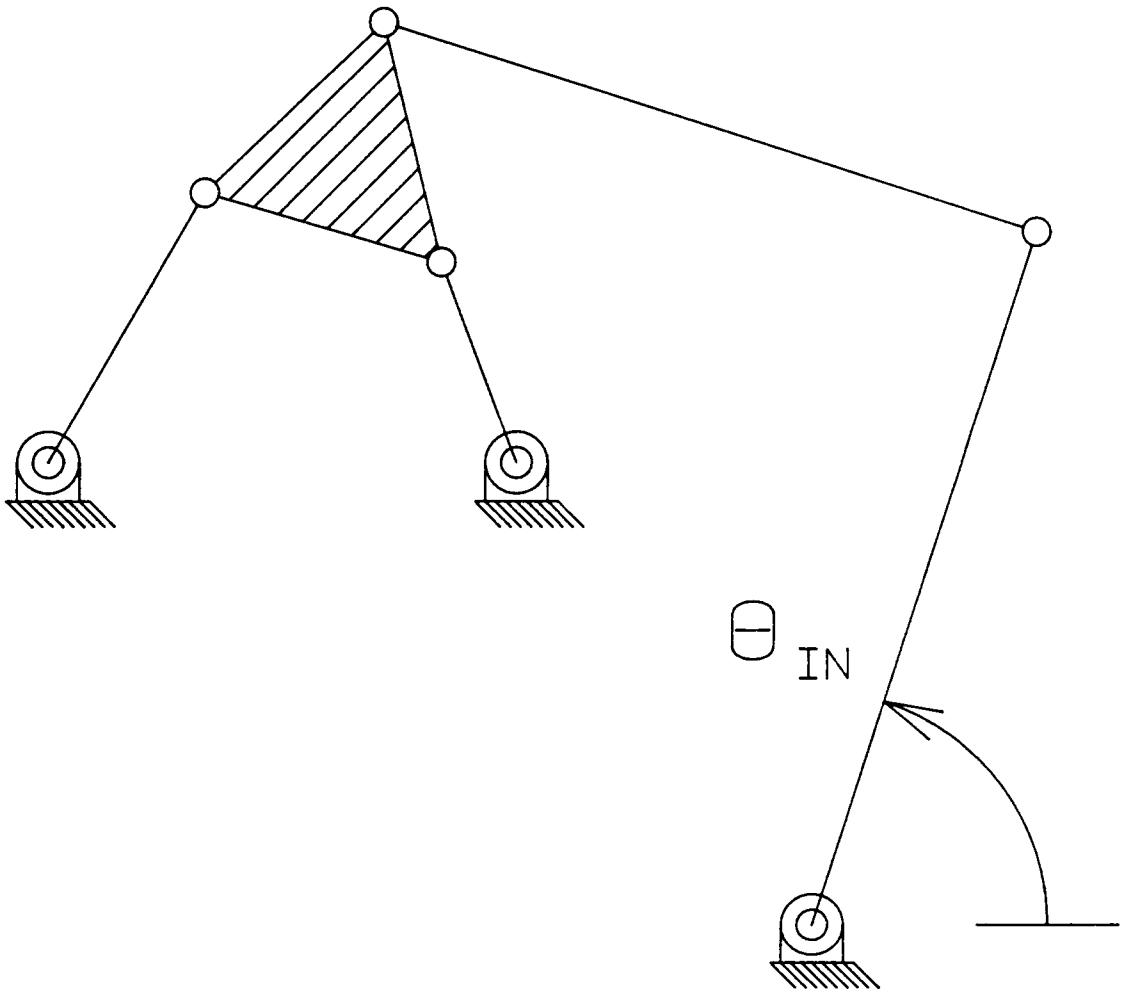

Figure 3.3
Stephenson III Mechanism

"N5R5" Manipulator

a = 0.80, b = 0.75, c = 1.00, d = 0.75, L = 0.90

$\theta_1 = 100.00, \theta_2 = 80.00;$ $x_H = 0.85, y_H = 1.29$

"N7R8" Manipulator

a = 0.80, b = 0.75, c = 1.00, d = 0.75, h = 1.20, p = 0.90

$\underline{G}_2 = (0.90,0.00), \underline{G}_3 = (1.80, -0.20)$

$\theta_1 = 100.00, \theta_2 = 80.00;$ $x_H = 1.85, y_H = 1.39$

"N6R6" Manipulator

a = 0.80, b = 0.75, c = 1.00, d = 0.75, h = 1.00, L = 0.90

$\theta_1 = 100.00, \theta_2 = 80.00, \theta_3 = 90.00;$ $x_H = 2.21, y_H = 1.51, \theta_H = -11.88$

"N8R9-1" Manipulator

a = 1.40, b = 1.00, c = 1.00, d = 1.00, f = 1.60, k = 0.90, p = 1.60

$\underline{G}_2 = (3.1348,0.3398), \underline{G}_3 = (2.40,3.68)$

$\theta_1 = 37.19, \theta_2 = 108.34, \theta_3 = 211.81;$ $x_H = 1.50, y_H = 1.83, \theta_H = 330.00$

"N8R9-2" Manipulator

a = 0.80, b = 0.75, c = 1.00, d = 0.75, k = 1.50, h = 0.90, p = 0.70

$\underline{G}_2 = (0.90,0.00), \underline{G}_3 = (2.00,0.30)$

$\theta_1 = 100.00, \theta_2 = 80.00, \theta_3 = 60.00;$ $x_H = 1.98, y_H = 2.15, \theta_H = 0.00$

"N8R7P2-3" Manipulator

a = 1.50, b = 1.00, c = 0.50, f = 1.30, l = 1.12,

$h_1 = 0.75, h_2 = 0.25, \beta_1 = 15.0, \beta_2 = 60.0$

$\theta_1 = 86.56, L_1 = 1.00, L_2 = 0.67;$ $x_H = -0.63, y_H = 2.15, \theta_H = 176.60$

"N8R6P3-4" Manipulator

c = 1.00

$\underline{G}_2 = (2.34,1.59), \underline{G}_3 = (-0.22,2.86)$

$L_1 = 1.00, L_2 = 1.14, L_3 = 1.15;$ $x_H = 0.67, y_H = 1.40, \theta_H = 20.00$

"N10R12" Manipulator

a = 2.00, b = 2.50, c = 1.00, d = 1.00, f = 3.00,
k = 1.80, p = 1.75, q = 2.25, r = 1.25

$\underline{G}_2 = (3.13,0.34)$, $\underline{G}_3 = (2.40,3.68)$, $\underline{G}_4 = (6.00,5.00)$

$\theta_1 = 10.21, \theta_2 = 80.35, \theta_3 = 339.73;$ $\quad x_H = 2.86, y_H = 3.43, \theta_H = 30.00$

3.5 graPHIGS Animation of Planar Robotic Mechanisms

This section describes computer graphics animation of planar robotic mechanisms. The IBM version of the PHIGS graphics subroutines, graPHIGS, is used as support software. PHIGS ("Programmer's Hierarchical Interactive Graphics System") is the proposed American National Standard for three dimensional computer graphics.

Manipulator animation is useful in the design of robotic mechanisms. Using the computer, manipulator motion may be viewed, avoiding the costly and time-consuming process of building physical prototypes. In this way, manipulators with varying dimensions may be compared. In addition to displaying kinematic position analysis results (both forward and inverse), the animation routines are also helpful in identifying potential problem areas. The areas of dynamics calculations (Chapter 5), workspace optimization (Chapter 6), and link interference (Chapter 7) benefitted from the animation routines.

An overview of the animation modelling process is presented here. Appendix C presents FORTRAN computer programs for the forward and inverse kinematic animation of the "N6R6" manipulator.

The core of the animation program for a manipulator is the forward or inverse kinematic position solution. The basic computer animation program may be used to graphically animate a large number of different manipulators. The geometry and kinematic position solution of the specific manipulator is substituted into the programs given in Appendix C.

In order to perform animation, the program solves the kinematic position problem repeatedly, according to user input. The user enters data through the valuators in event mode. A valuator is a logical input device which returns a real value that may be mapped to a dial box or a thumb wheel. Event mode allows the user application program to accept data from external input events as they occur. On an IBM 5080 terminal, the dial box is the valuator. One dial is used for each manipulator degree-of-freedom; for three degrees-of-freedom manipulators, dials 1 through 3 are used. The forward animation program equates the dial values with input actuators, either rotary or linear. The inverse animation program assigns x_H, y_H, and θ_H to dials 1, 2, and 3, respectively. The input data are passed to the kinematic solution subroutine. The solution is achieved, the structure emptied, and the new data associated with the structure. The workstation is then updated, causing the new image to appear on the screen and the old one to be erased. Due to the closed-form solutions and the capabilities of graPHIGS, the animation is smooth and the response is rapid.

Each program is started with an initial position. If the input valuators are set by the user such that the manipulator moves out of its physical workspace, the kinematic solution is not possible, and the last solution to assemble is used until the input values are within the manipulator motion range. There are generally multiple solutions to the forward and inverse position analysis problems for planar robotic mechanisms. The animation routines calculate all possible solutions and then display the solution closest to the previous location.

Appendix C.1 presents the forward kinematics animation program for the "N6R6" manipulator. Appendix C.2 presents minor modifications to this program necessary to produce the inverse kinematics animation routine for the same manipulator. In addition to the "N6R6" manipulator, forward and inverse animation routines were developed for the serial "N4R3" manipulator and the parallel "N8R9-1" robotic mechanism. Appendix C demonstrates FORTRAN code for the forward (Section C.1) and inverse (Section C.2) kinematic position solution of the "N6R6" manipulator, in subroutine COORD. The background theory appears in Sections 3.2.2 and 3.3.2. The CIRCLE Algorithm (Section 3.1.2) is implemented in subroutine SOLVPT, given in Section C.1.

Chapter 4 Velocity and Acceleration Analysis

In this chapter, forward and inverse derivative analysis is presented. When the forward or inverse kinematic position analysis is complete the velocity and acceleration solutions involve linear systems of equations. As stated in Chapter 3 there are generally multiple solutions to the kinematic position problem; for a given position the velocity and acceleration solutions are unique. Velocity and acceleration information is required for kinetostatic analysis. In addition, derivative analysis with position analysis provides complete robot motion specification.

Velocity analysis requires position information; acceleration analysis requires the velocity solution. Derivative analysis is presented in detail for the "N6R6" manipulator, shown in Fig. 2.4. The derivative problem for parallel manipulators is more involved than for serial manipulators, due to intermediate angles and their time derivatives. For the "N6R6" manipulator the intermediate unknowns $\dot{\phi}_1$, $\dot{\phi}_2$, $\ddot{\phi}_1$, and $\ddot{\phi}_2$ are determined simultaneously with the desired derivative values.

4.1 Forward Solution

The forward derivative problem solves for the velocity and acceleration of the hand given velocity and acceleration values for the input actuators. For the "N6R6" manipulator, the forward velocity and acceleration problems are: Given $\dot{\theta}_1$, $\dot{\theta}_2$, $\dot{\theta}_3$, $\ddot{\theta}_1$, $\ddot{\theta}_2$, and $\ddot{\theta}_3$, find $\dot{x}_H$, $\dot{y}_H$, $\dot{\theta}_H$, $\ddot{x}_H$, $\ddot{y}_H$, and $\ddot{\theta}_H$.

4.1.1 "N6R6" Forward Velocity Analysis

The vector loop closure equations used in forward kinematic position analysis of the "N6R6" manipulator are given below.

$$ae^{i\theta_1} + be^{i\phi_1} + ce^{i\phi_2} - de^{i\theta_2} = \underline{G}_2 - \underline{G}_1 \tag{4.1}$$

$$\underline{G}_2 + de^{i\theta_2} + ce^{i\phi} + he^{i\theta_H} = x_H + iy_H \tag{4.2}$$

The angle ϕ is directly related to the unknown intermediate angle ϕ_2 (recall that the ternary link is assumed equilateral).

$$\phi = \phi_2 - \frac{4\pi}{3} \tag{4.2a}$$

One time derivative of Eqs. 4.1 and 4.2 gives the velocity equations for the "N6R6" manipulator. The unknowns $\dot{\phi}_1$, $\dot{\phi}_2$ must be determined before evaluating the linear and angular velocities of the hand. The following equation is the time derivative of Eq. 4.1.

$$iae^{i\theta_1}\dot{\theta}_1 + ibe^{i\phi_1}\dot{\phi}_1 + ice^{i\phi_2}\dot{\phi}_2 - ide^{i\theta_2}\dot{\theta}_2 = 0 \tag{4.3}$$

Resolving Eq. 4.3 into real and imaginary components and separating the unknown terms leads to an equation of the following form.

$$[J]\{\dot{\phi}_{12}\} = \{B\} \tag{4.4}$$

The terms from Eq. 4.4 are as follows. The matrix $[J]$ is a Jacobian matrix.

$$[J] = \begin{bmatrix} -b\sin\phi_1 & -c\sin\phi_2 \\ b\cos\phi_1 & c\cos\phi_2 \end{bmatrix} \tag{4.4a}$$

$$\{\dot{\phi}_{12}\} = \begin{bmatrix} \dot{\phi}_1 \\ \dot{\phi}_2 \end{bmatrix} \tag{4.4b}$$

$$\{B\} = \begin{bmatrix} a\sin\theta_1\dot{\theta}_1 - d\sin\theta_2\dot{\theta}_2 \\ -a\cos\theta_1\dot{\theta}_1 + d\cos\theta_2\dot{\theta}_2 \end{bmatrix} \tag{4.4c}$$

The intermediate solution is obtained in closed-form by inverting Eq. 4.4.

$$\{\dot{\phi}_{12}\} = [J]^{-1}\{B\} \tag{4.5}$$

where:

$$[J]^{-1} = \frac{1}{|J|}\begin{bmatrix} c\cos\phi_2 & c\sin\phi_2 \\ -b\cos\phi_1 & -b\sin\phi_1 \end{bmatrix} \tag{4.5a}$$

$$|J| = bc(\cos\phi_1\sin\phi_2 - \cos\phi_2\sin\phi_1) \tag{4.5b}$$

The velocity of the hand is determined from a time derivative of Eq. 4.2, using $\dot{\phi}_2$ from Eq. 4.5. Relationships for $\dot{\phi}$ and $\dot{\theta}_H$ are required before evaluating the hand velocity. The angular velocity $\dot{\phi}$ is identical to that of $\dot{\phi}_2$, from a time derivative of Eq. 4.2a. The relative angle θ_3 is expressed in terms of the absolute angle θ_H and the angle ϕ_2.

$$\theta_3 = \theta_H - \phi_2 + \frac{\pi}{3} \tag{4.6}$$

The angular velocity $\dot{\theta}_H$ follows from the time derivative of Eq. 4.6.

$$\dot{\theta}_H = \dot{\theta}_3 + \dot{\phi}_2 \tag{4.7}$$

The hand velocity is now expressed using the above information.

$$\begin{bmatrix} \dot{x}_H \\ \dot{y}_H \\ \dot{\theta}_H \end{bmatrix} = \begin{bmatrix} -d\sin\theta_2 & -h\sin\theta_H & -(c\sin\phi + h\sin\theta_H) \\ d\cos\theta_2 & h\cos\theta_H & (c\cos\phi + h\cos\theta_H) \\ 0 & 1 & 1 \end{bmatrix} \begin{bmatrix} \dot{\theta}_2 \\ \dot{\theta}_3 \\ \dot{\phi}_2 \end{bmatrix} \tag{4.8}$$

Alternatively, the hand velocity may be written via the manipulator chain (a-b-c-h), using a different loop closure equation in place of Eq. 4.2. However, the form given above yields the same result with fewer terms.

4.1.2 "N6R6" Forward Acceleration Analysis

Acceleration analysis follows velocity analysis with a second time derivative of the position equations. Values obtained in the velocity section are required to solve for the unknown accelerations. The process again starts with an intermediate step, the second time derivative of Eq. 4.1.

$$iae^{i\theta_1}\ddot{\theta}_1 + ibe^{i\phi_1}\ddot{\phi}_1 + ice^{i\phi_2}\ddot{\phi}_2 - ide^{i\theta_2}\ddot{\theta}_2 - ae^{i\theta_1}\dot{\theta}_1^{\,2} - be^{i\phi_1}\dot{\phi}_1^2 -$$

$$ce^{i\phi_2}\dot{\phi}_2^2 + de^{i\theta_2}\dot{\theta}_2^{\,2} = 0 \tag{4.9}$$

The solution of intermediate unknowns $\ddot{\phi}_1$ and $\ddot{\phi}_2$ is similar to the velocity method of Section 4.1.1. The Jacobian matrix of Eq. 4.4a is used again.

$$[J]\{\ddot{\phi}_{12}\} = \{C\} \tag{4.10}$$

$$\{\ddot{\phi}_{12}\} = \begin{bmatrix} \ddot{\phi}_1 \\ \ddot{\phi}_2 \end{bmatrix} \tag{4.10a}$$

$$\{C\} = \begin{bmatrix} c_1 \\ c_2 \end{bmatrix} \tag{4.10b}$$

where:

$$c_1 = a\sin\theta_1\ddot{\theta}_1 - d\sin\theta_2\ddot{\theta}_2 + a\cos\theta_1\dot{\theta}_1{}^2 + b\cos\phi_1\dot{\phi}_1^2 + c\cos\phi_2\dot{\phi}_2^2 - d\cos\theta_2\dot{\theta}_2{}^2$$

$$c_2 = -a\cos\theta_1\ddot{\theta}_1 + d\cos\theta_2\ddot{\theta}_2 + a\sin\theta_1\dot{\theta}_1{}^2 + b\sin\phi_1\dot{\phi}_1^2 + c\sin\phi_2\dot{\phi}_2^2 - d\sin\theta_2\dot{\theta}_2{}^2$$

The solution of Eq. 4.10 is given below.

$$\{\ddot{\phi}_{12}\} = [J]^{-1}\{C\} \tag{4.11}$$

The angular acceleration $\ddot{\phi}$ is identical to that of $\ddot{\phi}_2$, from the second time derivative of Eq. 4.2a. The second time derivative of Eq. 4.6 is also required prior to evaluating the linear and angular accelerations of the hand.

$$\ddot{\theta}_H = \ddot{\theta}_3 + \ddot{\phi}_2 \tag{4.12}$$

The linear and angular accelerations of the hand are obtained by a second time derivative of Eq. 4.2.

$$\begin{bmatrix} \ddot{x}_H \\ \ddot{y}_H \\ \ddot{\theta}_H \end{bmatrix} = [D]\begin{bmatrix} \ddot{\theta}_2 \\ \ddot{\theta}_3 \\ \ddot{\phi}_2 \end{bmatrix} - \begin{bmatrix} d\cos\theta_2 & h\cos\theta_H & c\cos\phi \\ d\sin\theta_2 & h\sin\theta_H & c\sin\phi \\ 0 & 0 & 0 \end{bmatrix}\begin{bmatrix} \dot{\theta}_2{}^2 \\ \dot{\theta}_H{}^2 \\ \dot{\phi}_2^2 \end{bmatrix} \tag{4.13}$$

The matrix $[D]$ in Eq. 4.13 is the 3 x 3 matrix from Eq. 4.8.

4.2 *Inverse Solution*

In the inverse derivative problem, the velocity and acceleration of the input actuators are solved for given velocity and acceleration values of the manipulator hand. Derivative analysis is presented for the "N6R6" manipulator, shown in Fig. 2.4. The inverse velocity and acceleration problem for the "N6R6" manipulator is: given $\dot{x}_H$, $\dot{y}_H$, $\dot{\theta}_H$, $\ddot{x}_H$, $\ddot{y}_H$, and $\ddot{\theta}_H$, find $\dot{\theta}_1$, $\dot{\theta}_2$, $\dot{\theta}_3$, $\ddot{\theta}_1$, $\ddot{\theta}_2$, and $\ddot{\theta}_3$.

4.2.1 "N6R6" Inverse Velocity Analysis

The "N6R6" inverse velocity problem is solved in two steps. The first step solves for the unknowns $\dot{\theta}_2$ and $\dot{\phi}_2$ using one time derivative of Eq. 4.2 from the forward velocity analysis section. The second step uses a time derivative of the following equation to solve for $\dot{\theta}_1$ and $\dot{\phi}_1$ after the first step is complete.

$$\underline{G}_1 + ae^{i\theta_1} + be^{i\phi_1} + ce^{i(\phi_2+\frac{\pi}{3})} + he^{i\theta_H} = x_H + iy_H \tag{4.14}$$

The solution process for the first step is analogous to that presented in Section 4.1.2. The results are stated below.

$$[J_1]\{\dot{\gamma}_1\} = \{D\} \tag{4.15}$$

$$[J_1] = \begin{bmatrix} -d\sin\theta_2 & -c\sin\phi \\ d\cos\theta_2 & c\cos\phi \end{bmatrix} \tag{4.15a}$$

$$\{\dot{\gamma}_1\} = \begin{bmatrix} \dot{\theta}_2 \\ \dot{\phi}_2 \end{bmatrix} \tag{4.15b}$$

$$\{D\} = \begin{bmatrix} \dot{x}_H + h \sin\theta_H \dot{\theta}_H \\ \dot{y}_H - h \cos\theta_H \dot{\theta}_H \end{bmatrix} \tag{4.15c}$$

$$\{\dot{y}_1\} = [J_1]^{-1}\{D\} \tag{4.16}$$

$$[J_1]^{-1} = \frac{1}{|J_1|}\begin{bmatrix} c\cos\phi & c\sin\phi \\ -d\cos\theta_2 & -d\sin\theta_2 \end{bmatrix} \tag{4.16a}$$

$$|J_1| = cd(\cos\theta_2 \sin\phi - \cos\phi \sin\theta_2) \tag{4.16b}$$

The second solution step is similar, starting with the time derivative of Eq. 4.14.

$$[J_2]\{\dot{y}_2\} = \{E\} \tag{4.17}$$

$$[J_2] = \begin{bmatrix} -a\sin\theta_1 & -b\sin\phi_1 \\ a\cos\theta_1 & b\cos\phi_1 \end{bmatrix} \tag{4.17a}$$

$$\{\dot{y}_2\} = \begin{bmatrix} \dot{\theta}_1 \\ \dot{\phi}_1 \end{bmatrix} \tag{4.17b}$$

$$\{E\} = \begin{bmatrix} \dot{x}_H + c \sin(\phi_2 + \frac{\pi}{3})\dot{\phi}_2 + h \sin\theta_H \dot{\theta}_H \\ \dot{y}_H - c \cos(\phi_2 + \frac{\pi}{3})\dot{\phi}_2 - h \cos\theta_H \dot{\theta}_H \end{bmatrix} \tag{4.17c}$$

$$\{\dot{y}_2\} = [J_2]^{-1}\{E\} \tag{4.18}$$

$$[J_2]^{-1} = \frac{1}{|J_2|}\begin{bmatrix} b\cos\phi_1 & b\sin\phi_1 \\ -a\cos\theta_1 & -a\sin\theta_1 \end{bmatrix} \tag{4.18a}$$

$$|J_2| = ab(\cos\theta_1 \sin\phi_1 - \cos\phi_1 \sin\theta_1) \tag{4.18b}$$

The remaining unknown $\dot{\theta}_3$ is solved for from Eq. 4.7.

4.2.2 "N6R6" Inverse Acceleration Analysis

The "N6R6" inverse acceleration equations follow from a time derivative of the inverse velocity equations. The Jacobian matrices in this section are given in Eqs. 4.15a and 4.17a. The following equation is the second time derivative of Eq. 4.2.

$$\{\ddot{y}_1\} = [J_1]^{-1}\{F\} \tag{4.19}$$

$$\{\ddot{y}_1\} = \begin{bmatrix} \ddot{\theta}_2 \\ \ddot{\phi}_2 \end{bmatrix} \tag{4.19a}$$

$$\{F\} = \begin{bmatrix} \ddot{x}_H + h\sin\theta_H\ddot{\theta}_H + d\cos\theta_2\dot{\theta}_2{}^2 + c\cos\phi\dot{\phi}_2^2 + h\cos\theta_H\dot{\theta}_H{}^2 \\ \ddot{y}_H - h\cos\theta_H\ddot{\theta}_H + d\sin\theta_2\dot{\theta}_2{}^2 + c\sin\phi\dot{\phi}_2^2 + h\sin\theta_H\dot{\theta}_H{}^2 \end{bmatrix} \tag{4.19b}$$

A second time derivative of Eq. 4.14 produces the results for the second acceleration analysis step.

$$\{\ddot{y}_2\} = [J_2]^{-1}\{G\} \tag{4.20}$$

$$\{\ddot{y}_2\} = \begin{bmatrix} \ddot{\theta}_1 \\ \ddot{\phi}_1 \end{bmatrix} \tag{4.20a}$$

$$\{G\} = \begin{bmatrix} g_1 \\ g_2 \end{bmatrix} \tag{4.20b}$$

where:

$$g_1 = \ddot{x}_H + c\sin(\phi_2 + \tfrac{\pi}{3})\ddot{\phi}_2 + h\sin\theta_H\ddot{\theta}_H + a\cos\theta_1\dot{\theta}_1{}^2 + b\cos\phi_1\dot{\phi}_1^2 + c\cos(\phi_2 + \tfrac{\pi}{3})\dot{\phi}_2^2 + h\cos\theta_H\dot{\theta}_H{}^2 \tag{4.20c}$$

$$g_2 = \ddot{y}_H - c\cos(\phi_2 + \frac{\pi}{3})\ddot{\phi}_2 - h\cos\theta_H\ddot{\theta}_H + a\sin\theta_1\dot{\theta}_1{}^2 + b\sin\phi_1\dot{\phi}_1^2 +$$

$$c\sin(\phi_2 + \frac{\pi}{3})\dot{\phi}_2^2 + h\sin\theta_H\dot{\theta}_H{}^2 \qquad (4.20d)$$

The third actuator acceleration $\ddot{\theta}_3$ is obtained from Eq. 4.12.

4.3 "N6R6" Center of Mass Accelerations

The link center-of-mass accelerations are required in kinetostatic analysis, presented in Chapter 5; these may be determined after the manipulator acceleration analysis is complete. The formulas given below result from two successive time derivatives of the mass center vector position equations. The links are assumed to be homogeneous and symmetric; therefore, the mass centers are located at the link centroids. The vector accelerations are resolved into x and y components for computational purposes.

$$a_{g2x} = -\frac{a}{2}(\sin\theta_1\ddot{\theta}_1 + \cos\theta_1\dot{\theta}_1{}^2) \qquad (4.21a)$$

$$a_{g2y} = \frac{a}{2}(\cos\theta_1\ddot{\theta}_1 - \sin\theta_1\dot{\theta}_1{}^2) \qquad (4.21b)$$

$$a_{g3x} = -a(\sin\theta_1\ddot{\theta}_1 + \cos\theta_1\dot{\theta}_1{}^2) - \frac{b}{2}(\sin\phi_1\ddot{\phi}_1 + \cos\phi_1\dot{\phi}_1^2) \qquad (4.21c)$$

$$a_{g3y} = a(\cos\theta_1\ddot{\theta}_1 - \sin\theta_1\dot{\theta}_1{}^2) + \frac{b}{2}(\cos\phi_1\ddot{\phi}_1 - \sin\phi_1\dot{\phi}_1^2) \qquad (4.21d)$$

$$a_{g4x} = -a(\sin\theta_1\ddot{\theta}_1 + \cos\theta_1\dot{\theta}_1{}^2) - b(\sin\phi_1\ddot{\phi}_1 + \cos\phi_1\dot{\phi}_1^2) -$$

$$\frac{\sqrt{3}}{3}c(\sin\frac{\pi}{6}\ddot{\phi}_2 + \cos\frac{\pi}{6}\dot{\phi}_2^2) \qquad (4.21e)$$

$$a_{g4y} = a(\cos\theta_1\ddot{\theta}_1 - \sin\theta_1\dot{\theta}_1^{\,2}) + b(\cos\phi_1\ddot{\phi}_1 - \sin\phi_1\dot{\phi}_1^2) + \frac{\sqrt{3}}{3}c\,(\cos\frac{\pi}{6}\ddot{\phi}_2 - \sin\frac{\pi}{6}\dot{\phi}_2^2) \qquad (4.21f)$$

$$a_{g5x} = -\frac{d}{2}(\sin\theta_2\ddot{\theta}_2 + \cos\theta_2\dot{\theta}_2^{\,2}) \qquad (4.21g)$$

$$a_{g5y} = \frac{d}{2}(\cos\theta_2\ddot{\theta}_2 - \sin\theta_2\dot{\theta}_2^{\,2}) \qquad (4.21h)$$

$$a_{g6x} = -d(\sin\theta_2\ddot{\theta}_2 + \cos\theta_2\dot{\theta}_2^{\,2}) - c(\sin\phi\ddot{\phi}_2 + \cos\phi\dot{\phi}_2^2) - \frac{h}{2}(\sin\theta_H\ddot{\theta}_H + \cos\theta_H\dot{\theta}_H^{\,2}) \qquad (4.21i)$$

$$a_{g6y} = d(\cos\theta_2\ddot{\theta}_2 - \sin\theta_2\dot{\theta}_2^{\,2}) + c(\cos\phi\ddot{\phi}_2 - \sin\phi\dot{\phi}_2^2) + \frac{h}{2}(\cos\theta_H\ddot{\theta}_H - \sin\theta_H\dot{\theta}_H^{\,2}) \qquad (4.21j)$$

4.4 Remaining Manipulators

Derivative analysis for the "N6R6" manipulator is representative for planar robotic mechanisms in general. The procedure generally starts with multiple vector loop closure position equations and proceeds with successive time derivatives. Solved values may be required in ensuing steps. This section briefly discusses the derivative problems for the remaining manipulators of Figs. 2.1 - 2.9.

The derivative problem for the "N4R3" serial manipulator is relatively simple because there are no intermediate angles in the serial chain. The "N5R5" manipulator is similar to the "N6R6"; only one loop is required because the "N5R5" does not have the additional link ex-

tending from the coupler triangle. The "N7R8" and "N8R9-2" manipulators are similar to the "N5R5" manipulator; extra loop equations are required due to the extra legs built onto the basic five-bar chain. The forward problem for the "N8R9-1" manipulator starts with the position equations in Appendix A, Eqs. A.1a and A.1b to solve for the intermediate unknowns simultaneously. The inverse problem for this manipulator is to solve for the unknowns of the three legs independently. The "N10R12" manipulator is identical to the "N8R9-1" in terms of the derivative problem. Manipulators with prismatic joints (such as the "N8R7P2-3" and "N8R6P3-4") follow the same basic procedures discussed for the revolute joint manipulators. The equations are more involved due to the Coriolis component of acceleration.

Chapter 5 Kinetostatic Analysis

Along with the preceding kinematic analyses, dynamic analysis is required for complete robot design and control. Kinetostatics solves for the internal joint forces and input driving torques given the manipulator position, velocity, and acceleration, plus the external loading. This chapter presents a general kinetostatic analysis method for planar robotic mechanisms.

Authors in the area of closed-loop robotic manipulators list dynamic characteristics among the advantages of the parallel manipulator configuration over serial manipulators. The basis for this is that parallel manipulators may be designed with all driving motors attached to the ground link, thus reducing dynamic inertia. The claim of superior dynamic performance of parallel manipulators has not been substantiated quantitatively. This chapter uses the theory developed to quantitatively study the aforementioned dynamic claim for various manipulator topologies. Power requirement comparisons are made between three different planar manipulators. These manipulators are the serial "N4R3", parallel-serial "N6R6", and fully parallel "N8R9-1", pictured in Figs. 2.1, 2.4, and 2.5, respectively.

FORTRAN computer routines have been developed in order to facilitate power comparisons. For a given manipulator input, the routine performs the following steps: inverse kinematic position analysis, inverse velocity and acceleration analysis, and kinetostatic analysis. In general, there are multiple solutions for the inverse kinematic position solution of a

robotic mechanism. Corresponding to each solution, there is a unique derivative and dynamic solution.

5.1 *Kinetostatic Calculations*

In this section, kinetostatic analysis is presented for planar robotic mechanisms. In the kinetostatic problem, the manipulator motion (position, velocity, and acceleration) is given, along with the external forces and torques. The associated internal forces and driving torques are calculated. Kinetostatic analysis is the opposite of true dynamics analysis where the input torques are specified while the manipulator velocities and accelerations are calculated. Kinetostatic analysis does not involve time explicitly. The theory developed in this section is applicable to any planar mechanism or planar robotic mechanism.

5.1.1 Kinetostatics Matrix Method

A matrix method is applied in the kinetostatic solution. The solution of a linear system of equations yields the desired torques and forces. This method was adapted from the presentation in Mabie and Reinholtz (1987).

A free-body diagram which identifies all internal and external forces and moments is drawn for each moving link. Figure 5.1a shows a general free-body diagram for an arbitrary two-joint link i with the associated force conventions defined. The unknown internal joint force f_{i-1} is taken to be negative, while the unknown force f_i is defined as positive. These forces are denoted by curved lines in Fig. 5.1a because their directions are unknown. For link i, Newton's second law is applied for both forces and moments.

$$f_i - f_{i-1} = m_i \underline{a}_{gi} - \underline{EE}_i \qquad (5.1a)$$

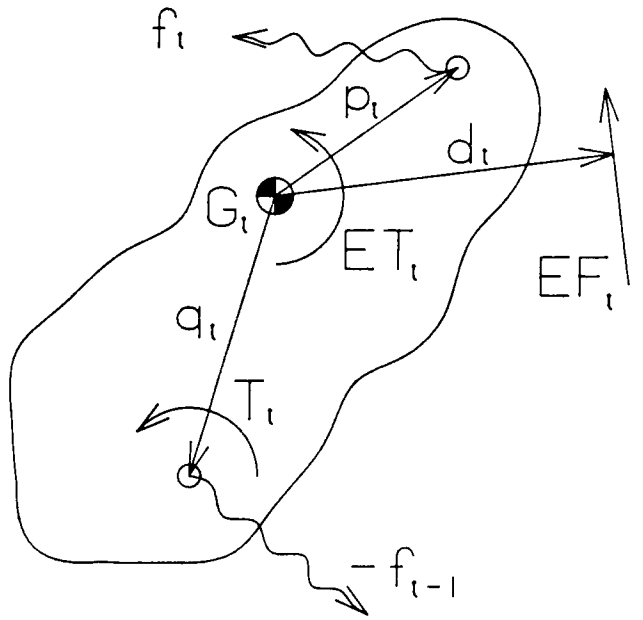

5.1a
General

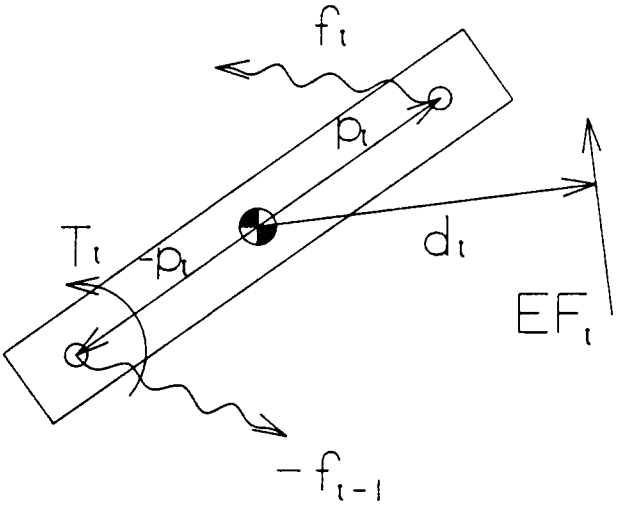

5.1b
Simplified

Figure 5.1
Dynamic Free-Body-Diagrams
for Two-Jointed Links

$$\underline{p}_i \times \underline{f}_i - \underline{q}_i \times \underline{f}_{i-1} + \underline{I}_i = I_i \underline{\alpha}_i - \underline{EI}_i - \underline{d}_i \times \underline{EF}_i \qquad (5.1b)$$

The external force resultant for link i is represented by $\underline{EF}_i$ and $\underline{EI}_i$ is the resultant of external moments. The vector $\underline{a}_{gi}$ is the linear acceleration of the center of gravity of link i, while $\underline{\alpha}_i$ is the angular acceleration of link i. The term $\underline{I}_i$ denotes the unknown driving torque which appears only on directly actuated links.

The force summation vector equation yields two scalar equations, one each for the x and y directions in the plane. The moment summation vector equation gives one scalar equation because moment vectors are perpendicular to the manipulator plane. Therefore, for each moving link, three linear scalar equations result. There are 3(n-1) equations for kinetostatic modeling, where n is the number of manipulator links, including ground. The unknowns are f_k and $\underline{I}_j$, where k goes from 1 to the number of internal forces and j goes from 1 to the number of freedoms of the manipulator. As in the discussion above, each unknown vector force represents two scalar unknowns, while each unknown vector driving torque is one scalar unknown. The condition $2k + j = 3(n - 1)$ must be satisfied to ensure the existence of a unique solution to the kinetostatics problem.

The following simplifying assumptions are made in the kinetostatic solutions of this chapter. No external torques are considered. The only external force allowed is a single planar force at the manipulator hand. Therefore, $\underline{EI}_i$ is always zero, and $\underline{EF}_i$ is zero when i is not the hand link.

Each two-joint link is assumed to be a uniform, symmetrical body with mass center midway between the two joints. This condition leads to

$$\underline{q}_i = -\underline{p}_i \qquad (5.2)$$

With these simplifications, the free-body diagram of link i reduces to that shown in Fig. 5.1b. The three scalar equations for any two-jointed link are given below.

$$f_{ix} - f_{(i-1)x} = m_i a_{gix} - EF_x \qquad (5.3a)$$

$$f_{iy} - f_{(i-1)y} = m_i a_{giy} - EF_Y \tag{5.3b}$$

$$p_{ix} f_{iy} - p_{iy} f_{ix} + p_{ix} f_{(i-1)y} - p_{iy} f_{(i-1)x} + T_i = I_i \alpha_i - d_X EF_Y + d_Y EF_X \tag{5.3c}$$

If i is not the hand link, the EF_x and EF_y terms are zero. For links which have more than two joint connections, additional terms arise in Eqs. 5.3. Figure 5.2 shows the equilateral ternary link from the "N6R6" manipulator. The force f_3 is taken to be negative, while the forces f_4 and f_6 are defined to be positive. The summation of forces and moments yields the following vector equations.

$$f_4 + f_6 - f_3 = m_4 \underline{a}_{g4} \tag{5.4a}$$

$$\underline{p}_4 \times f_4 + \underline{r}_4 \times f_6 - \underline{q}_4 \times f_3 = I_4 \ddot{\phi}_2 \tag{5.4b}$$

The angles of Fig. 5.2 and the associated position vectors of Eqs. 5.4 are as follows.

$$\beta_1 = \phi_2 + \frac{\pi}{6} \qquad \beta_2 = \phi_2 - \frac{\pi}{6} \qquad \beta_3 = \phi_2 + \frac{\pi}{2} \tag{5.5a}$$

$$q_{4X} = -LH \cos \beta_1 \qquad q_{4Y} = -LH \sin \beta_1 \tag{5.5b}$$

$$p_{4X} = LH \cos \beta_2 \qquad p_{4Y} = LH \sin \beta_2 \tag{5.5c}$$

$$r_{4X} = LH \cos \beta_3 \qquad r_{4Y} = LH \sin \beta_3 \tag{5.5d}$$

After writing the three equations for each moving manipulator link, the solution of the kinetostatic problem is obtained by solving the resulting linear system of order 3(n-1).

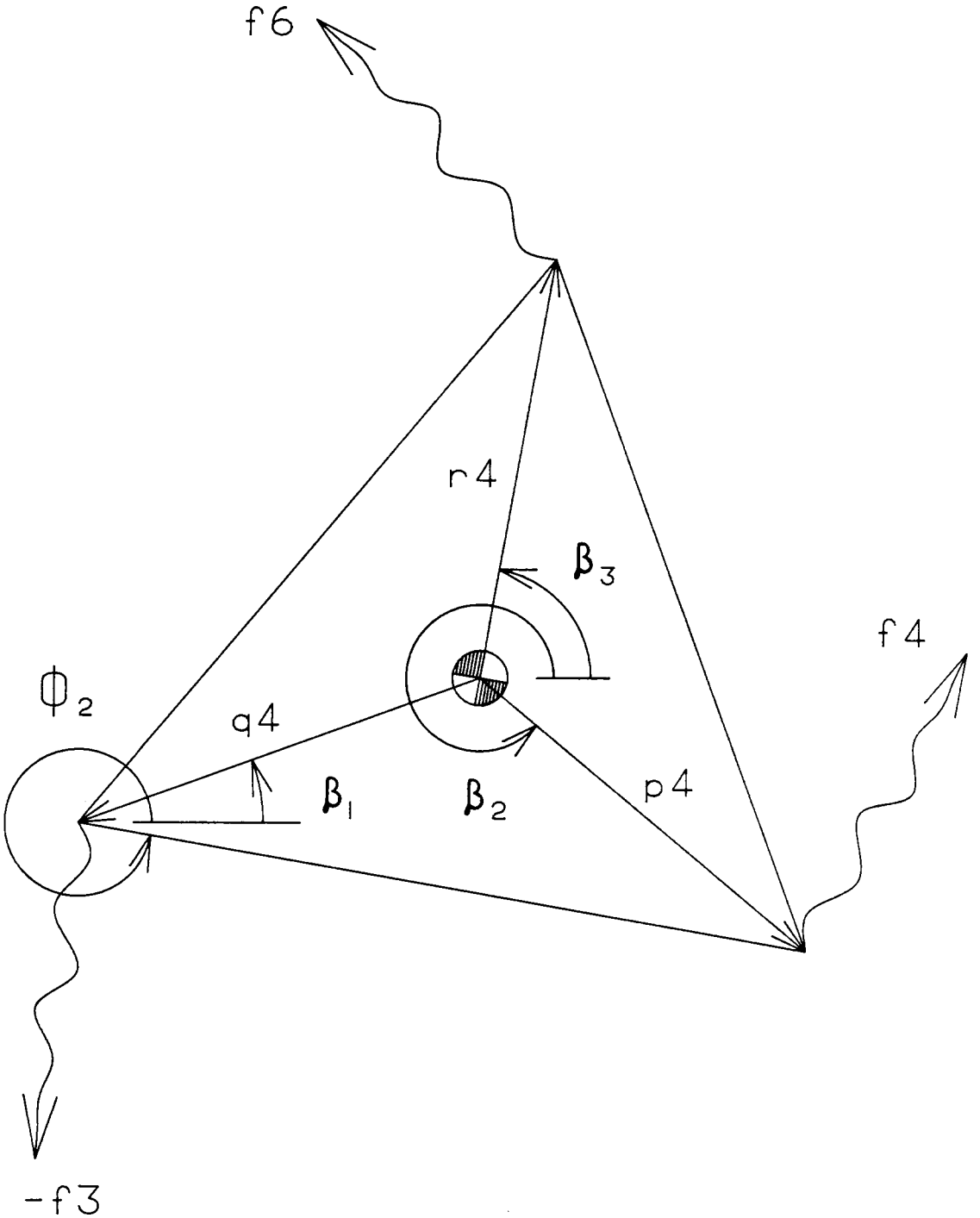

Figure 5.2
Dynamic Free-Body-Diagram
for Three-Jointed Links

5.1.2 "N6R6" Kinetostatics

The link free-body diagrams for the "N6R6" manipulator are shown in Fig. 5.3. There are five moving links and thus fifteen scalar dynamic equations. The fifteen unknowns are six internal forces and three driving torques.

The sixth link is in a serial configuration, extending from the parallel configuration of the remainder of the manipulator. Therefore, the last three equations are solved directly. The resulting coupled linear system of order twelve is given in Eq. 5.7.

$$f_{6X} = EF_X - m_6 a_{g6x} \tag{5.6a}$$

$$f_{6Y} = EF_Y - m_6 a_{g6y} \tag{5.6b}$$

$$T_3 = I_6 \ddot{\theta}_H + p_{6Y}(f_{6X} + EF_X) - p_{6X}(f_{6Y} + EF_Y) \tag{5.6c}$$

$$\begin{bmatrix}
-1 & 0 & 1 & 0 & & & & & & & & \\
0 & -1 & 0 & 1 & & & & & & & & \\
-p_{2Y} & p_{2X} & -p_{2Y} & p_{2X} & 1 & & & & & & & \\
0 & 0 & -1 & 0 & 0 & 1 & & & & & & \\
 & & 0 & -1 & 0 & 0 & 1 & & & & & \\
 & & -p_{3Y} & p_{3X} & 0 & -p_{3Y} & p_{3X} & & & & & \\
 & & & & & -1 & 0 & 1 & & & & \\
 & & & & & 0 & -1 & 0 & 1 & & & \\
 & & & & & q_{4Y} & -q_{4X} & -p_{4Y} & p_{4X} & & & \\
 & & & & & & & -1 & 0 & 1 & & \\
 & & & & & & & 0 & -1 & 0 & 1 & \\
 & & & & & & & -p_{5Y} & p_{5X} & -p_{5Y} & p_{5X} & 1
\end{bmatrix}
\begin{bmatrix} f_{1X} \\ f_{1Y} \\ f_{2X} \\ f_{2Y} \\ T_1 \\ f_{3X} \\ f_{3Y} \\ f_{4X} \\ f_{4Y} \\ f_{5X} \\ f_{5Y} \\ T_2 \end{bmatrix}
=
\begin{bmatrix} A_2 \\ B_2 \\ C_2 \\ A_3 \\ \beta_3 \\ C_3 \\ A_4 \\ B_4 \\ C_4 \\ A_5 \\ B_5 \\ C_5 \end{bmatrix} \tag{5.7}$$

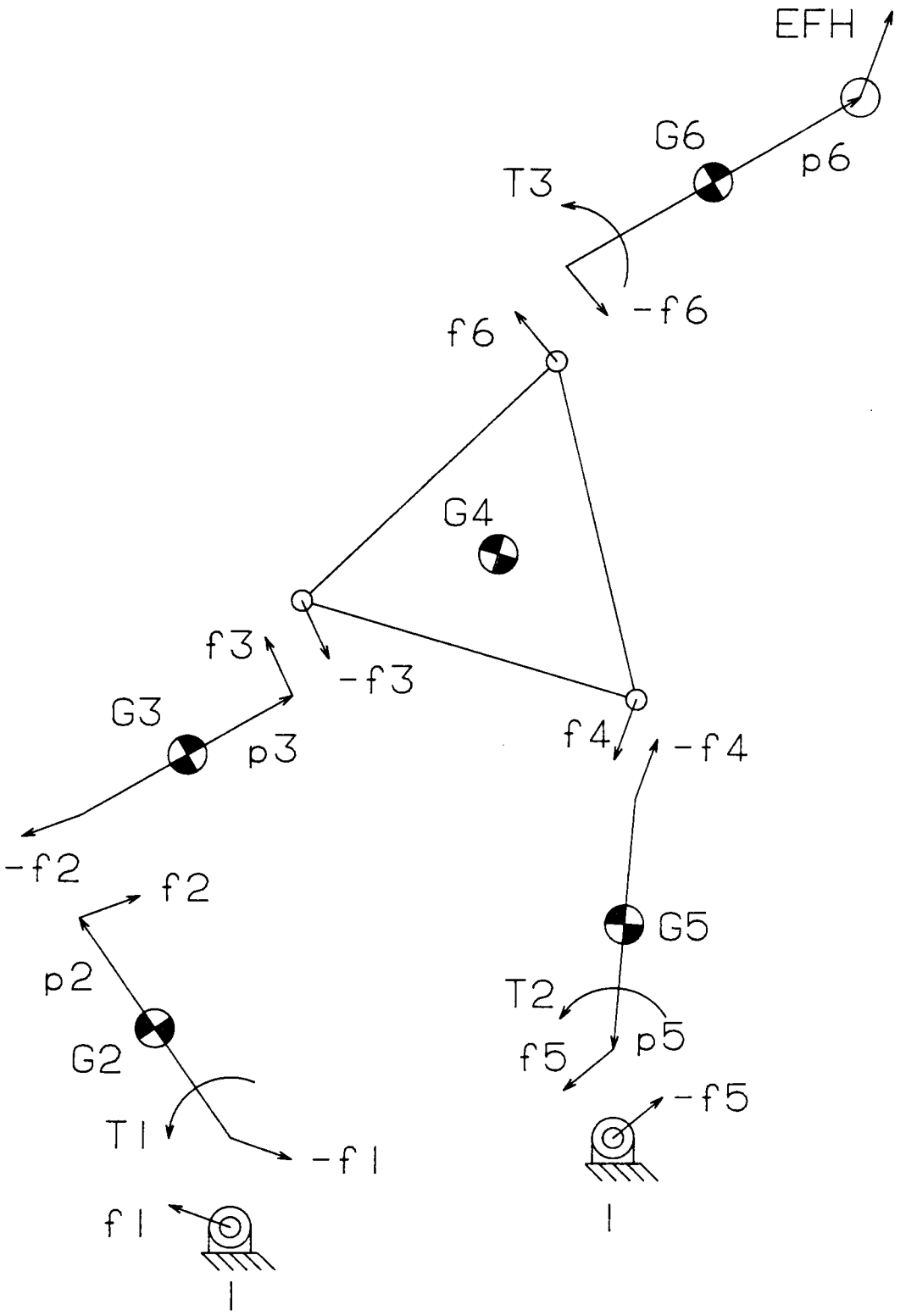

Figure 5.3
Dynamic Free-Body-Diagrams
for "N6R6" Manipulator

The link midpoint position vectors are defined as follows.

$$p_{2X} = \frac{a}{2}\cos\theta_1 \qquad p_{2Y} = \frac{a}{2}\sin\theta_1 \tag{5.7a}$$

$$p_{3X} = \frac{b}{2}\cos\phi_1 \qquad p_{3Y} = \frac{b}{2}\sin\phi_1 \tag{5.7b}$$

$$p_{5X} = \frac{-d}{2}\cos\theta_2 \qquad p_{5Y} = \frac{-d}{2}\sin\theta_2 \tag{5.7c}$$

$$p_{6X} = \frac{h}{2}\cos\theta_H \qquad p_{6Y} = \frac{h}{2}\sin\theta_H \tag{5.7d}$$

The terms of the right-hand side of Eq. 5.7 are given below.

$$A_i = m_i a_{gix} \qquad i = 2,3,4,5 \tag{5.7e}$$

$$B_i = m_i a_{giy} \qquad i = 2,3,4,5 \tag{5.7f}$$

$$C_i = I_i \ddot{\alpha}_i \qquad i = 2,3,5 \tag{5.7g}$$

$$C_4 = I_4 \ddot{\phi}_2 - r_{4Y} f_{6X} - r_{4X} f_{6Y} \tag{5.7h}$$

5.1.3 "N4R3" and "N8R9-1" Kinetostatics

The "N4R3" manipulator has three moving links and therefore nine scalar dynamic equations. There are three unknown internal vector forces and three unknown driving torques for a total of nine unknowns. Due to the serial nature of the "N4R3" manipulator, the dynamics equations are solved algebraically, avoiding the need for a linear equation solver. The "N8R9-1" manipulator's seven moving links and thus twenty-one dynamic equations are used to solve for the twenty-one unknowns: nine internal vector forces and three driving torques.

The "N8R9-1" configuration is fully parallel. Therefore, the resulting linear system of order twenty-one is irreducible in the general case.

5.1.4 Power Requirement

The power requirement for a manipulator is calculated from the summation of the products of driving torque and angular velocity. For the manipulators in this chapter, the following equation is used to calculate the required power.

$$P = |T_1\dot{\theta}_1| + |T_2\dot{\theta}_2| + |T_3\dot{\theta}_3| \tag{5.8}$$

The absolute value signs are necessary because the angular velocities may be driven in opposite directions. In Eq. 5.8, the relative angular velocities must be used. For example, the "N6R6" manipulator has a moving motor that drives the serial link. The relative angular velocity of this link, $\dot{\theta}_3$, is given in Eq. 4.7. Relative angular velocities must be used for the "N4R3" manipulator. For the "N8R9-1" manipulator, all motors are attached to ground, and thus the absolute and relative input angular velocities are the same.

5.2 *Power Requirement Comparisons*

A FORTRAN computer program was written for each manipulator configuration to facilitate the large calculation effort required for kinetostatic analysis. The inverse kinematics routine solves for the multiple manipulator input parameters given the hand position and orientation. The inverse velocity and acceleration routine determines the necessary link angular velocities and accelerations to provide the specified hand motion. A kinetostatic routine incorporating the matrix method discussed earlier then solves for the unknown driving torques

and joint forces. Following this, Eq. 5.8 is used to calculate power requirement. The inverse kinematics calculations are performed once; after this, the inverse velocity and acceleration, followed by the dynamics routine are called for each unique assembly of the manipulator.

For each specified manipulator position and orientation, m power requirements are calculated, where m is the number of inverse kinematic position solutions. The value of m is two, four, and eight for the "N4R3", "N6R6", and "N8R9-1" manipulators, respectively. Power information is desired for points covering the entire workspace, for all hand orientation angles. Therefore, due to the large number of power requirement combinations, only the minimum/maximum behavior is studied. Only the minimum and maximum power requirements are stored for each position and orientation of the hand. For the "N4R3" manipulator, both values are used. However, for the "N8R9-1" manipulator, only the extrema of the eight possibilities are returned. For each workspace position, hand orientation angles vary from 0 to 2π radians; the minimum power requirement for all assemblies and orientation angles is stored. Likewise, the maximum is stored, which bounds the power requirements over the workspace.

The manipulators compared are designed to have approximately the same reachable and dextrous workspaces as shown in Fig. 5.4, where the dimensions are centimeters. Reachable and dextrous workspaces are discussed in Section 6.2. The reachable workspace boundary is solid in Figs. 5.4a, 5.4b, and 5.4c, and the dextrous workspace boundary is dashed. The reachable workspaces of these three manipulators are identical, a solid circular disk of radius 93 cm. The dextrous workspaces of the "N4R3" and "N6R6" manipulators are identical solid circles with a radius of 67 cm. The dextrous workspace of the "N8R9-1" manipulator is non-circular, but of similar size. The same velocity, acceleration, and manipulator hand force are specified for each manipulator for all positions considered. The dynamics routine calculates the maximum and minimum power required to drive the manipulator given the input values.

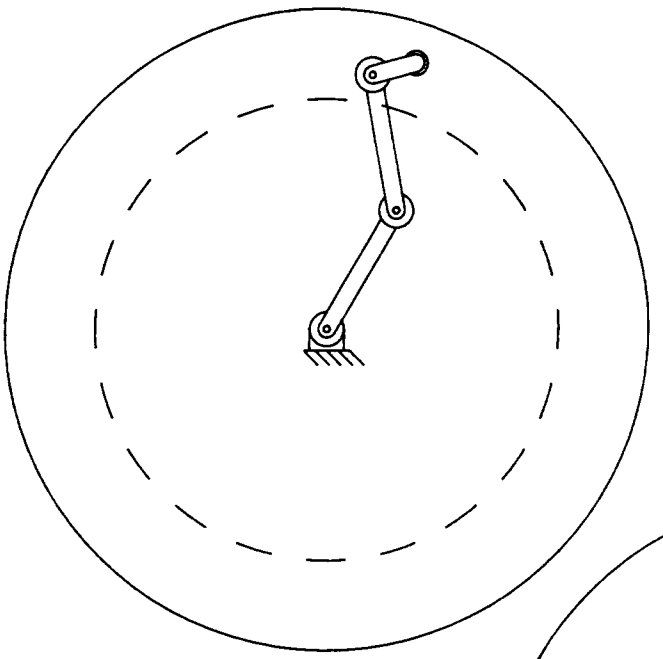

5.4a "N4R3"
R2=R3=40.0; R4=13.0

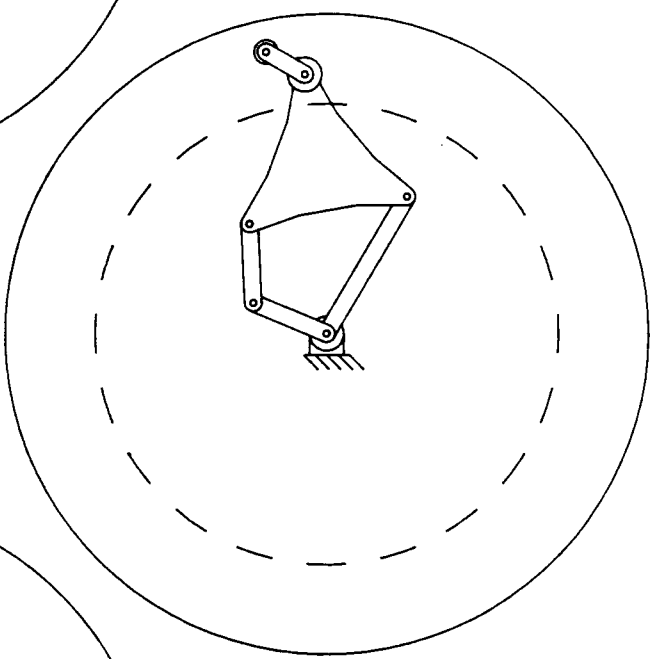

5.4b "N6R6"
a=b=23.1; c=d=46.2
h=13.0

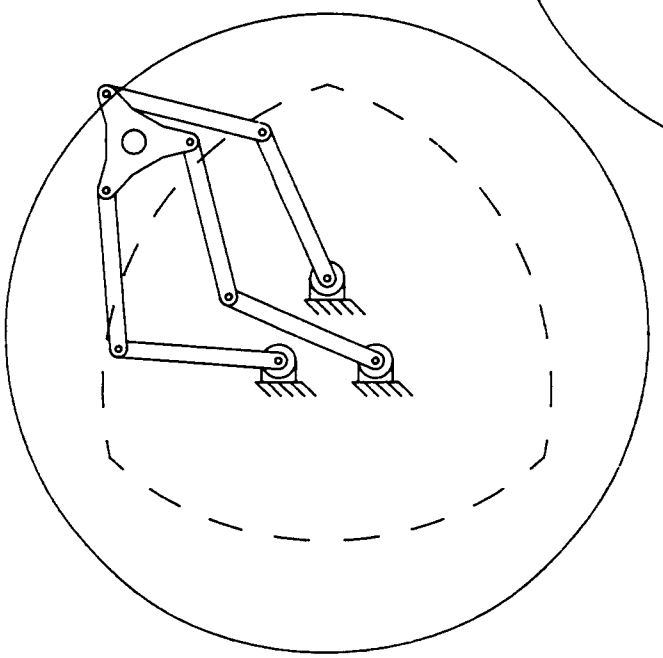

5.4c "N8R9-1"
a=b=f=d=p=k=46.5
c=L=28.0

Figure 5.4
Dynamic Comparison Manipulators

5.2.1 Physical Manipulator Parameters

The link masses and inertias are determined with the following assumptions, for comparison purposes only. The material is steel, with a mass density of 7834 $\frac{kg}{m^3}$. The binary links have a square cross-section with a 5 cm side. The ternary links are equilateral triangles with a thickness of 0.50 cm. The mass moment of inertia about the center of gravity of a homogeneous equilateral triangle with side L and mass m is derived to be

$$I_{zz} = \frac{75}{324} mL^2 \tag{5.9}$$

The motors have a mass of 9.0 kg and a radius of 8 cm. The hand fixture mass is 4.5 kg with a radius of 5 cm. The above assumptions, plus the given link sizes, yield the following mass and inertia values. The units for mass are *kg*, and the units for mass moment of inertia are kgm^2.

"N4R3" Manipulator

$m_2 = m_3 = 16.83; \quad m_4 = 7.05$

$I_2 = I_3 = 0.50; \quad I_4 = 0.03$

"N6R6" Manipulator

$m_2 = m_3 = 4.52; \quad m_4 = 12.62; \quad m_5 = 9.05; \quad m_6 = 7.05$

$I_2 = I_3 = 0.02; \quad I_4 = 0.85; \quad I_5 = 0.16; \quad I_6 = 0.03$

"N8R9-1" Manipulator

$m_i = 9.11 \quad i = 2,....,8; \; i \neq 4; \quad m_4 = 5.83$

$I_i = 0.17 \quad i = 2,....,8; \; i \neq 4; \quad I_4 = 0.03$

5.2.2 Manipulator Loading Conditions

To include variation in the dynamic comparison, two different loading conditions are used: light and heavy. A loading condition includes the linear and angular velocity and acceleration of the hand, plus force applied at the hand. The values are such that neither acceleration nor the external force dominates the results. The heavy loading condition given below includes non-zero accelerations, but with constant velocity values. The discrete locations considered thus do not take motion from one point to the next into consideration. The units for linear and angular velocities and accelerations are $\frac{m}{s}$, $\frac{\text{rad}}{s}$, $\frac{m}{s^2}$ and $\frac{\text{rad}}{s^2}$. The force units are *N*.

Light

$\dot{x}_H = \dot{y}_H = 0.10; \quad \dot{\theta}_H = 0.06$

$\ddot{x}_H = \ddot{y}_H = 0.01; \quad \ddot{\theta}_H = 0.00$

$F_H = (-14.14, -14.14)$

Heavy

$\dot{x}_H = \dot{y}_H = 0.20; \quad \dot{\theta}_H = 0.12$

$\ddot{x}_H = \ddot{y}_H = 0.04; \quad \ddot{\theta}_H = 0.06$

$F_H = (-56.57, -56.57)$

5.2.3 Results of Power Comparisons

The results for the computer kinetostatic comparisons are given in combinations of MAXIMUM/MINIMUM power and HEAVY/LIGHT loading conditions. The results are graphically presented in Figs. 5.5 and 5.6. Only the MINIMUM-LIGHT and MAXIMUM-HEAVY results are included, which bounds the power requirements for each manipulator. Figure 5.5 shows

the MINIMUM-LIGHT contour plots results. The MAXIMUM-HEAVY results of Fig. 5.6 are three-dimensional surfaces.

The area covered in Figs. 5.5 and 5.6 is a square of side 1.30 m. This square approximately covers the dextrous workspace of each manipulator, and is approximately inscribed in the reachable workspace circle of each manipulator (see Figs. 5.4a, 5.4b, and 5.4c). The unit of power is Watts.

The computer dynamics results for the MAXIMUM-HEAVY case of all three manipulators include locations with very large power requirements, in excess of 1×10^9 Watts. These locations represent singularities where at least one pair of links nearly lines up. This condition leads to high angular velocities and accelerations, and thus high torques and power requirement. In order to provide graphs that are readable for the entire area in question, the MAXIMUM-HEAVY results for each manipulator are filtered. The maximum power value allowed on Figs. 5.6a, 5.6b, and 5.6c is 500 Watts. No filtering is necessary for the MINIMUM-LIGHT cases.

For the MINIMUM-LIGHT condition reported in Figs. 5.5a, 5.5b, and 5.5c the three manipulators behave similarly. The overall power range is narrow: 0.1 - 4.8 Watts. The "N6R6" manipulator requires the least power over the entire range, followed by the"N8R9-1" and "N4R3" manipulators.

The MAXIMUM-HEAVY case is more significant for manipulator design. The performance of the "N6R6" and "N4R3" manipulators is similar: The large power values are in the center of the area, and most of the power values are below 100 Watts. The "N6R6" manipulator has a slightly smaller power requirement than the "N4R3" manipulator. The "N8R9-1" manipulator power requirement is much greater. From Fig. 5.6c, most of the power values are at the filter value of 500 Watts.Except for points near dynamic singularities, most "N8R9-1" power requirement values are between 500 and 600 Watts.

In conclusion, the fully parallel "N8R9-1" manipulator has an overall power requirement roughly five times higher than the parallel-serial "N6R6" and serial "N4R3" manipulators. For the "N8R9-1" manipulator, the dynamic inertia is lower because the three motors are stationary. However, this effect is offset because the fully parallel manipulator link lengths are

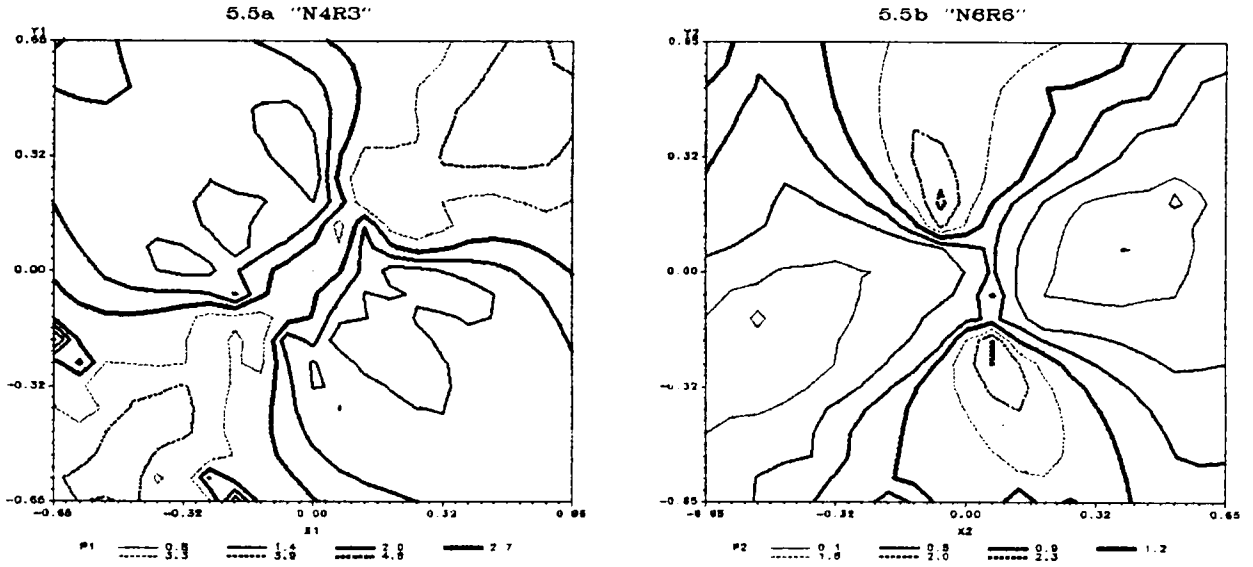

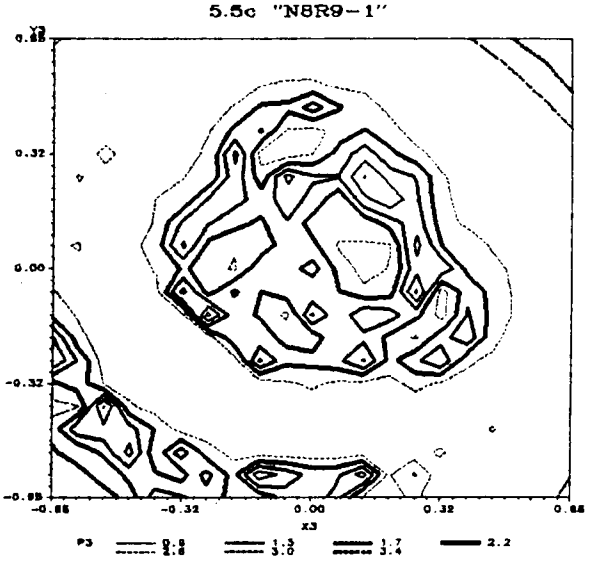

Figure 5.5
MINIMUM/LIGHT Dynamics Results

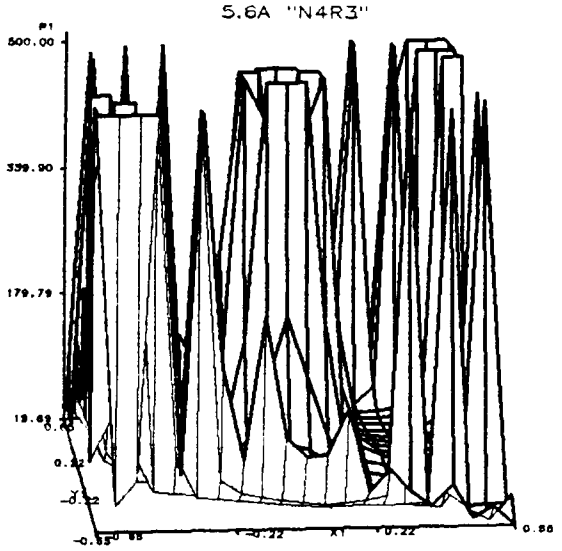

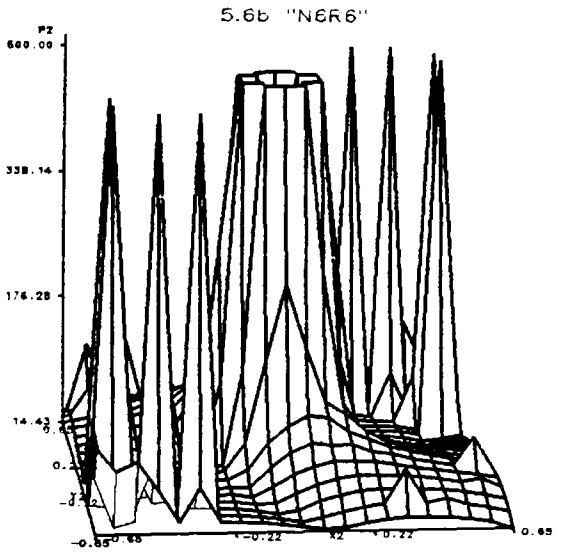

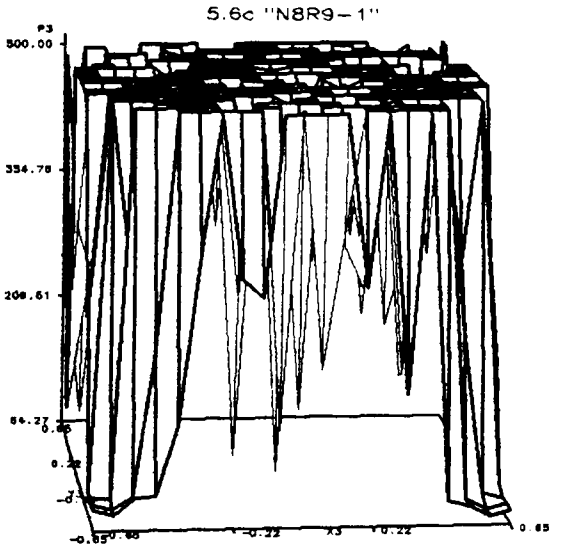

Figure 5.6
MAXIMUM/HEAVY Dynamics Results

large relative to the other two types, in order to reach the same planar area. In addition, the "N8R9-1" manipulator may be assembled in more positions than the other manipulators, which leads to more kinematic positions near dynamic singularities.

The "N6R6" parallel-serial manipulator configuration requires the least power input and the "N4R3" serial manipulator is not significantly higher. The parallel-serial manipulator has two fixed and one moving motor. From workspace analysis of parallel robotic mechanisms (Chapter 6) the parallel-serial configuration is far superior to the fully parallel manipulator in terms of maximum workspace area. This means that relatively shorter links are required to reach the same area as the fully parallel case. The serial manipulator has the best workspace performance; however, the two moving motors may offset this advantage.

This chapter has shown that parallel robotic mechanisms may require significantly higher power when they are designed to provide the same workspace as serial robots. However, this does not mean that parallel robots are undesireable for dynamic reasons. On the contrary, parallel manipulators have high stiffness and load bearing characteristics which make them excellent alternatives to serial robots for applications where a large workspace is not required.

Chapter 6 Workspace Optimization

One drawback of parallel robotic mechanisms is reduced workspace compared to serial robots of similar dimensions. In order to become competitive, the workspace of parallel manipulators must be maximized. This chapter is concerned with efficient workspace determination and optimization of robotic mechanisms.

The reachable workspace of a manipulator is defined as the volume in space whose boundary is the limit of the manipulator hand reach, regardless of the hand orientation. If a point is reachable with only one specific hand orientation, it is within the reachable workspace. The dextrous workspace is the maximum volume attainable by the manipulator hand in all possible hand orientations and thus is generally a subset of the reachable workspace. For planar manipulators, the above definitions apply when "volume" is replaced by "area".

The theory of this chapter may be used to find workspace area and shape for a planar robotic mechanism, given the link lengths, size of ternary links, and location of fixed pivots. The following are possible definitions of "optimum" workspace: total workspace area; general shape of workspace; maximum hand reach; continuity of workspace; and location of fixed pivots. In this chapter the optimization objective is maximum workspace area.

Section 6.1 presents a numerical technique for workspace determination, applied to the reachable workspace of the six manipulators from Chapter 2 with no prismatic joints,

shown in Figs. 2.2 - 2.6 and 2.9. Optimization using the numerical technique is not mathematically rigorous, because it relies on user interaction.

Section 6.2 presents closed-form methods for determination and optimization of reachable and dextrous workspaces. The manipulators studied in the second part of this chapter are the "N5R5", "N6R6", and "N8R9-1" robotic mechanisms. These manipulators have the largest reachable workspace areas from the numerical optimization method.

The current chapter presents kinematic optimization. To be complete it must be extended to include deflection constraints, dynamic characteristics, link interference problems, and other practical considerations.

6.1 *Numerical Workspace Optimization*

This section presents a numerical method for reachable workspace determination of planar robotic mechanisms. Optimization is achieved by using this algorithm repeatedly and viewing the results from perturbations in the input parameters. This process is aided by graPHIGS computer representation of the results.

6.1.1 General Numerical Workspace Determination

The numerical method for workspace determination is based on the closed-form inverse kinematic solution (Section 3.2). The method is attractive because each different robotic mechanism is dealt with by substituting the appropriate inverse kinematics assembly subroutine. The numerical method involves moving the position of the hand, plus orientation for three degree-of-freedom manipulators, and determining where the manipulator assembles, using the inverse kinematic solution.

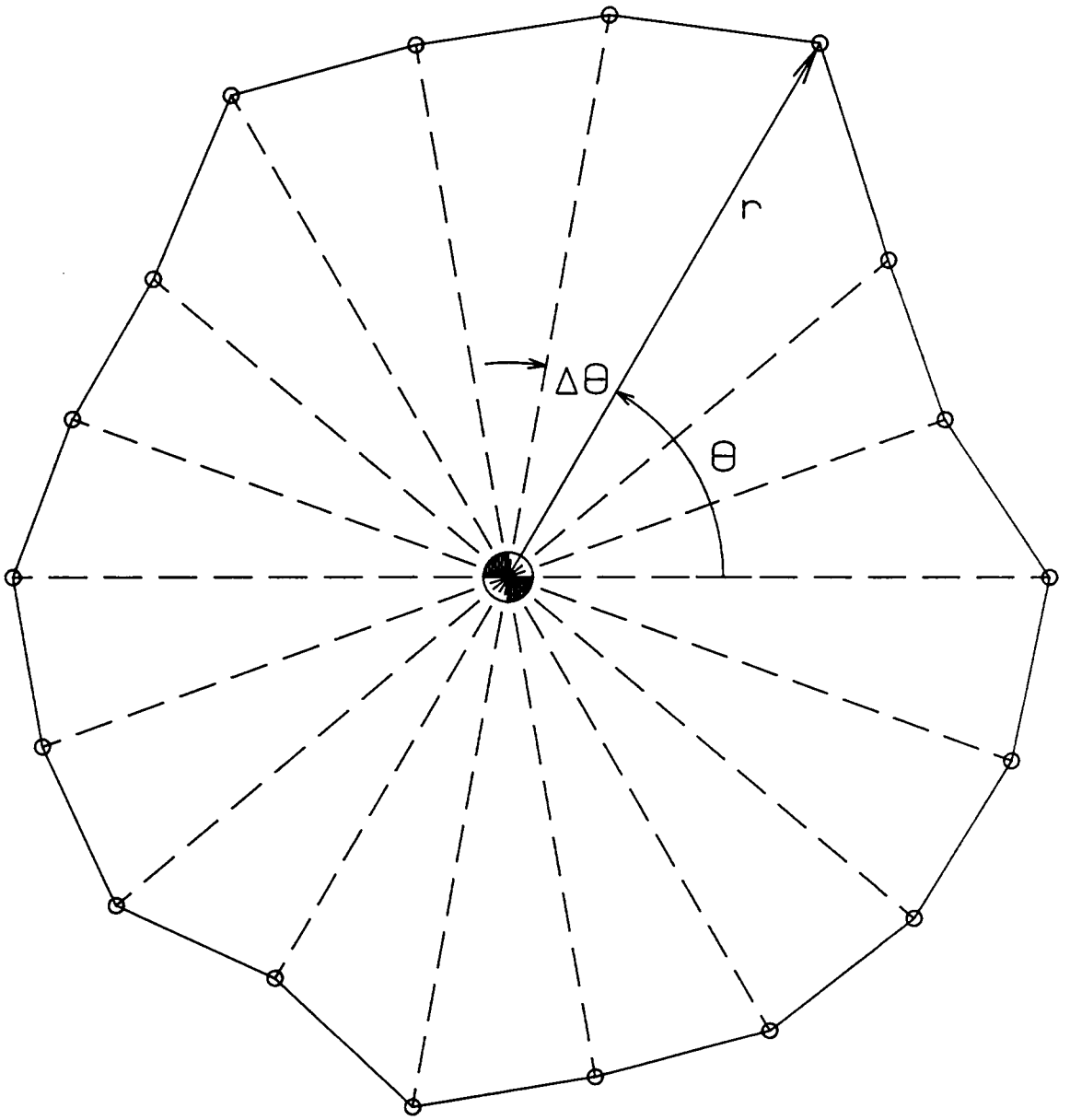

Figure 6.1
Numerical Workspace Determination

Figure 6.1 shows a graphical application of the above description. Workspace determination is based from the centroid of the fixed pivots. At $\theta = 0$, the maximum reach of the hand is found from bisection, starting from a hand location for which the robot assembles and a second one which fails to assemble. The maximum assembly radius is stored. Then θ is increased by $\Delta\theta = \frac{2\pi}{n}$, where the plane is divided into n regions, and again the maximum assembly radius is found. After the limiting hand position for $\theta = 0$ is found, the following radii are found more quickly because the previous assembly radius is used as the starting point. A small Δr is added or subtracted until the limit of assembly along the given ray is found. The workspace data is saved in an array of maximum radii along each $\Delta\theta$. For two degree-of-freedom robots, the above description is sufficient to determine the outer workspace limit. Manipulators with three degrees-of-freedom require the specification of hand orientation in addition to the position. The above method is repeated for hand orientation angles from 0 to 2π in small steps. The array of radii is stored, saving the maximum value for a given θ over all θ_H values.

For determining the inner workspace limits, the procedure is similar except that the minimum assembly radii are stored, rather than the maximum.

The above algorithm is computationally efficient because the assembly calculations are closed-form. For a given planar workspace the approximate area is found from a summation of all the triangular areas. The inner areas are subtracted from the outer, when they exist.

A FORTRAN program is used to perform the workspace algorithm. The optimization takes place through user interaction, varying the fixed parameters while noting the workspace results. To facilitate this process, a computer graphics subroutine using graPHIGS displays each calculated workspace on an IBM 5080 terminal. Along with the resulting shape, the area and maximum hand reach are displayed.

6.1.2 Application to Specific Manipulators

The workspace optimization routine described in the previous section has been adapted to the six manipulators pictured in Figs. 2.2 - 2.6 and 2.9. The present section discusses details of the individual workspace optimization routines. The "N5R5", "N7R8", "N6R6", and "N8R9-2" use the following link normalization criteria, respectively, for the purpose of comparing various manipulator configurations.

$$a + b + LH + d = 1.0 \tag{6.1a}$$

$$a + b + +c + d + LH + p = 1.0 \tag{6.1b}$$

$$a + b + c + d + h = 1.0 \tag{6.1c}$$

$$a + b + c + d + LH + h + p = 1.0 \tag{6.1d}$$

For the above four manipulators, the interior space of non-assembly is found numerically, based on the centroid of fixed pivots.

The normalization equations for the "N8R9-1" and "N10R12" manipulators, respectively, are given below.

$$a + b + d + f + k + p + LH = 1.0 \tag{6.1e}$$

$$a + b + d + f + k + p + r + q + LH = 1.0 \tag{6.1f}$$

For these two manipulators, internal spaces of non-assembly are centered about the fixed pivots, when they occur. The optimization routines for these two robots incorporate a numerical inner void determination centered around each fixed pivot.

The results for the numerical reachable workspace optimization are summarized in Table 6.1 and displayed in Figs. 6.2a - 6.2f. These figures are drawn to the same scale for relative comparison purposes. From Table 6.1, the manipulators with the three largest optimum reachable workspaces are the "N6R6", "N5R5", and "N8R9-1". These three manipulators

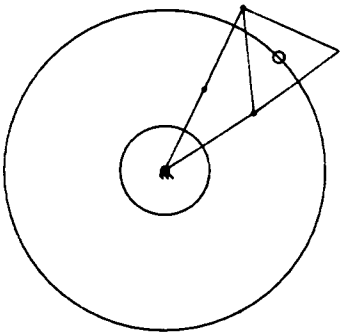

6.2a "N5R5"
a=b=0.26; c=d=0.30

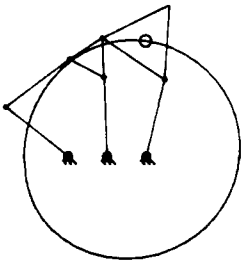

6.2b "N7R8"
a=b=d=p=0.198
h=0.186; L=0.10

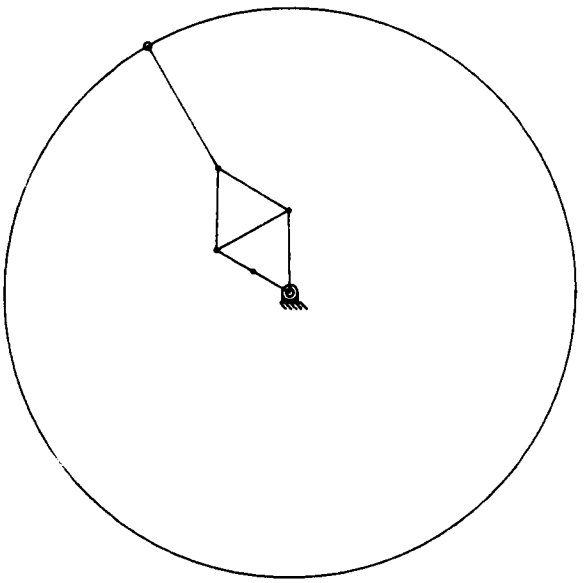

6.2c "N6R6"
a=b=0.109; c=d=0.211
h=0.360

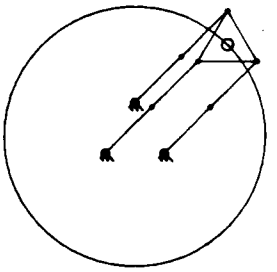

6.2d "N8R9-1"
a=b=f=d=p=k=0.153
c=L=0.142

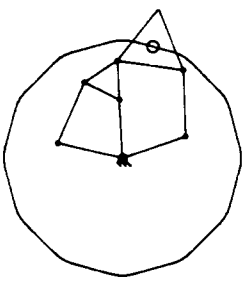

6.2e "N8R9-2"
a=b=k=h=p=0.165
c=0.097; d=0.146

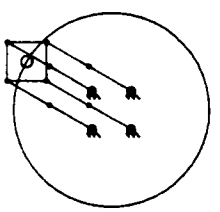

6.2f "N10R12"
a=b=f=d=p=k=q=r=0.117
c=L=0.090

Figure 6.2
Numerical Optimum
Reachable Workspace Results

are studied further in the following section, where closed-form determination and optimization is presented for both reachable and dextrous workspaces.

Table 6.1 Optimum Numerical Reachable Workspace Results

NAME	AREA	R_{max}	CIRCLE	PIVOTS
"N6R6"	1.6719	0.7295	yes	same
"N5R5"	0.6090	0.4590	yes	same
"N8R9-1"	0.2942	0.3060	yes	distinct
"N8R9-2"	0.2709	0.2990	no	same
"N7R8"	0.2321	0.3353	no	distinct
"N10R12"	0.1720	0.2340	yes	distinct

6.2 *Closed-Form Workspace Optimization*

This section presents geometrical closed-form determination and optimization of reachable and dextrous workspaces of parallel robotic mechanisms. For each manipulator and workspace type, optimal criteria are developed and the maximum workspace area is determined.

The "N5R5", "N6R6", and "N8R9-1" manipulators of Figs. 2.2, 2.4, and 2.5 are selected for detailed study in this section. These manipulators have the largest reachable workspace areas from the numerical workspace study in Section 6.1. The methods of this section may be adapted to handle various planar robotic mechanisms.

6.2.1 "N5R5" Manipulator

The "N5R5" robotic mechanism is a five-bar linkage, as shown in Fig. 2.2. This device has two degrees of freedom; the hand position, (x_H, y_H) is controlled. Therefore, no distinction is made between the reachable and dextrous workspace, because the angular orientation of the hand is not specified independently.

A method is presented to geometrically determine in closed form the workspace of a "N5R5" manipulator of general dimensions. Factors leading to optimum workspace characteristics are developed simultaneously. The "N5R5" workspace is maximized according to these optimal criteria.

Referring to Fig. 2.2, the triad a-b-LH is viewed as a three link serial manipulator, which connects the left fixed pivot to the hand. Likewise, the dyad d-LH is viewed as a serial two link manipulator, connecting the right fixed pivot to the hand. As mentioned previously, the angular orientation of the triangular hand link cannot be controlled independently for this two degree of freedom manipulator. However, this angle, ϕ, must be considered in workspace determination because the two manipulator sub-chains must assemble at the same hand point. The angle ϕ is a compatibility condition for assembly in the following development.

Prior to the development of the workspace for the "N5R5" manipulator, the concept of angular cognates (Myklebust and Tesar, 1971) is used to determine the manipulator hand traces for planar three-link and two-link serial chains, with the orientation of the end link fixed in each case.

Figure 6.3a shows a three-link serial chain with the end link orientation fixed at ϕ_1 . The concept of angular cognates is that any order of assembly of links a, b, and LH results in the same hand position provided the absolute orientations of the links are preserved. Therefore, the end link LH may be attached to the ground link, followed by links a and b, as shown in dashed lines in Fig. 6.3a. The angle ϕ_1 is still fixed, and thus link LH forms an extension of the ground link. The resulting trace of the tip of link b is identical to the hand trace of the

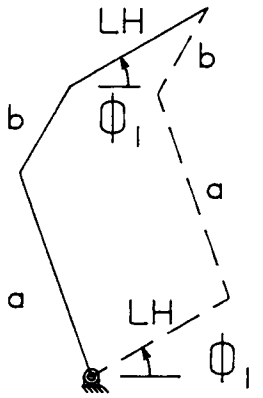

6.3a
Angular Cognate

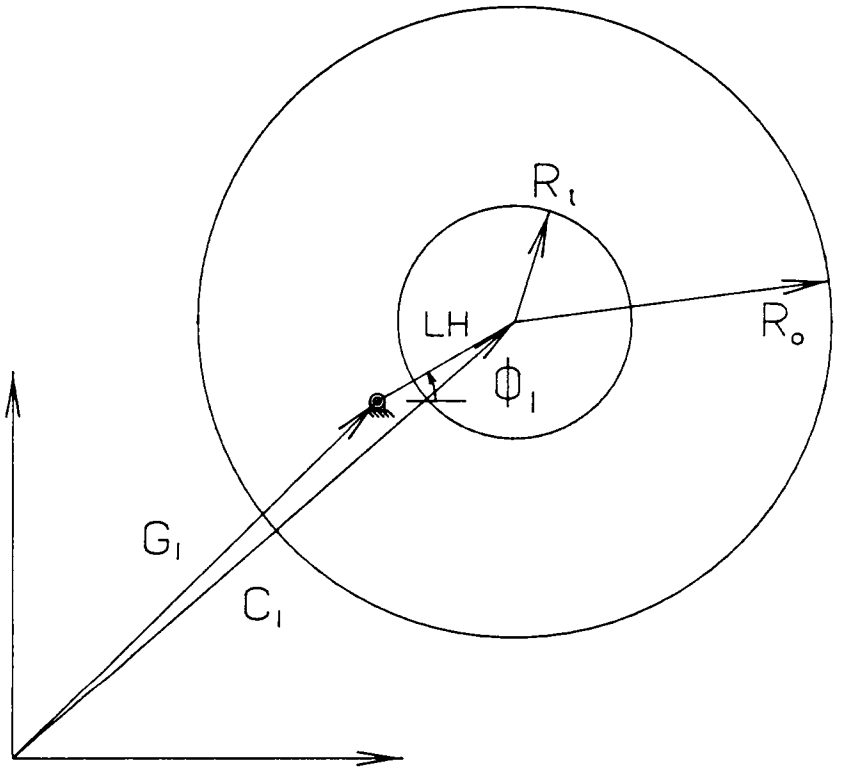

6.3b
Associated Hand Area

Figure 6.3
Three-Link Serial Chain
with Fixed Hand Angle

original chain. This trace is a concentric ring, shown in Fig. 6.3b, with the following center and radii, where $\underline{G}_1$ represents the fixed pivot location in the global coordinate system.

$$\underline{C}_1 = \underline{G}_1 + LHe^{I\phi_1} \tag{6.2}$$

$$\phi_1 = \phi + \frac{\pi}{6} \tag{6.2a}$$

$$R_o = a + b \tag{6.3a}$$

$$R_i = |a - b| \tag{6.3b}$$

Figure 6.4a displays a two-link serial chain with the end link orientation fixed at ϕ_2. An angular cognate of the original serial chain is shown in dashed lines in Fig. 6.4a. The resulting trace of the tip of link d is identical to the hand trace of the original chain. This trace displayed in Fig. 6.4b is the boundary of a circle with radius d and the following vector locating the center.

$$\underline{C}_2 = \underline{G}_2 + LHe^{I\phi_2} \tag{6.4}$$

$$\phi_2 = \phi + \frac{5\pi}{6} \tag{6.4a}$$

Where $\underline{G}_2$ is the vector locating the fixed pivot in the global coordinate system.

Given the above behavior for subchains a-b-LH and d-LH, the workspace of the "N5R5" manipulator for a given ϕ is the intersection of the solid circular disk and the circular curve, as shown in Figs. 6.5a and 6.5b. Assembly is assured through the compatibility angles ϕ_1 and ϕ_2. The overall workspace is found by incrementing ϕ through 0 - 2π radians. The intersection mentioned above is a circular arc for a given ϕ. The union of all of these circular arcs forms a plane area, which is the total workspace of the "N5R5" manipulator.

In order to maximize the "N5R5" workspace, the two centers $\underline{C}_1$ and $\underline{C}_2$ must be as close as possible for all values of ϕ, in order to reduce workspace limitations. The distance

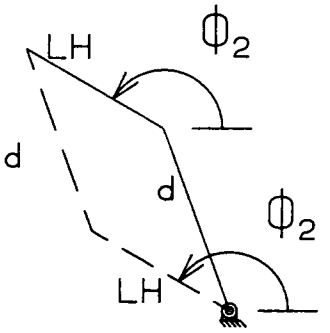

6.4a
Angular Cognate

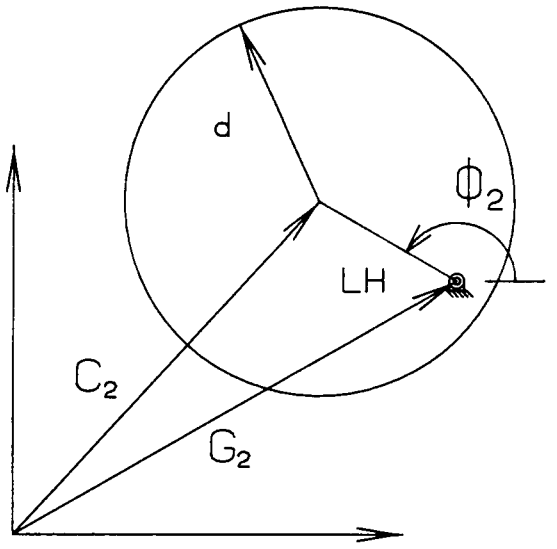

6.4b
Associated Hand Angle

Figure 6.4
Two-Link Serial Chain
with Fixed Hand Angle

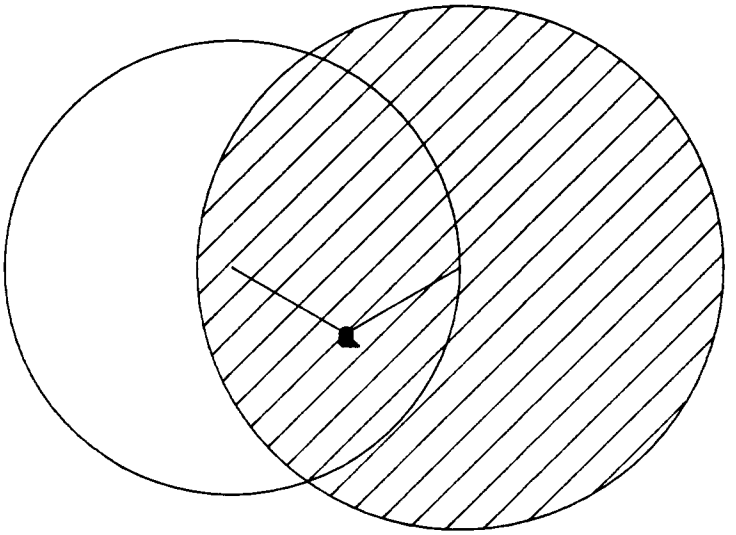

6.5a
Workspace Intersection

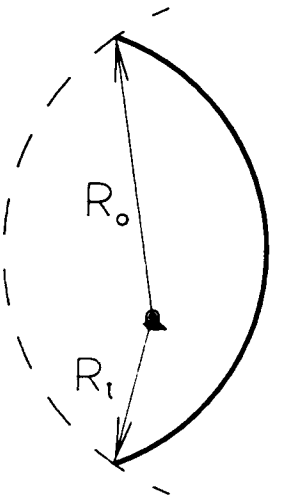

6.5b
Intersection Detail

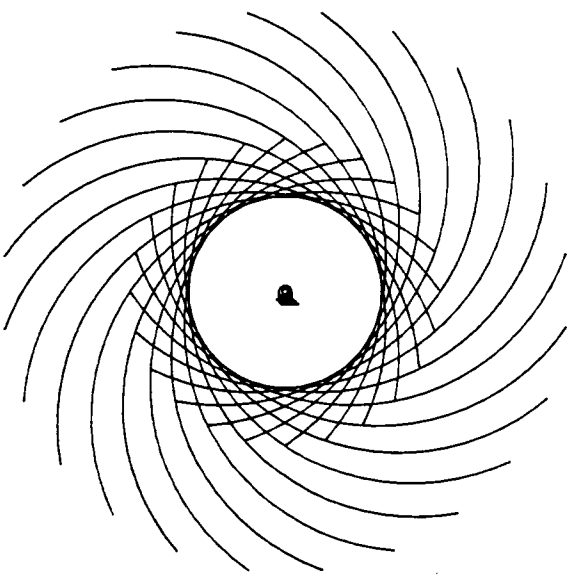

6.5c
Overall Workspace

Figure 6.5
"N5R5" Workspace Determination

between the two centers is constant and minimized when L = 0, i.e. the two fixed pivots occupy the same point. From Fig. 6.3b and Eq. 6.3b, if a=b then the radius of the inner circle goes to zero, which reduces workspace limitations. In addition to the normalization condition, Eq. 6.1a, another condition is required to express all unknowns in terms of one variable. From trial and error, this extra optimal criterion is equal lengths for the link d and the equilateral ternary hand link. The optimal conditions for the "N5R5" manipulator are summarized below.

$$L = 0 \tag{6.5a}$$

$$a = b \tag{6.5b}$$

$$c = d = \sqrt{3}\,LH \tag{6.5c}$$

Figures 6.5a and 6.5b show the workspace intersection with $\phi = 0$ for a "N5R5" manipulator that satisfies the optimal criteria of Eqs. 6.5. Considering all ϕ , the overall workspace is a disk with radii R_o and R_i, centered at the fixed pivot. This fact is demonstrated in Fig. 6.5c, where the intersection for $\phi = 0$ has been rotated about the fixed pivot. Clearly, the resulting workspace is a planar area.

From Eqs. 6.1a and 6.5, the unknowns a, b, and LH are expressed in terms of d. Equation 6.5c gives LH; a and b are as follows.

$$a = b = 0.50 - 0.7887d \tag{6.6}$$

The workspace area is maximized using a univariate search in d. The optimization is performed graphically, using CADAM as a tool. The optimum value is obtained by varying d and graphically solving for the associated radii. This process is repeated until the workspace behavior is known for the entire range of d.

The results from the graphical solution are presented in Table 6.2 and Fig. 6.6. Figure 6.6a shows the inner and outer workspace radii as a function of d, and Fig. 6.6b shows the associated workspace area. The optimum value for d is 0.3100, which yields a workspace bounded by circles of radii $R_o = 0.4630$, $R_i = 0.1310$ and area A = 0.6195.

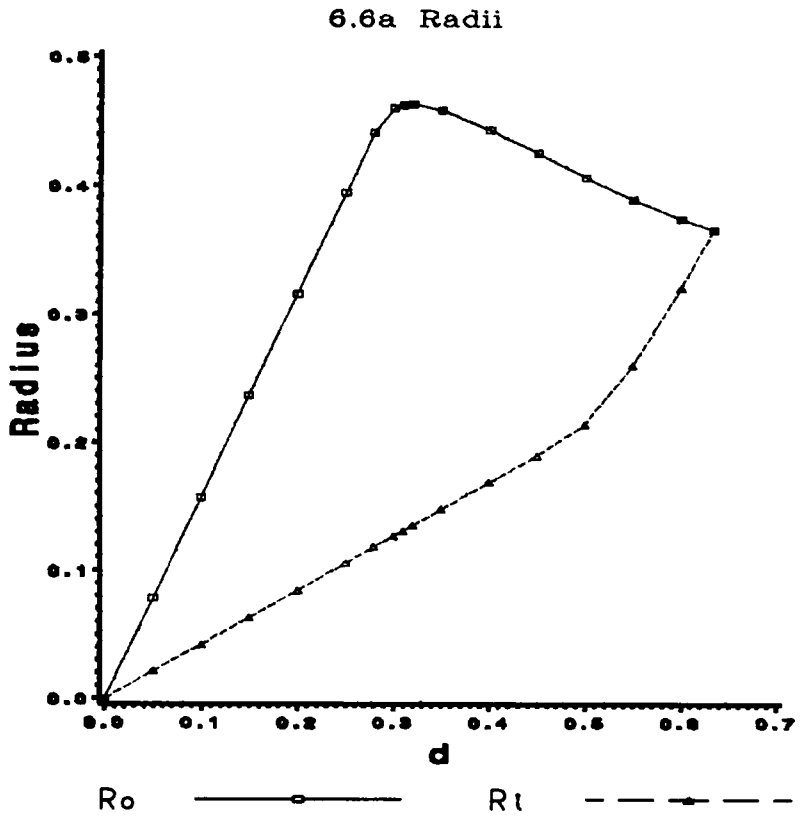

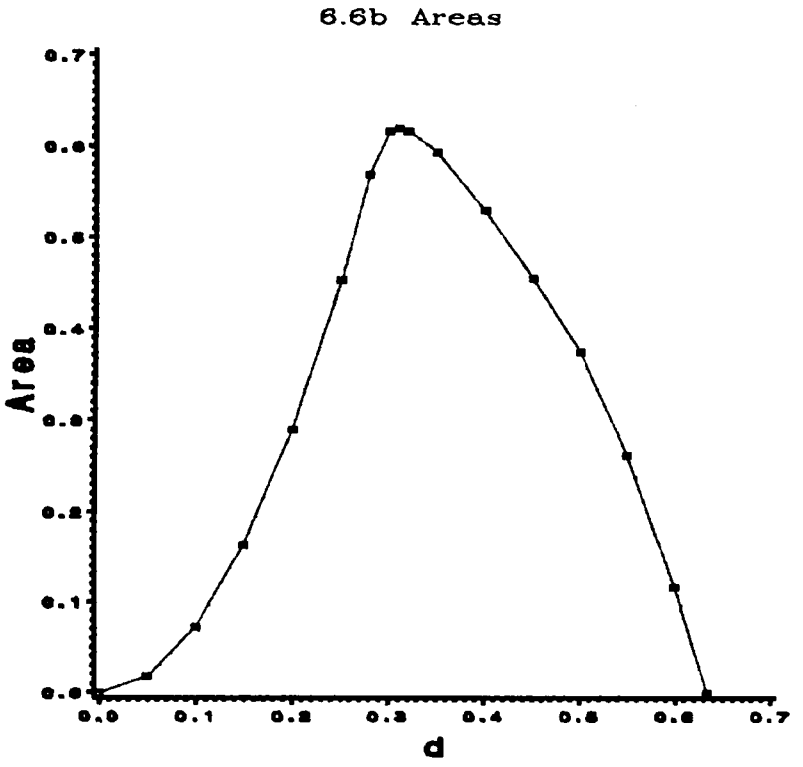

Figure 6.6
"N5R5" Optimum Workspace Results

Table 6.2 Optimum "N5R5" Workspace Data

d	R_o	R_i	A
0.0000	0.0000	0.0000	0.0000
0.2000	0.3155	0.0845	0.2903
0.2800	0.4416	0.1184	0.5686
0.3000	0.4609	0.1268	0.6168
0.3100	0.4630	0.1310	0.6195
0.3200	0.4634	0.1352	0.6172
0.3500	0.4590	0.1479	0.5932
0.4000	0.4439	0.1691	0.5292
0.5000	0.4065	0.2145	0.3746
0.6000	0.3742	0.3208	0.1166
0.6340	0.3660	0.3660	0.0000

From d = 0 to d = 0.28, and from d = 0 to d = 0.45, respectively, the R_o and R_i curves are linear. In these ranges, the the outer and inner radii are (d + LH) and (d-LH), respectively. Outside of these ranges, the circular disk of radius (a + b) imposes a restriction such that the outer radius increases at a smaller rate while the inner radius grows at a greater pace with increasing d.

The workspace area is parabolic in the range d = 0 to d = 0.28, due to the linear radii. Beyond the maximum area location, d = 0.3100, the inner and outer radii approach a common value of 0.3660 at d = 0.634. The area accordingly drops to zero. Manipulator assembly is not possible for d values greater than 0.634, as evident from Eq. 6.6. The optimum "N5R5" manipulator is shown along with its maximized workspace in Fig. 6.7.

All "N5R5" manipulator workspaces represented by Figs. 6.6a and 6.6b are concentric disks with an internal void. A solid workspace is possible only if the optimal condition of Eq. 6.5c is replaced by d = LH. This condition forces the circle of radius d to pass through the fixed pivot, which forms a solid planar area upon rotation through all ϕ. For solid workspaces, the optimum workspace has R_o = 0.4398, A = 0.6076, and d = 0.2300. Even with the condition d = LH, workspaces with an internal void result for $d > 1/3$. This is due to restrictions caused by the intersecting circular disk of radius (a + b).

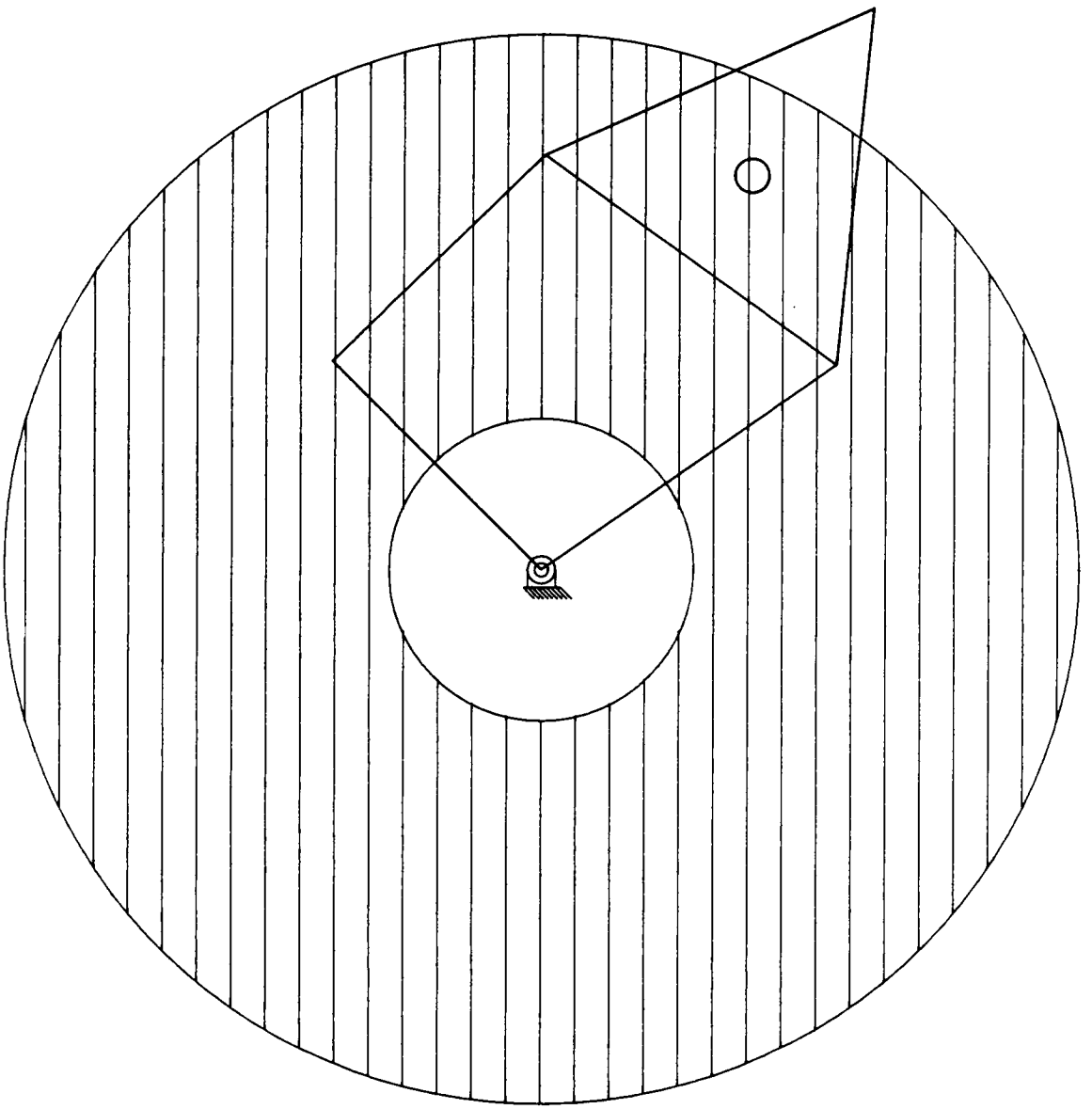

Figure 6.7
"N5R5" Optimum Workspace

6.2.2 "N6R6" Manipulator

6.2.2.1 "N6R6" Reachable Workspace

The "N6R6" manipulator is pictured in Fig. 2.4. This device possesses three degrees-of-freedom; workspace determination must involve the hand orientation angle θ_H. The "N5R5" workspace method is adapted to determine the workspace reach of the "N6R6" manipulator for a fixed value of θ_H . The overall manipulator workspace is found by rotating this area through all hand orientation values. Workspace maximization is performed following the geometric workspace determination. The reachable workspace is treated first, followed by the dextrous workspace.

The following procedure is used for determination of the hand trace for a given fixed but arbitrary value of θ_H . The "N6R6" manipulator is comprised of two serial manipulators: four-link chain a-b-c-h and three-link chain d-c-h. The hand angle for both subchains must be the same. In addition, there is a second compatibility angle, ϕ_2, required to ensure assembly of the two subchains.

If the compatibility angles θ_H and ϕ_2 are fixed, the geometric topology degenerates to a five-bar linkage comprised of three-link chain a-b-L1 and two-link chain d-L2, shown in Fig. 6.8a. Concluding from the "N5R5" workspace theory, the "workspace" for fixed values of θ_H and ϕ_2 is a circular arc formed by the intersection of the circular disk of radius (a + b) and the circle of radius d. The workspace area for a given θ_H value is found by incrementing the second compatibility angle, ϕ_2, which rotates the intersection arc to form a plane area.

Thus far, the method described is identical to that for the "N5R5" manipulator. The major difference is that L_1 and L_2 vary with ϕ_2 . As shown in Fig. 6.8a, the values for L_1, ϕ_A, L_2 and ϕ_B are functions of θ_H and ϕ_2.

$$L_1 = \sqrt{p^2 + q^2} \tag{6.7a}$$

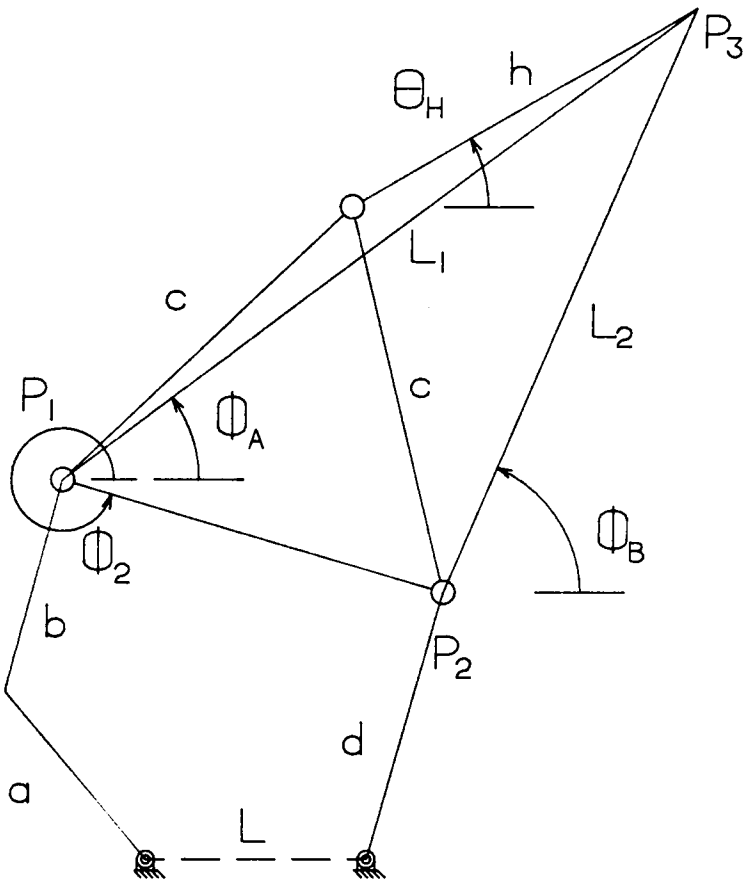

6.8a
Geometry with
Fixed Φ_2

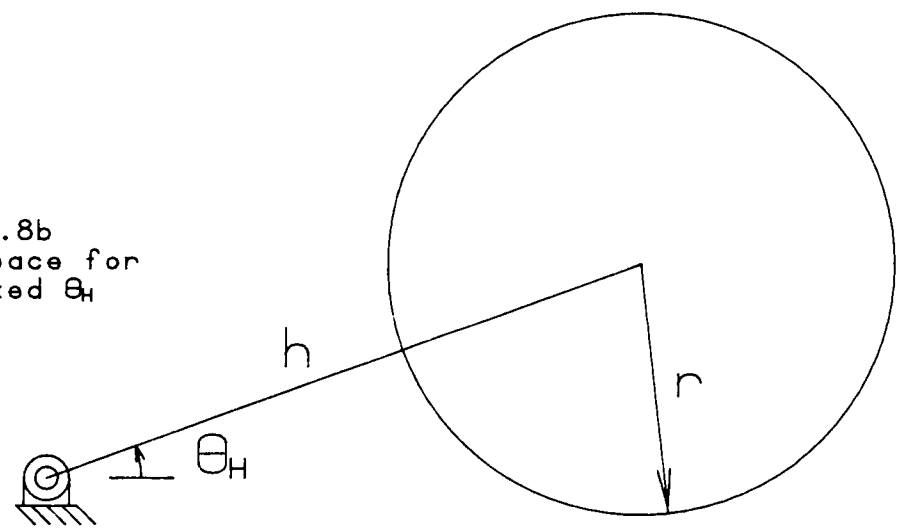

6.8b
Workspace for
Fixed θ_H

Figure 6.8
"N6R6" Manipulator with Fixed θ_H

$$\phi_A = \tan^{-1}\frac{q}{p} \tag{6.7b}$$

$$p = P_{3x} - P_{1x} = c\cos(\phi_2 + \frac{\pi}{3}) + h\cos\theta_H \tag{6.7c}$$

$$q = P_{3y} - P_{1y} = c\sin(\phi_2 + \frac{\pi}{3}) + h\sin\theta_H \tag{6.7d}$$

$$L_2 = \sqrt{s^2 + t^2} \tag{6.8a}$$

$$\phi_B = \tan^{-1}\frac{t}{s} \tag{6.8b}$$

$$s = P_{3x} - P_{2x} = c\cos(\phi_2 + \frac{2\pi}{3}) + h\cos\theta_H \tag{6.8c}$$

$$t = P_{3y} - P_{2y} = c\sin(\phi_2 + \frac{2\pi}{3}) + h\sin\theta_H \tag{6.8d}$$

The centers of the circular disk and circle, respectively, are:

$$\underline{C}_1 = \underline{G}_1 + L_1 e^{i\phi_A} \tag{6.9a}$$

$$\underline{C}_2 = \underline{G}_2 + L_2 e^{i\phi_B} \tag{6.9b}$$

Workspace determination for a fixed θ_H is difficult because $\underline{C}_1$ and $\underline{C}_2$ vary with ϕ_2. The workspace determination and subsequent maximization is accomplished through geometry and graphical solution with the aid of CADAM.

For a given θ_H, incrementing through all ϕ_2 values yields the hand area shown in Fig. 6.8b. The area is not circular for the general case, but this is an optimal characteristic. The value of r must be maximized relative to h in order to provide maximum workspace. Optimal criteria are developed through geometric considerations.

The condition a = b is specified for the "N6R6" manipulator, in order to limit workspace reduction. This ensures no internal void in the circular disk centered about $\underline{C}_1$. Figure 6.9a shows an example case for $L \neq 0$ and $c \neq d$. All of the intersections are different and there is

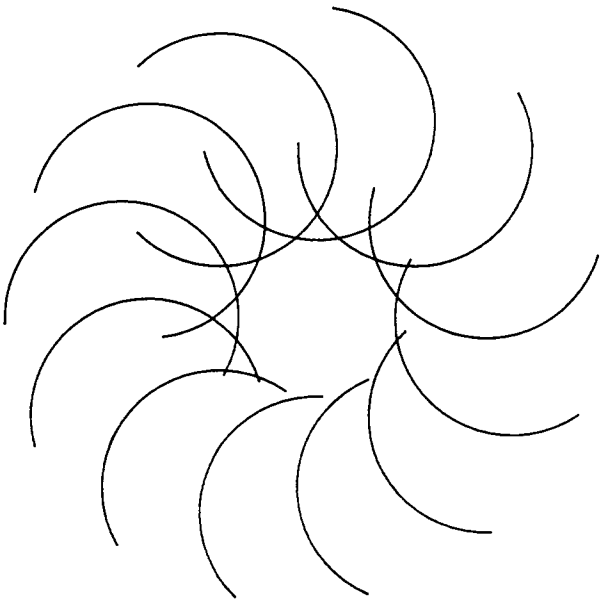

6.9a
$L \neq 0;\quad c \neq d$

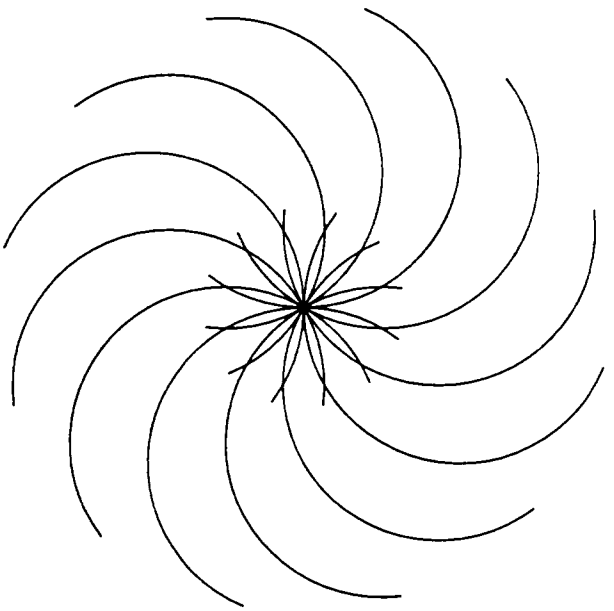

6.9b
$L = 0;\quad c = d$

Figure 6.9
"N6R6" Workspace Detail
with Fixed θ_H

a void in the center of the area. The example in Fig. 6.9b has L=0 and c=d. In this case, the intersections are identical. In addition, the intersections pass through a common point, and thus form a solid area upon rotation through angle ϕ_2. The optimal conditions are Eqs. 6.5a, 6.5b, and Eq. 6.5c. The normalization equation is Eq. 6.1c.

The link length h is varied in workspace maximization. One more equation is required to solve for the unknowns a, b, c, and d when h is given. This extra equation is an optimal criterion which maximizes r. It was found that maximum r results when the circle and circular disk are of equal size, which leads to the following, using Eq. 6.5b.

$$a = \frac{d}{2} \tag{6.10}$$

Using Eqs. 6.5, 6.10, and 6.1c, d is related to h.

$$d = \frac{1-h}{3} \tag{6.11}$$

The associated value of r (defined in Fig. 6.8b) is the following.

$$r = \sqrt{3}\,d \tag{6.12}$$

The overall workspace of the "N6R6", formed by incrementing θ_H , is a concentric ring with the following outer and inner radii, making use of Eq. 6.11.

$$R_o = h + \sqrt{3}\,d = 0.4226h + 0.5774 \tag{6.13a}$$

$$R_i = h - \sqrt{3}\,d = 1.5774h - 0.5774 \tag{6.13b}$$

The inner and outer radii are linear functions in h. From Eq. 6.13b, the inner radius is zero at h = 0.3660. For $h < 0.3660$, Eq. 6.13b gives a negative value for R_i which physically implies that the overall workspace has no interior void. The overall "N6R6" workspace behavior is summarized in Table 6.3 and Fig. 6.10. All workspaces form concentric circular rings, with an internal void for $h > 0.3660$.

Table 6.3 Optimum "N6R6" Reachable Workspace Data

h	R_o	R_i	A
0.0000	0.5774	0.0000	1.0472
0.1000	0.6196	0.0000	1.2061
0.2000	0.6619	0.0000	1.3763
0.3000	0.7041	0.0000	1.5577
0.3660	0.7320	0.0000	1.6836
0.4000	0.7464	0.0536	1.7412
0.5000	0.7887	0.2111	1.8142
0.6000	0.8309	0.3690	1.7412
0.7000	0.8732	0.5268	1.5236
0.8000	0.9155	0.6845	1.1610
0.9000	0.9577	0.8423	0.6528
1.0000	1.0000	1.0000	0.0000

The workspace area is

$$A = \pi(R_o^2 - R_i^2) \tag{6.14}$$

where R_i is zero up to h = 0.3660. Substituting Eqs. 6.13a and 6.13b into Eq. 6.14, the h value which gives maximum area is found by equating $\frac{dA}{dh}$ to zero. The result is h = 1/2.

The overall workspace maximum area is A = 1.8142 at h = 0.5000, with R_o = 0.7887 and R_i = 0.2111. The optimum area free of internal voids is A = 1.6836 at h = 0.3660 and R_o = 0.7320. Figure 6.11a shows the optimum "N6R6" manipulator reachable workspace.

6.2.2.2 "N6R6" Dextrous Workspace

Associated with each "N6R6" manipulator optimum reachable workspace case, the dextrous workspace is null. Referring to Fig. 6.8b, a dextrous workspace exists only when $h \leq r$. For the "N6R6" manipulators reported in Fig. 6.10 obeying this condition, the dextrous workspace is relatively small compared to the reachable workspace. For these cases, the radii of the reachable and dextrous workspaces, respectively, are given below.

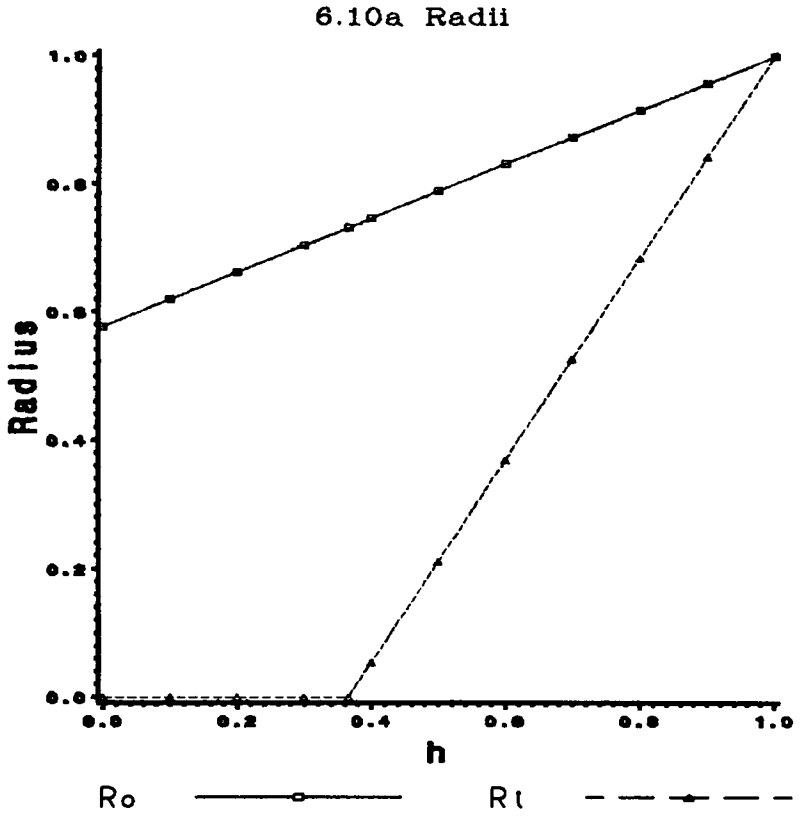

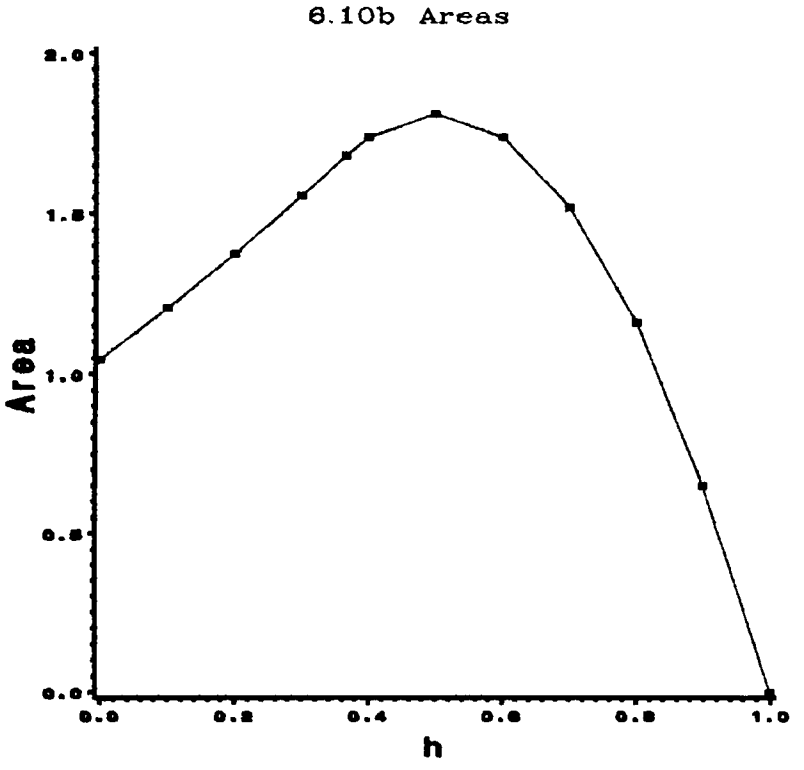

Figure 6.10
"N6R6" Optimum Reachable Workspace Results

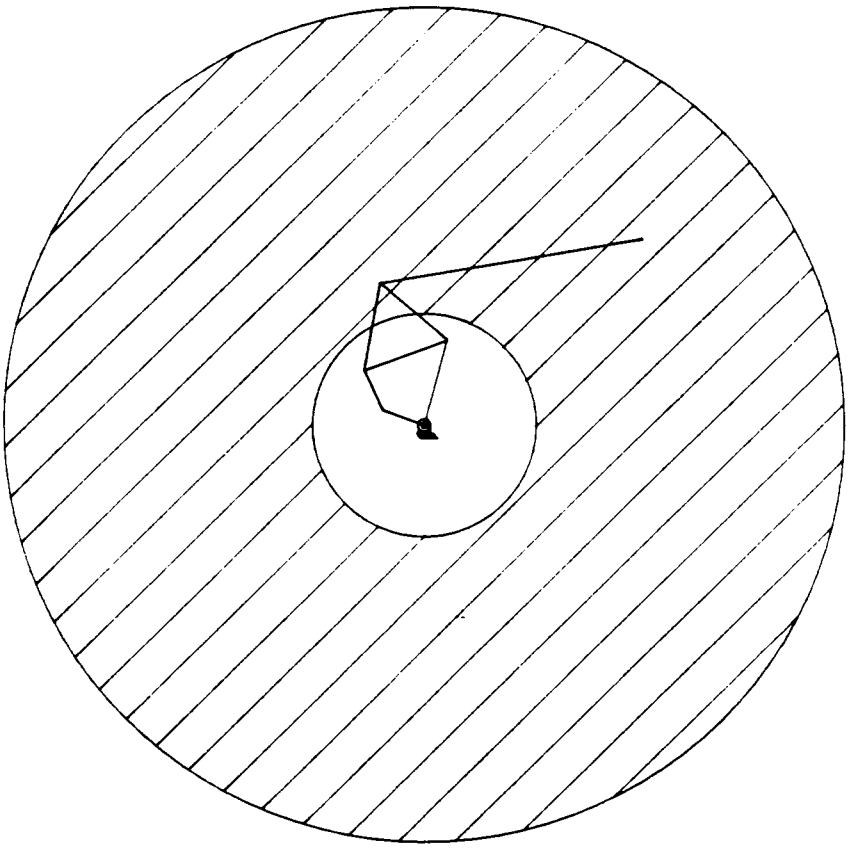

6.11a Reachable

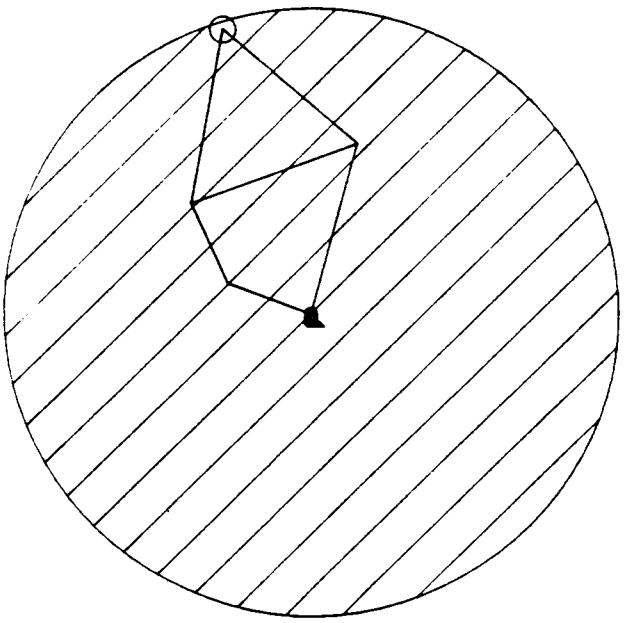

6.11b Dextrous

Figure 6.11
"N6R6" Optimum Workspaces

$$R_R = r + h \tag{6.15a}$$

$$R_D = r - h \tag{6.15b}$$

For those manipulators with h = r, the dextrous workspace is a single point, with zero area.

The maximum dextrous workspace occurs when the dextrous and reachable workspaces are identical. For the "N6R6" manipulator this condition implies that h = 0, from Fig. 6.8b. Physically this represents an "N6R6" manipulator with a rotational degree of freedom at the ternary link tip. The dextrous workspace maximization is thus performed in the same manner as that of the "N5R5" manipulator (Section 6.2.1). The two subchains involved are three-link serial chain a-b-c and two-link serial chain d-c. The hand orientation angle θ_H has no effect in the procedure because h=0. The coupler triangle compatibility angle ϕ_2 must be satisfied by both sub-chains.

The centers of the circular disk and circle are rotated by $\frac{\pi}{3}$ radians due to the "N6R6" geometry.

$$\underline{C}_1 = \underline{G}_1 + ce^{i\beta_1} \tag{6.16}$$

$$\beta_1 = \phi_2 + \frac{\pi}{3} \tag{6.16a}$$

$$\underline{C}_2 = \underline{G}_2 + ce^{i\beta_2} \tag{6.17}$$

$$\beta_2 = \phi_2 + \frac{2\pi}{3} \tag{6.17a}$$

The optimal conditions are Eqs. 6.5a, 6.5b, 6.5c, and h=0; the normalization constraint is Eq. 6.1c. The length of d is varied independently in workspace maximization. Table 6.4 and Fig. 6.12 display the optimization results. The maximum area is A = 1.0474 at d = 1/3. This optimum coincides with the upper limit for solid workspaces. In Table 6.4, the entry for d = 0.2500 represents the case where the circle and disk intersect in one point; d = 0.2680 is the

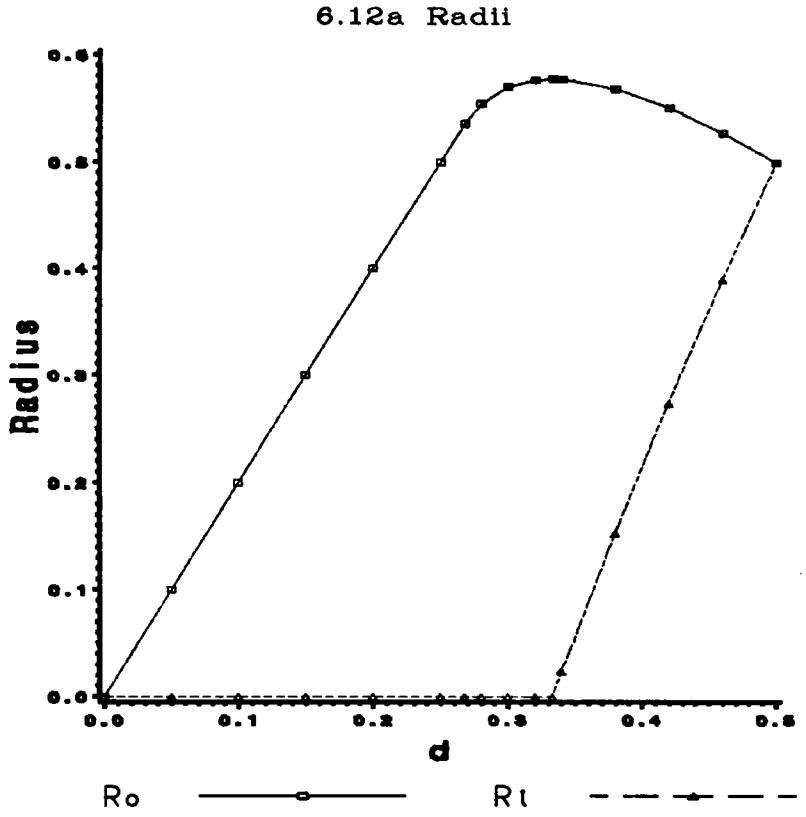

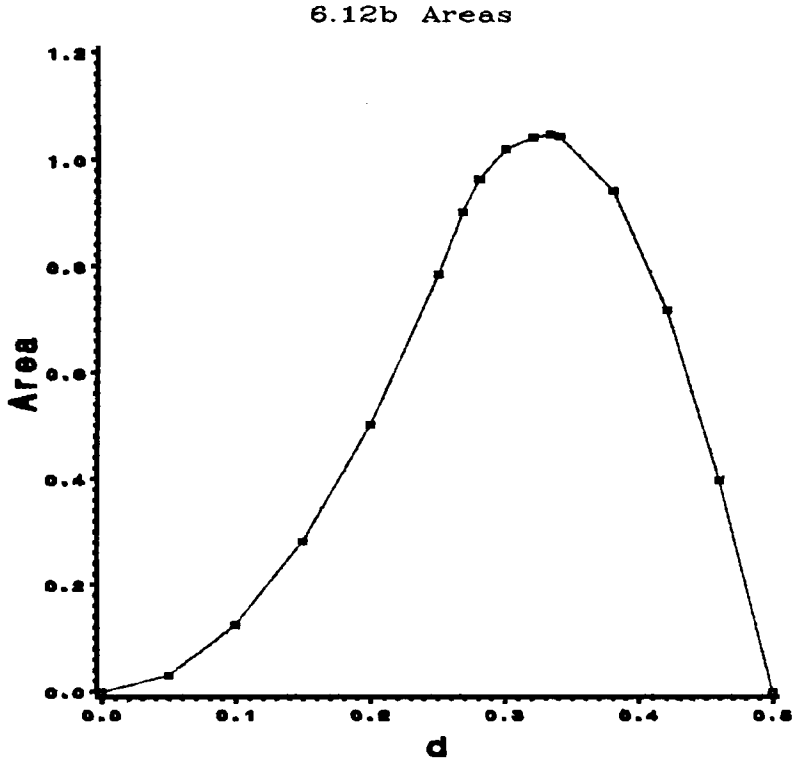

Figure 6.12
"N6R6" Optimum Dextrous Workspace Results

upper limit for the linear range. Figure 6.11b shows the optimum "N6R6" manipulator, along with its maximum dextrous workspace.

Table 6.4 Optimum "N6R6" Dextrous Workspace Data

d	R_o	R_i	A
0.0000	0.0000	0.0000	0.0000
0.2500	0.5000	0.0000	0.7854
0.2680	0.5360	0.0000	0.9026
0.2800	0.5542	0.0000	0.9649
0.3000	0.5700	0.0000	1.0207
0.3200	0.5763	0.0000	1.0434
0.3333	0.5774	0.0000	1.0474
0.3400	0.5771	0.0229	1.0446
0.3800	0.5684	0.1527	0.9417
0.4200	0.5509	0.2737	0.7181
0.4600	0.5275	0.3890	0.3988
0.5000	0.5000	0.5000	0.0000

6.2.3 "N8R9-1" Manipulator

The "N8R9-1" parallel robotic mechanism is shown in Fig. 2.5. In the following, a geometrical method is applied to determine the reachable and dextrous workspaces of this manipulator. After this development, a closed-form method is presented for calculating the workspace area for a fixed hand angle of a "N8R9-1" manipulator with general dimensions. Optimal reachable and dextrous workspaces are then discussed.

Since a manipulator must be a general purpose device, symmetry is an important design consideration. The "N8R9-1" manipulators considered in this chapter have the following symmetry.

$$a = f = p; \qquad b = d = k \tag{6.18}$$

Additionally, the fixed pivots lie on the vertices of an equilateral triangle and the triangular hand link is equilateral.

The "N8R9-1" manipulator is composed of three planar serial three degree-of-freedom chains: a-b-LH, f-d-LH, and p-k-LH. Each serial sub-chain connects a different fixed pivot to the manipulator hand. Given the above symmetry conditions, all serial triads are of equal size.

The hand trace area for a fixed but arbitrary θ_H value of triad a-b-LH is presented in Fig. 6.3b The hand reach area for the remaining two "N8R9-1" manipulator sub-chains is similar in form. The difference lies in the offset angles ϕ_2 and ϕ_3, dictated by the manipulator geometry. The three "N8R9-1" triads must assemble at the same hand orientation angle. The concentric ring for the first "N8R9-1" leg has the inner and outer radii defined by Eqs. 6.3. The radii for the other two legs are found in an analogous way. The centers $\underline{C}_1$ and $\underline{C}_2$ are given by Eqs. 6.2 and 6.4, with ϕ replaced by θ_H. The center of the third circle is given by

$$\underline{C}_3 = \underline{G}_3 + LHe^{I\phi_3} \tag{6.19}$$

$$\phi_3 = \theta_H - \frac{\pi}{2} \tag{6.19a}$$

The manipulator workspace area for a given θ_H is the intersection of the three concentric rings, one for each serial sub-chain. Figure 6.13a shows a sample workspace which demonstrates this intersection for $\theta_H = 0$. It is established for the "N5R5" manipulator in Section 6.2.1 that the condition a=b forced the inner radius of the ring to zero, causing the concentric ring to be a solid circle, and reducing workspace limitations. Figure 6.13b shows an example of this fact, where the dimensions are similar to those in Fig. 6.13a, but with a=b, f=d, and p=k. These conditions, along with Eq. 6.18, give the following.

$$a = b = f = d = p = k \tag{6.20}$$

The normalization condition is given in Eq. 6.1e.

Using Eqs. 6.1e and 6.20, the radii of the circles in Fig. 6.13b are:

$$a + b = 2a = \frac{1 - LH}{3} \tag{6.21}$$

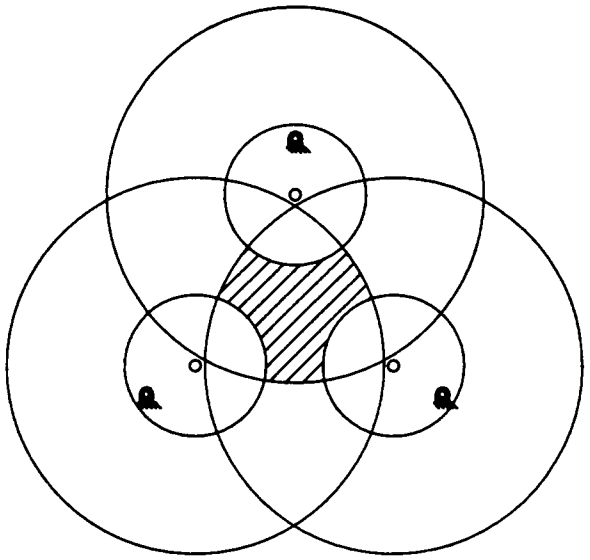

6.13a
$\theta_H = 0$

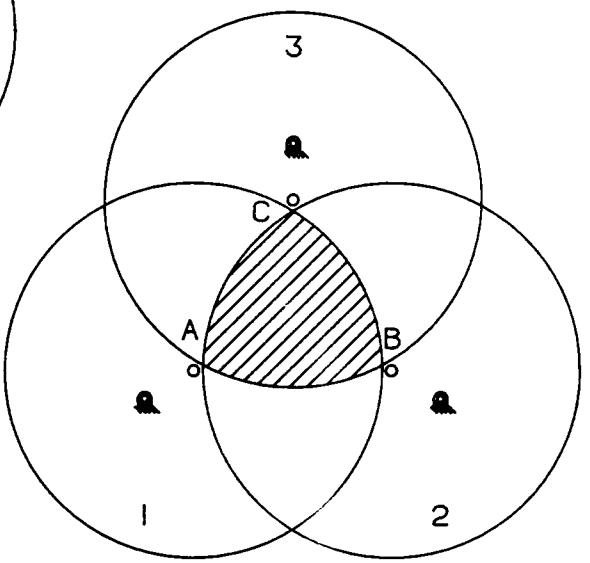

6.13b
$\theta_H = 0$; a=b

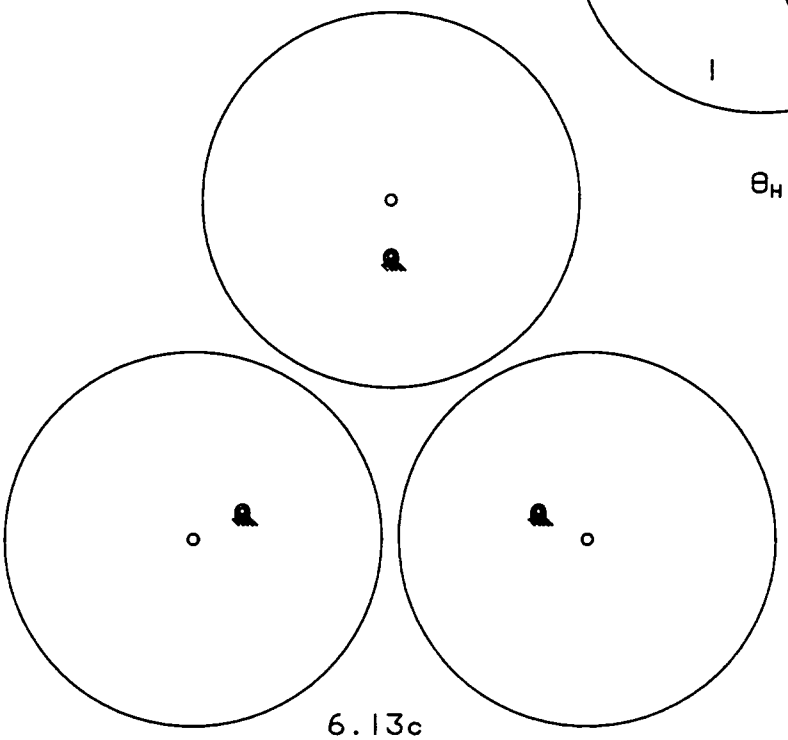

6.13c
$\theta_H = \pi$; a=b

Figure 6.13
"N8R9-1" Workspace Intersections

From the geometry of Figs. 6.13b and 6.13c, for a "N8R9-1" manipulator of given dimensions and fixed θ_H , the largest hand area occurs for $\theta_H = 0$, while $\theta_H = \pi$ yields the smallest hand area. The reason for this is that the centers of the circles are nearest each other for a hand angle of zero, and farthest apart for a hand angle of π. The hand areas for all other θ_H values are intermediate in size to these two extreme conditions. The reachable workspace is generated by $\theta_H = 0$, and the dextrous workspace by $\theta_H = \pi$.

Given the normalization equation, Eq. 6.1e, limits of the reachable and dextrous workspaces are now developed. From Eqs. 6.20 and 6.21, the manipulator parameters a, b, f, d, p, and k are expressed in terms of LH. To specify a "N8R9-1" manipulator fully, the ground pivot distance L must also be given. The parameters L and LH are varied in workspace maximization.

From the geometry of Fig. 2.5, the maximum and minimum coupler hand size for which a reachable workspace exists is calculated as follows. Equation 6.21 is used for simplification.

$$LH_{max} = (a+b) + \frac{\sqrt{3}}{3}L = \frac{\sqrt{3}L+1}{4} \qquad (6.22a)$$

$$LH_{min} = \frac{\sqrt{3}}{3}L - (a+b) = \frac{\sqrt{3}L-1}{2} \qquad (6.22b)$$

The maximum coupler hand size for which a dextrous workspace exists is given by Eq. 6.23. The minimum hand size is LH = 0.

$$LH_{max} = (a+b) - \frac{\sqrt{3}}{3}L = \frac{1-\sqrt{3}L}{4} \qquad (6.23)$$

Figure 6.14a shows the ranges in the L-LH plane where reachable (entire shaded area) and dextrous (cross-hatched area) workspaces exist. Along the respective boundaries, the reachable and dextrous workspaces are a single point, with zero area.

The workspace area for a "N8R9-1" manipulator of fixed dimensions and θ_H is determined as follows, adapted from Gosselin and Angeles (1987a). The workspace area shown in

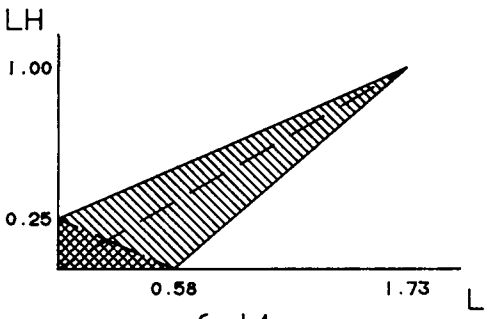

6.14a
L-LH Plane

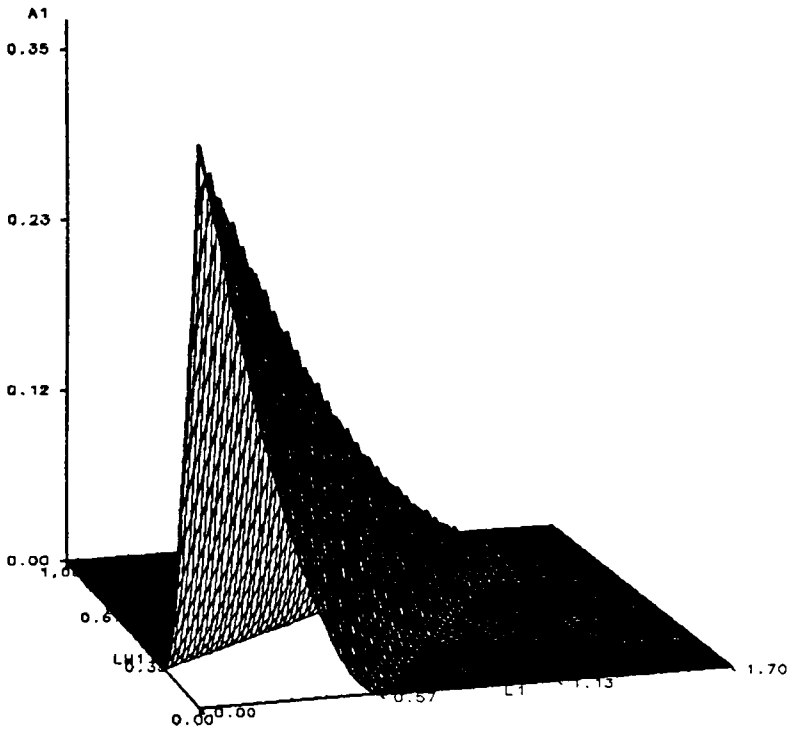

6.14b
Reachable

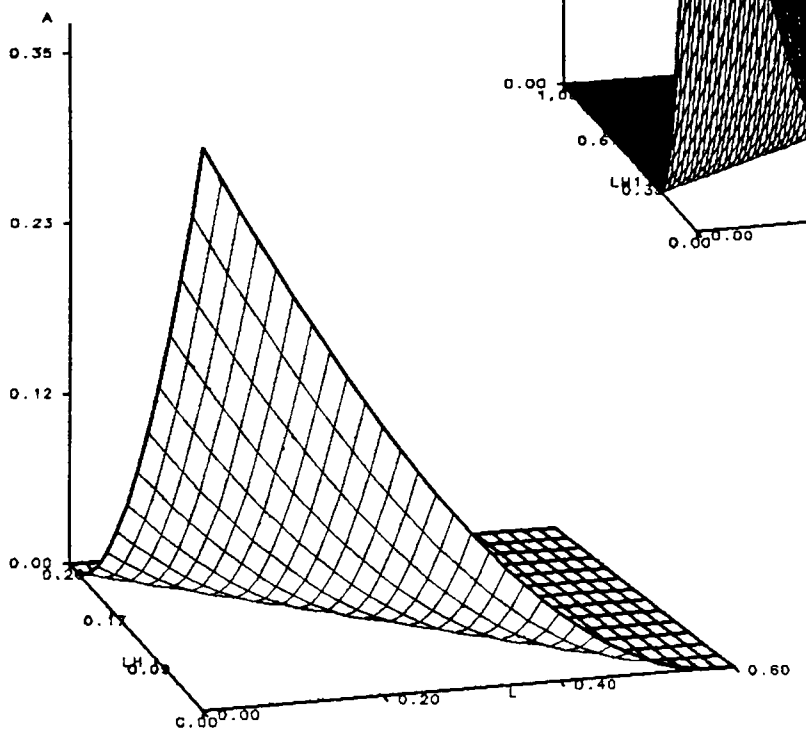

6.14c
Dextrous

Figure 6.14
"N8R9-1" Optimum Workspace Areas

Fig. 6.13b is calculated using boundary integration; the boundary is broken into three parts, one for each of the circles forming the workspace border.

$$A(\theta_H) = a(A_1 + A_2 + A_3) \tag{6.24}$$

$$A_1 = C_{1x}(\sin\theta_{C1} - \sin\theta_{B1}) - C_{1y}(\cos\theta_{C1} - \cos\theta_{B1}) + 2a(\theta_{C1} - \theta_{B1}) \tag{6.24a}$$

$$A_2 = C_{2x}(\sin\theta_{A2} - \sin\theta_{C2}) - C_{2y}(\cos\theta_{A2} - \cos\theta_{C2}) + 2a(\theta_{A2} - \theta_{C2}) \tag{6.24b}$$

$$A_3 = C_{3x}(\sin\theta_{B3} - \sin\theta_{A3}) - C_{3y}(\cos\theta_{B3} - \cos\theta_{A3}) + 2a(\theta_{B3} - \theta_{A3}) \tag{6.24c}$$

In Eqs. 6.24a, 6.24b, and 6.24c, θ_{ij} (i = A,B,C; j = 1,2,3) denotes the angle between point i and center $\underline{C}_j$ of circle j. Equation 6.24 is written in a more convenient form using the Cartesian coordinates of points A, B, and C.

$$A(\theta_H) = \frac{1}{2}(AA_1 + AA_2 + AA_3) + 12a\sin^{-1}\left(\frac{D}{4a}\right) \tag{6.25}$$

$$AA_1 = C_{1x}(C_y - B_y) - C_{1y}(C_x - B_x) \tag{6.25a}$$

$$AA_2 = C_{2x}(A_y - C_y) - C_{2y}(A_x - C_x) \tag{6.25b}$$

$$AA_3 = C_{3x}(B_y - A_y) - C_{3y}(B_x - A_x) \tag{6.25c}$$

In Eq. 6.25, D is the distance between A and B (also between B and C and between C and A, from symmetry). Using Eq. 6.25, the workspace area is calculated for both reachable and dextrous workspaces over the L-LH ranges indicated in Fig. 6.14a.

6.2.3.1 "N8R9-1" Reachable Workspace

Figure 6.14b shows the area calculation results for reachable workspace (θ_H = 0). This three-dimensional surface represents workspace area for all possible L-LH combinations.

The maximum obtainable workspace area is A = 0.3491 at L = LH = 0. This optimal "N8R9-1" manipulator has degenerated to a two-link serial manipulator with a rotational degree of freedom at the tip of the second link, as shown in Fig. 6.15a. The three manipulator legs coincide and the fixed pivots occupy the same location. Although this is a mathematical optimum, some of the advantages of parallel manipulators will be lost.

The workspace area decreases from this optimum to zero area on the border of the L-LH range shown in Fig. 6.14a. For a given value of L, the optimum reachable workspace is a solid circular area. This optimum is achieved when the centers $\underline{C}_1$, $\underline{C}_2$, and $\underline{C}_3$, given by Eqs. 6.2, 6.4, 6.19, coincide. This results when the following condition is satisfied.

$$LH = \frac{\sqrt{3}}{3}L \qquad (c = L) \tag{6.26}$$

Equation 6.26 states that the optimum reachable workspace occurs when the equilateral triangles of the fixed pivots and the hand are of the same size. Figure 6.15b shows the optimum circular reachable workspace given L = 0.10; the dashed trilobe boundary represents the associated dextrous workspace. The optimum circular area is calculated from $A = \pi r^2$ where the radius is obtained from Eq. 6.21 using Eq. 6.26.

$$A = \frac{\pi}{9}\left[\frac{L}{3}(L - 2\sqrt{3}) + 1\right] \tag{6.27}$$

The optimum reachable workspace area for any L value is displayed by the ridge in Fig. 6.14b. This ridge is aligned $\frac{\pi}{6}$ radians from the L axis (shown as a dashed line projected onto the L-LH plane of Fig. 6.14a) due to the condition given in Eq. 6.26.

6.2.3.2 "N8R9-1" Dextrous Workspace

The dextrous workspace ($\theta_H = \pi$) area results are shown in Fig. 6.14c. Again the optimum is A = 0.3491 at L = LH = 0. Centers $\underline{C}_1$, $\underline{C}_2$, and $\underline{C}_3$ coincide for the dextrous work-

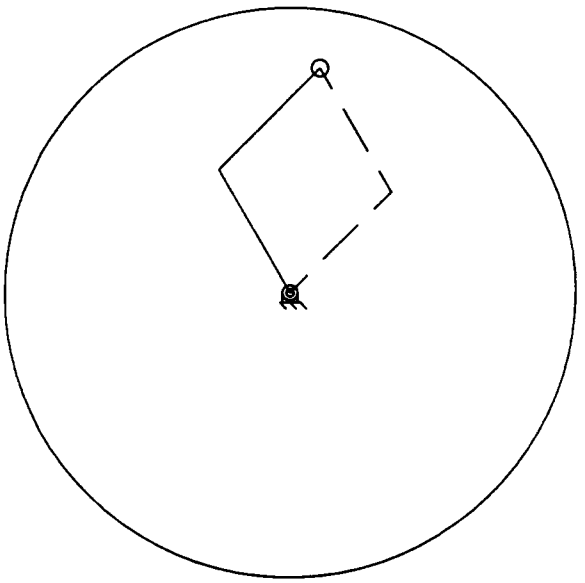

6.15a
L=0.0; LH=0.0

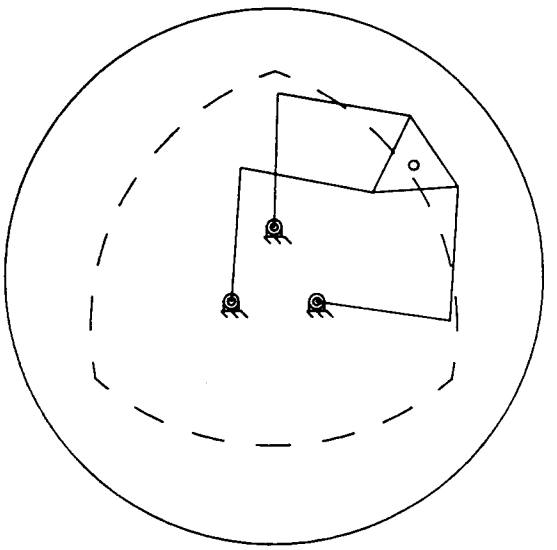

6.15b
L=0.10; LH=0.0577

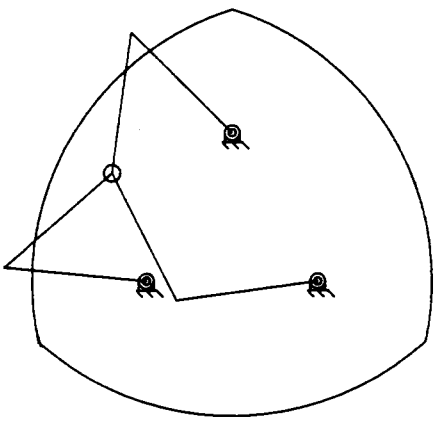

6.15c
L=0.20; LH=0.0

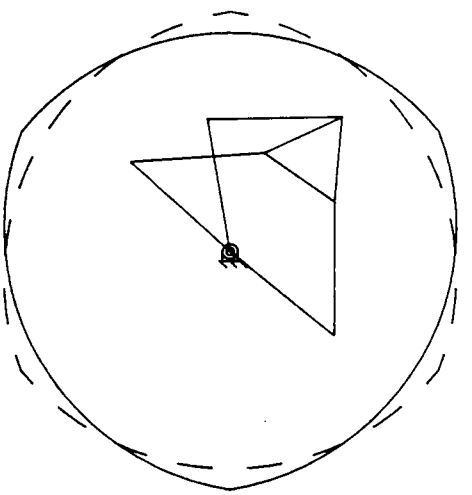

6.15d
L=0.0; LH=0.0577

Figure 6.15
"N8R9-1" Optimum Workspaces

space only when L = LH = 0. At this point the dextrous and reachable workspaces are identical; this is the only circular dextrous workspace possible.

For a given L value, the optimum dextrous workspace is obtained when it is the same as the reachable workspace, which leads to LH = 0. When this condition is met, the centers $\underline{C}_1$, $\underline{C}_2$, and $\underline{C}_3$ are fixed over θ_H , which produces the same workspace for all hand orientation angles. The A-L, LH=0 planes are identical in Figs. 6.14b and 6.14c. Figure 6.15c shows an example dextrous (and reachable) workspace with L = 0.20.

Additionally, for a given value of LH along L=0, the resulting reachable and dextrous workspaces are of the same area, but with inverted trilobe shapes. The A-LH, L=0 planes on Figs. 6.14b and 6.14c are the same. An example for this case is shown in Fig. 6.15d, with LH = 0.0577; again the reachable workspace is denoted by the solid curve and the dextrous workspace by the dashed curve.

Dextrous workspace area reduces rapidly to zero at the dextrous line in Fig. 6.14a. For many "N8R9-1" manipulators represented in Fig. 6.14b, the dextrous workspace is non-existent.

The optimum workspace results for the manipulators presented in Sections 6.2.1 - 6.2.3 are kinematic optima. That is, the areas reported cannot be increased given the same configuration and normalization equations; however, the optima all have degenerative characteristics which make them behave like serial manipulators. For example, the ground pivots may occupy the same location. Thus, some parallel advantages such as stiffness may be reduced. The optimum dimensions would be different when considering dynamic or stiffness optimization in addition to maximum hand reach.

Chapter 7 Link Interference Detection

Link interference is a potential problem in the application of robotic mechanisms. Increased numbers of links and greater kinematic complexity compared with a serial robot configuration lead to a greater possibility of one or more pairs of robot links interfering. The mathematical theory developed thus far makes no allowances for link interference possibilities. Subjects such as kinematic position simulation, forward dynamics calculations, and workspace optimization are not complete without a consideration of link interference.

Link interference during a given motion task for planar robotic mechanisms may be guarded against in two ways. The first is to provide a sophisticated robot controller which does not allow motion to proceed into any ranges where link interference occurs. The second alternative involves geometric design such that link interference never occurs for a given robotic mechanism topology.

A general planar link interference determination method is developed in this section. The method requires position information at each point in the range of robot motion. Manipulator links are assumed to be lines and link interference is determined for isolated positions only; no check is made to determine if the manipulator moves through an interference point to arrive at the location under consideration.

Special cases in link interference are identified and dealt with. The method has been coded into a FORTRAN program, which is used to determine the effects of link interference

on the optimum reachable and dextrous workspaces developed in Chapter 6, Sections 6.2.1, 6.2.2, and 6.2.3. Finally, geometric conditions for the elimination of link interference are presented. The dextrous and reachable workspaces of the "N6R6" and "N8R9-1" manipulators are re-optimized considering the freedom of link interference constraint.

7.1 Position-Dependent Link Interference Detection

For most simple planar one degree-of-freedom mechanisms, link interference is avoided by positioning each link, including ground fixtures, on a separate plane. This technique may be used to reduce link interference in planar robotic mechanisms; however, in general, the link interference problem is not eliminated.

Figure 7.1 shows the two degree-of-freedom "N5R5" manipulator with four possible Z-plane configurations, where the X-Y plane is the plane of the paper. Parametric link interference detection depends on the specific manipulator configuration. The configuration of Fig. 7.1d is used for link interference determination in the present section. From Fig. 7.1d it is seen that only links b and d can interfere. The "N6R6" manipulator (Fig. 2.4) is also treated with the configuration of Fig. 7.1d, if it is assumed that the hand link h achieves a full rotation on a plane separate from the remaining links. Figure 7.2 shows the "N8R9-1" manipulator along with its Z-plane configuration. On level one, three pairs of links may intersect: a-f, f-p, p-a; possible second level conflicts are b-d, d-k, k-b.

7.1.1 General Link Interference Detection

A link interference detection method is presented by Keil, Myklebust, and Reinholtz (1985). This method is general but the application thrust of the paper is towards planar

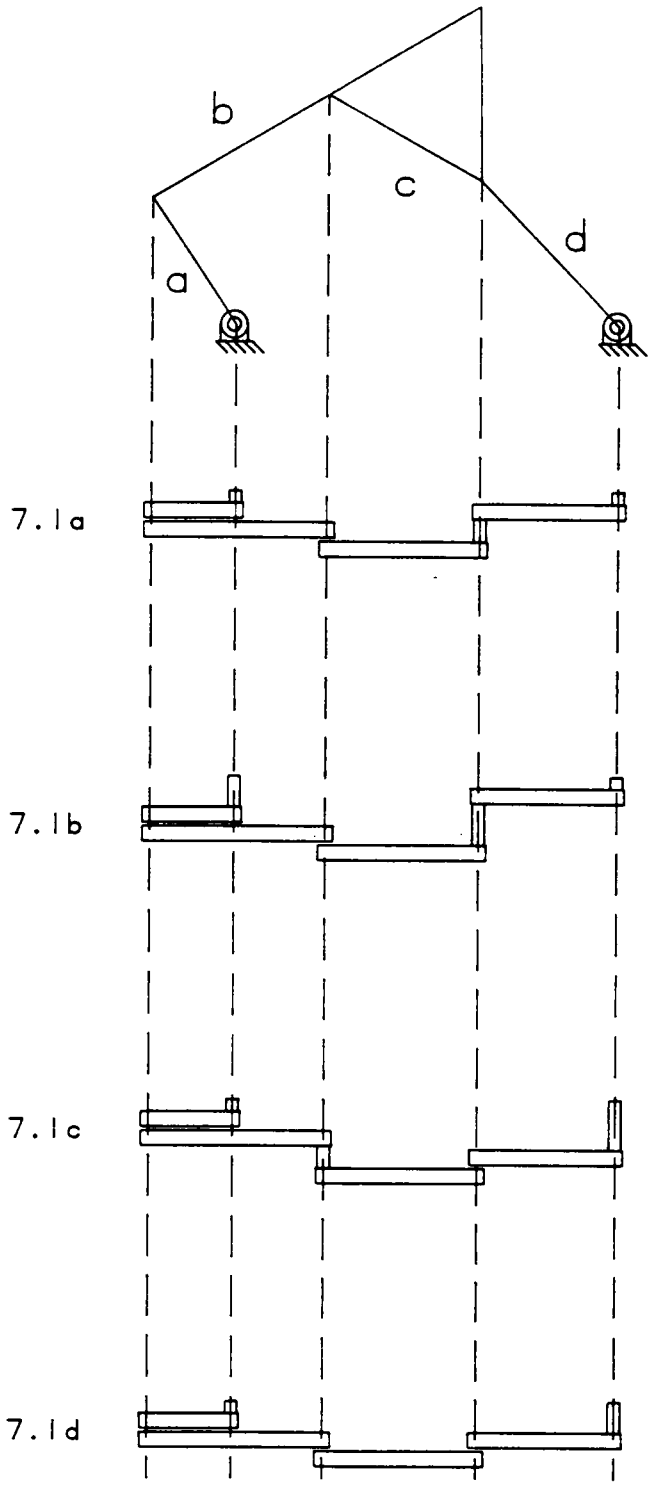

Figure 7.1
Z-Plane Configurations
for the "N5R5" Manipulator

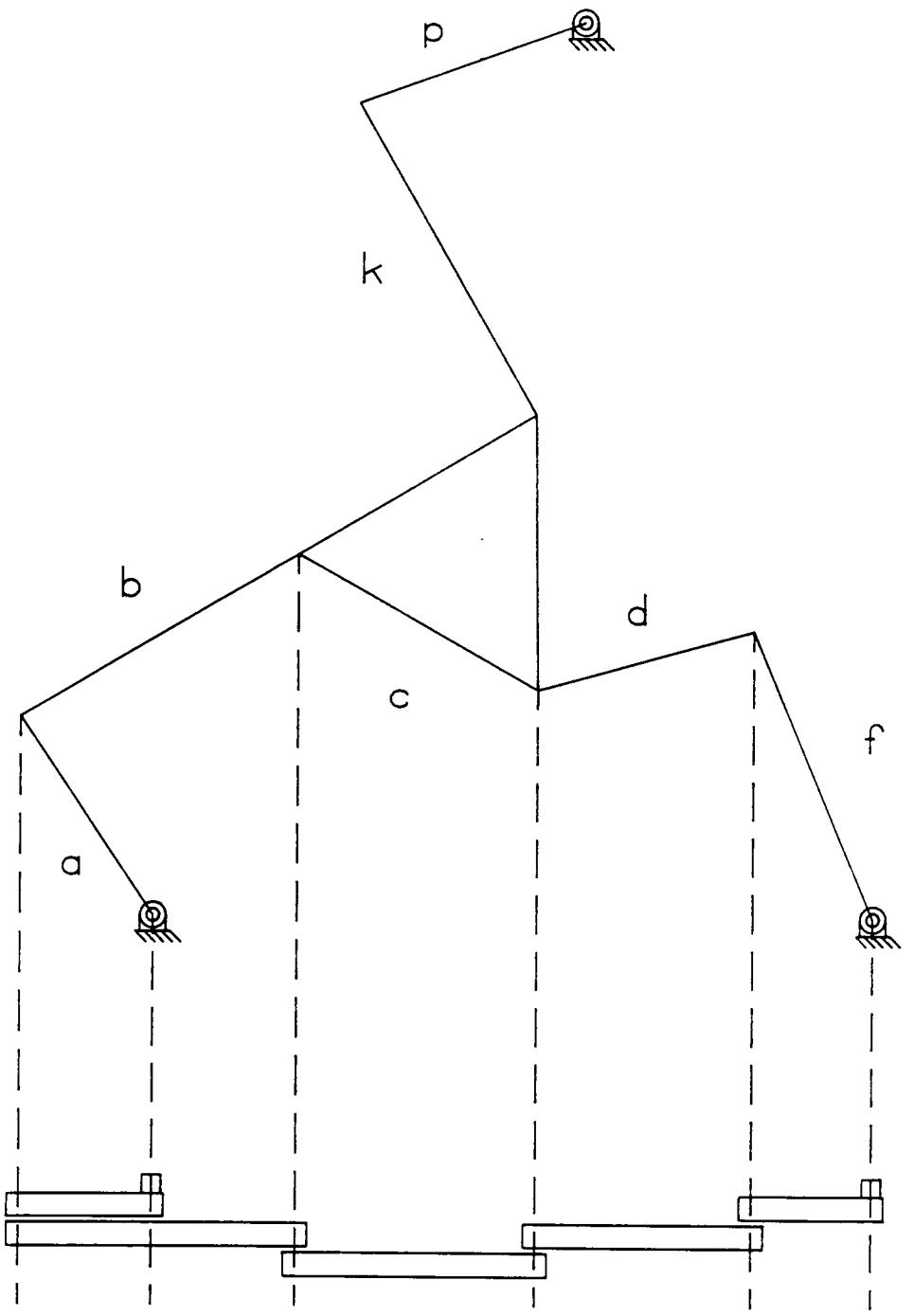

Figure 7.2
Z-Plane Configuration
for the"N8R9-1" Manipulator

mechanisms. The above method is not directly applied in this section because the link interference check in this chapter is limited to those links which may appear on the same Z-plane. A closed-form method for link interference determination between two general planar links on the same Z-plane is presented in this section. The method determines if a pair of co-planar links intersects. This algorithm is repeated for each pair of links which may conflict in a given position of a robotic mechanism.

Figure 7.3a shows two planar links which intersect at point $\underline{PTI}$. The respective endpoints of links L_1 and L_2 are $\underline{P}_1, \underline{P}_2$ and $\underline{P}_3, \underline{P}_4$. referred to the global origin. Point $\underline{PTI}$ is solved algebraically as follows. The slopes of the two lines are:

$$m_1 = \frac{P_{2y} - P_{1y}}{P_{2x} - P_{1x}} \tag{7.1a}$$

$$m_2 = \frac{P_{4y} - P_{3y}}{P_{4x} - P_{3x}} \tag{7.1b}$$

The equations for L_1 and L_2 are written in point-slope form. The unknown PTI_y is equated from both lines. The unknown PTI_x is then solved, and substituted into either line equation (Eq. 7.2a) to determine PTI_y.

$$PTI_y = m_1(PTI_x - P_{1x}) + P_{1y} = m_2(PTI_x - P_{3x}) + P_{3y} \tag{7.2a}$$

$$PTI_x = \frac{m_1 P_{1x} - m_2 P_{3x} + P_{3y} - P_{1y}}{m_1 - m_2} \tag{7.2b}$$

Link interference occurs when the following conditions are satisfied (see Fig 7.3a).

$$\underline{P_1PTI} < \underline{P_1P_2} \quad AND \quad \underline{P_2PTI} < \underline{P_1P_2} \tag{7.3a}$$

$$\underline{P_3PTI} < \underline{P_3P_4} \quad AND \quad \underline{P_4PTI} < \underline{P_3P_4} \tag{7.3b}$$

The term $\underline{P_1P_2}$ is the Euclidean length between endpoints $\underline{P}_1$ and $\underline{P}_2$; the remaining terms are defined analogously.

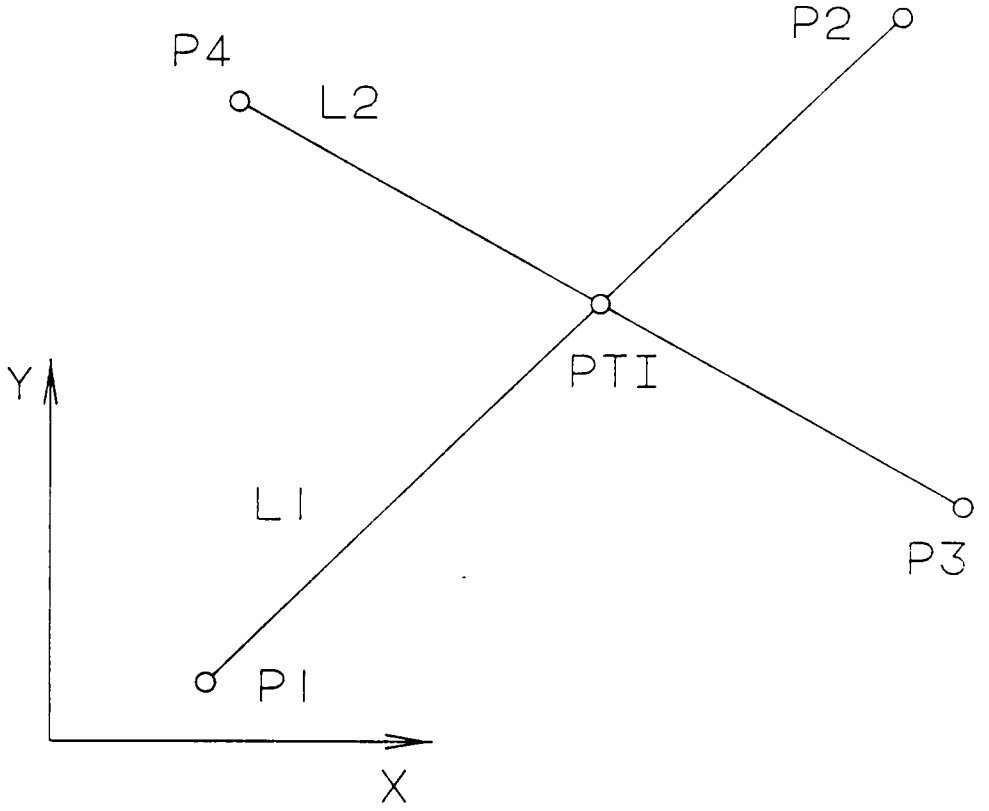

7.3a
General

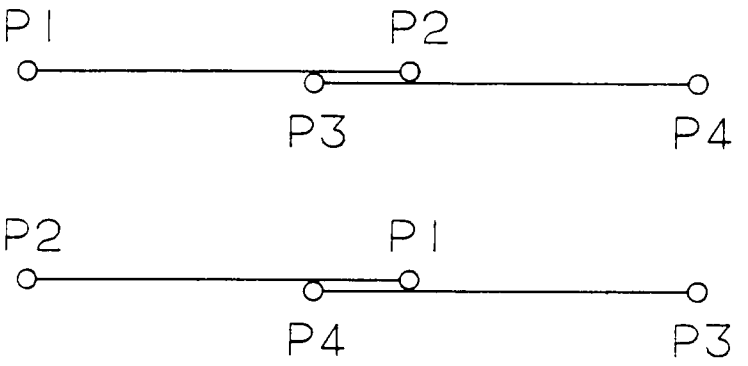

7.3b
m1 = m2 = 0

Figure 7.3
Planar Link Interference Detection

$$\underline{P_1P_2} = \sqrt{(P_{2x} - P_{1x})^2 + (P_{2y} - P_{1y})^2} \tag{7.4}$$

If at least one of the conditions of Eqs. 7.3a and 7.3b is violated, the pair of links is free from interference.

7.1.2 Special Cases in Link Interference Detection

The above theory describes general link interference determination. The following special cases must be considered and solved in order to produce a robust algorithm.

The above calculation for $\underline{PTI}$ fails when the two links are parallel. When this case occurs, the two slopes from Eqs. 7.1a and 7.1b are equal, and the denominator of Eq. 7.2b is zero. The physical interpretation is that the intersection point of two parallel lines is at infinity. Provided that no link or fixed pivot dimensions are zero, interference is not possible between two parallel links.

The second special case is infinite slope, occurring when one of the links is vertical. If both links are vertical, they are parallel and covered by the above discussion. If link L_1 is vertical, the denominator of Eq. 7.1a is zero, leading to infinite slope. Alternate solution #1 for intersection point $\underline{PTI}$, used when line L_1 is vertical, is as follows. The unknown PTI_x is the X-coordinate of either endpoint, $\underline{P_1}$ or $\underline{P_2}$. This value is substituted into the right side of Eq. 7.2a to solve for the unknown PTI_y.

$$PTI_x = P_{1x} \tag{7.5a}$$

$$PTI_y = m_2(P_{1x} - P_{3x}) + P_{3y} \tag{7.5b}$$

Similarly, alternate solution # 2 for $\underline{PTI}$ is used when link L_2 is vertical.

$$PTI_x = P_{3x} \tag{7.6a}$$

$$PTI_y = m_1(P_{3x} - P_{1x}) + P_{1y} \qquad (7.6b)$$

For both alternate solutions dealing with infinite slope, the interference conditions are again given by Eqs. 7.3a and 7.3b.

The third special case arises when both slopes are zero, leading to zero denominator in Eq. 7.2b. The physical behavior is either no intersection, or infinitely many along the line segment of intersection. If either slope m_1 or m_2 is non-zero, the previously developed theory may be used. When $m_1 = m_2 = 0$, and both links lie on the same Y-coordinate, interference is determined using the following logic, with reference to Fig. 7.3b. Link interference occurs when either Eq. 7.7a or Eq. 7.7b is satisfied.

$$P_{2x} > P_{3x} \quad AND \quad P_{4x} > P_{1x} \qquad (7.7a)$$

$$P_{1x} > P_{4x} \quad AND \quad P_{3x} > P_{2x} \qquad (7.7b)$$

Figure 7.4 shows the flow chart for the position dependent link interference determination algorithm, including all of the special cases.

7.2 Effect of Link Interference on Optimum Workspaces

In this section the theory of Section 7.1 is applied to determine the effects of link interference on planar robotic mechanism workspaces. Specifically, the optimized workspaces of the "N5R5", "N6R6", and "N8R9-1" manipulators are scrutinized. These workspaces were developed in Chapter 6 without regard to link interference.

There are multiple solutions to the inverse kinematic position problem for these robotic mechanisms; the "N8R9-1" has eight solutions, while the "N5R5" and "N6R6" each have four solutions. Therefore, to better understand the nature of the link interference problem, two distinctions are used for each reachable and dextrous workspace reported in this section. The

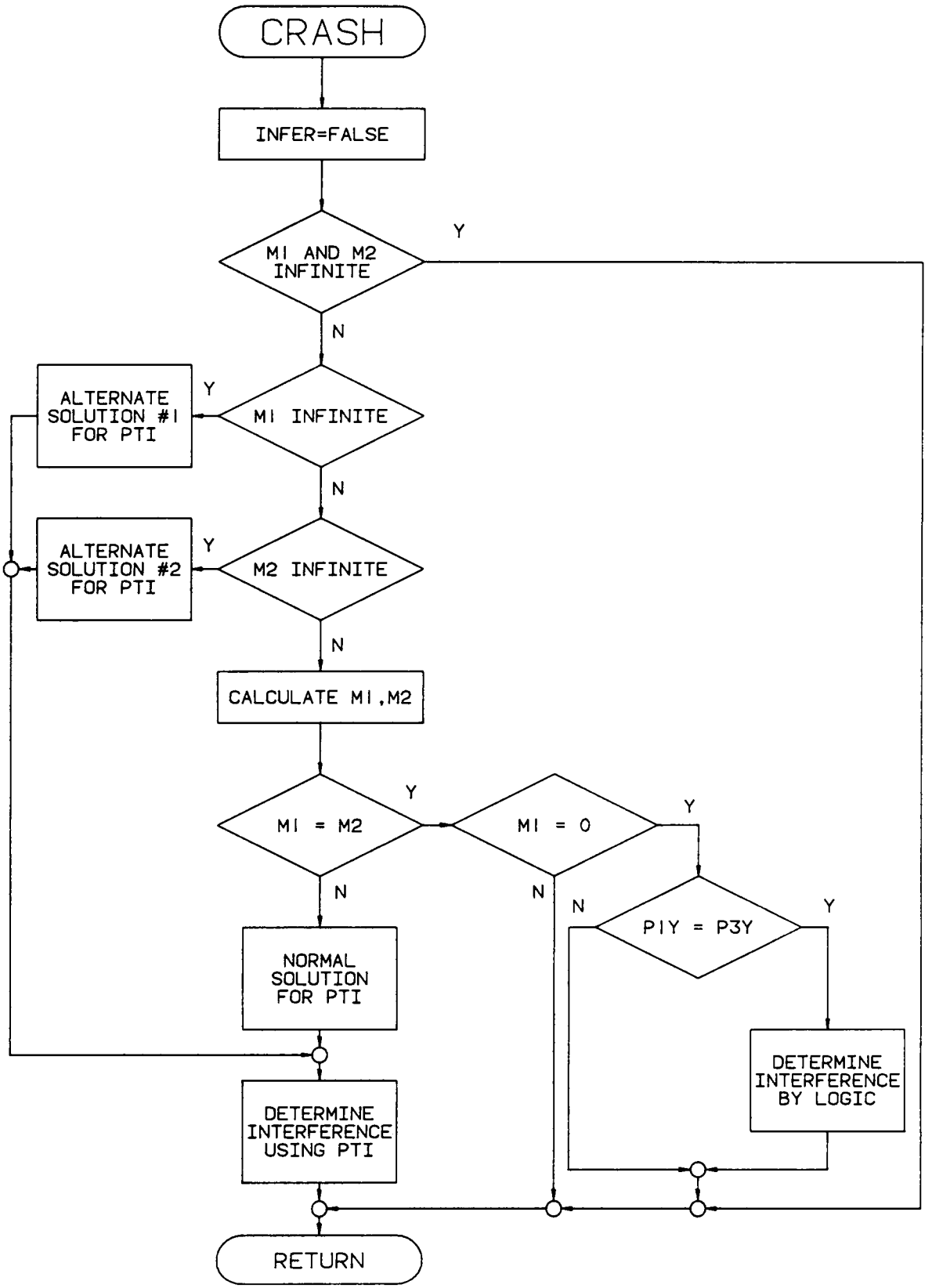

Figure 7.4
Link Interference Algorithm Flowchart

"one-free" attribute denotes that at least one of the multiple kinematic position solutions is free from link interference. The "totally-free" designation implies that the workspace shown is free of link interference in all possible solutions. The "totally-free" workspace is a greater restriction and thus its area is always less than or equal to that of the "one-free" workspace.

From the "N8R9-1" geometry of Fig. 2.5 it is evident that if one solution exists, then all eight solutions assemble mathematically. However, for both the "N5R5" and "N6R6" manipulators, either zero, two, or four solutions are possible, due to the associated geometries. The computer link interference routine need only be applied to solutions that assemble mathematically.

7.2.1 "N5R5" Manipulator

The optimum workspace of the "N5R5" planar robotic mechanism is shown in Fig. 6.7. This manipulator workspace is unaffected by link interference. That is, the "one-free" and "totally-free" workspaces are identical to the original optimum workspace of Fig. 6.7.

7.2.2 "N6R6" Manipulator

The "N6R6" reachable optimum workspace (without internal void) is a solid circle of radius r = 0.7320. The effect of link interference on this optimum workspace is shown in Figs. 7.5a and 7.5b, presenting the "one-free" and "totally-free" workspaces, respectively. The mathematical optimum workspace (r = 0.7320) is represented by the dashed circle on Figs. 7.5a and 7.5b. The "N6R6" "one-free" workspace has a slightly reduced boundary and two small internal voids. The "totally-free" workspace has the same boundary as the "one-free", but more internal voids. In Section 6.2.2.1, the "N6R6" reachable workspace is optimized such

that the associated dextrous workspace is null. Therefore, the "one-free" and "totally-free" dextrous workspaces do not exist for the optimum reachable workspace case.

Without considering link interference, the optimum dextrous workspace of the "N6R6" manipulator is a solid circle with r = 0.5774, shown in Fig. 6.11b. The "N6R6" dextrous "one-free" and "totally-free" workspaces are shown in Figs. 7.6a and 7.6b, respectively. The mathematical boundary is preserved in Fig. 7.6a, with the exception of two notches. There is also an internal void. Again, the "totally-free" workspace is similar, but more restricted.

7.2.3 "N8R9-1" Manipulator

For the "N8R9-1" manipulator, the optimum workspace depends on the specified fixed pivot distance, L. For L = 0.10, the optimum mathematical reachable workspace is given in Fig. 6.15b, along with the associated dextrous workspace. The reachable workspace is circle of radius R = 0.3141 and thus area A = 0.3099; the dextrous workspace is a "triangle" with circular arc sides and area A = 0.1420.

The reachable "one-free" workspace is not shown because it is identical to the reachable workspace given in Fig. 6.15b. That is, for the reachable workspace of this optimum "N8R9-1" manipulator, all points in the mathematical workspace have at least one solution free of link interference. The reachable "totally-free" workspace is shown in Fig. 7.7a. The optimum mathematical workspace boundary (R = 0.3141) is evident, but there is a serious reduction in area due to link interference.

The dextrous "one-free" workspace of this "N8R9-1" manipulator, shown in Fig. 7.7b, also has a greatly reduced area when considering link interference. The dashed lines show the mathematical dextrous workspace boundary. The dextrous "totally-free" workspace is null; there are no points totally free of link interference in the dextrous workspace of this optimum manipulator.

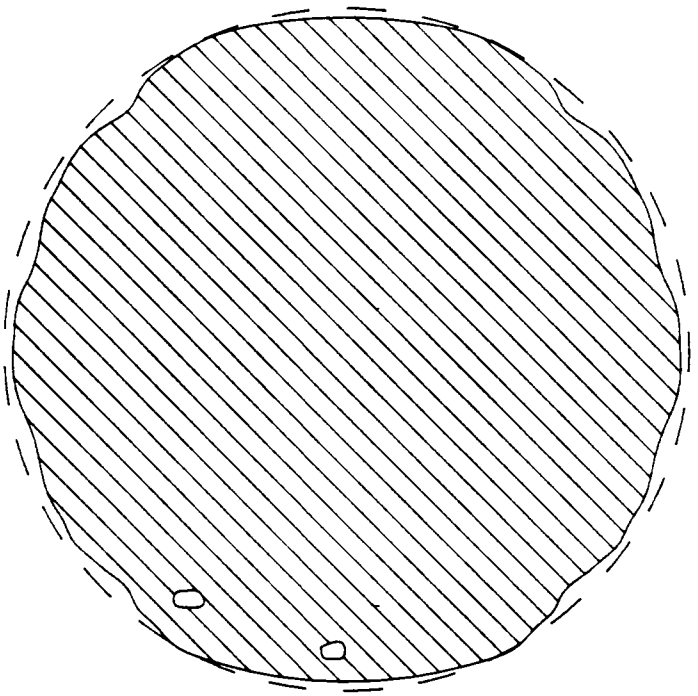

7.5a
"One-Free"

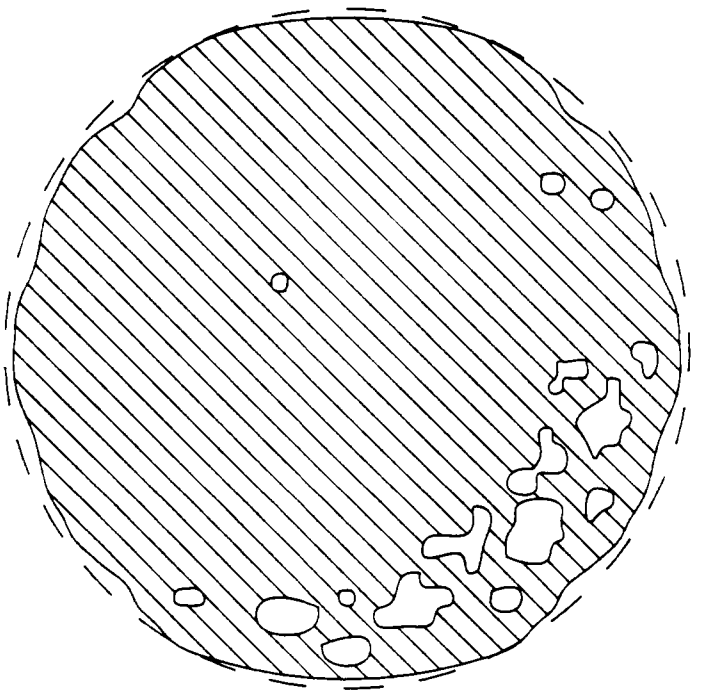

7.5b
"Totally-Free"

Figure 7.5
"N6R6" Reachable Workspace
Considering Link Interference

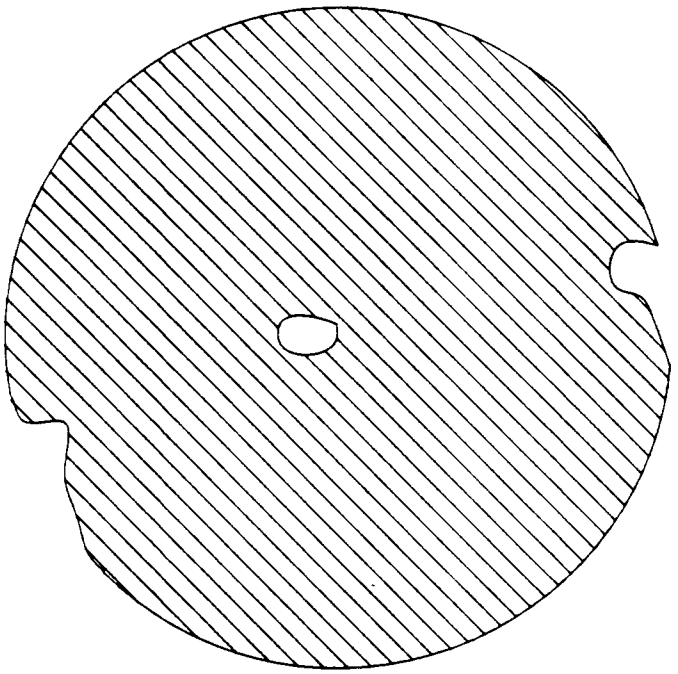

7.6a
"One-Free"

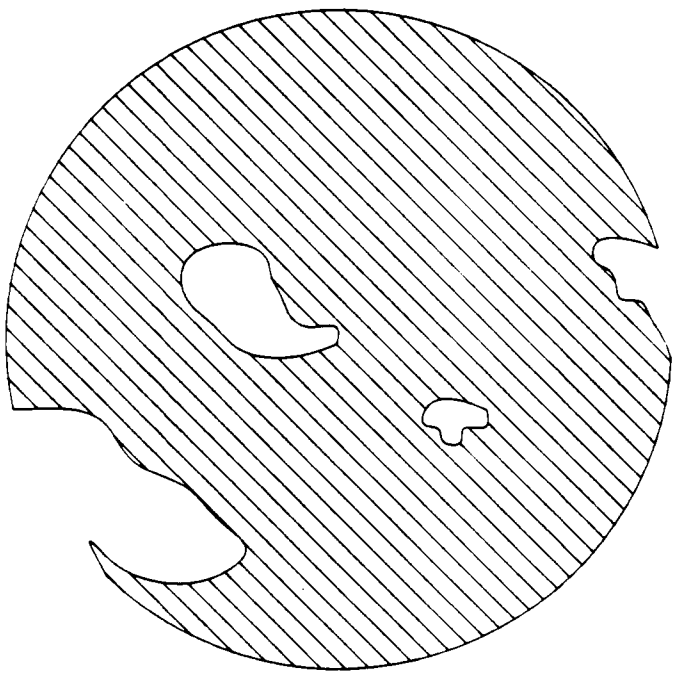

7.6b
"Totally-Free"

Figure 7.6
"N6R6" Dextrous Workspace
Considering Link Interference

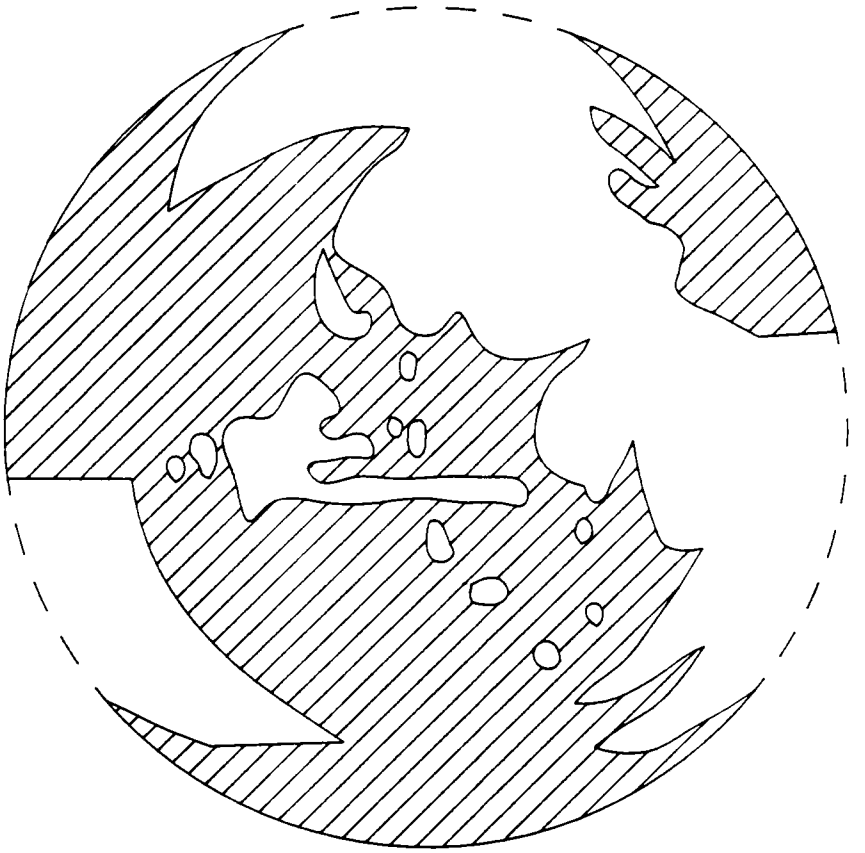

7.7a
Reachable "Totally-Free"

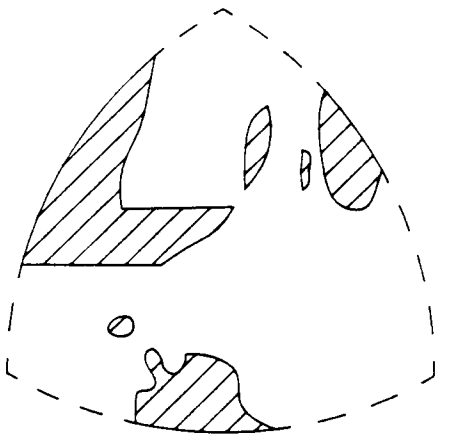

7.7b
Dextrous "One-Free"

Figure 7.7
"N8R9-1" Workspace
Considering Link Interference

7.3 *Link Interference-Free Workspace Optimization*

In this section, the reachable and dextrous workspaces of the "N6R6" and "N8R9-1" manipulators are re-optimized subject to the constraint of freedom from link interference. The method is independent of position information. The treatment is not presented in detail because it is similar to the closed-form workspace development in Chapter 6. The Z-plane configurations of the above manipulators are shown in Figs. 7.1 and 7.2. As stated in the previous section, the "N5R5" optimum mathematical workspace developed in Chapter 6 is already free from link interference and thus warrants no further treatment.

7.3.1 "N6R6" Manipulator

In the "N6R6" manipulator only one link pair (b-d) has a possibility of interference. From the connectivity geometry, these two links never interfere if the following condition is satisfied.

$$b + d \leq c \tag{7.8}$$

This is not a necessary condition. That is, if this condition is violated, freedom from link interference may be possible. This statement is evidenced by the "N5R5" optimum workspace example.

For interference-free "N6R6" workspace optimization, the optimal criterion c=d (Eq. 6.5c) is replaced by Eq. 7.8 with equality as the limiting case. The remaining optimal criteria (Eqs. 6.5a, 6.5b, and 6.10) and normalization condition (Eq. 6.1c) are still used.

The re-optimization results are as follows. The optimum "N6R6" reachable workspace is a planar concentric disk with $R_o = 0.7800$ and $R_i = 0.2200$, occurring at h=0.50. The associated area is A = 1.7597, a 3% reduction compared to the mathematical optimum "N6R6"

reachable workspace. The optimum workspace without an internal void occurs at h = 0.359; it is a circular disk of radius R = 0.718 and area A = 1.6196, representing a 4% reduction. In this section, the percent area reduction refers to the decrease from the original mathematical optimum area. Therefore, the "reduced" areas in the re-optimization may represent larger areas when link interference is considered.

The optimization process for the dextrous "N6R6" workspace free of link interference again replaces the constraint c=d by Eq. 7.8. With this exception, the remaining optimal criteria and normalization equation are the same as those developed in Chapter 6. All possible "N6R6" manipulators obeying these conditions are circular disks , with an internal void. The condition c=d is required to provide a solid workspace; this is not possible excepting the trivial case b=0. The optimization result is d = 0.250, $R_o = 0.5639$ and $R_i = 0.1711$, and area A = 0.9070, which is a 13% reduction from the mathematical optimum dextrous "N6R6" manipulator workspace.

7.3.2 "N8R9-1" Manipulator

The geometry of the "N8R9-1" manipulator shown in Fig. 7.2 indicates that links a-f-p and b-d-k may interfere. From the connectivity geometry, the following non-necessary conditions ensure freedom from link interference in all manipulator motion ranges.

$$a + f \leq L \qquad b + d \leq c \tag{7.9a}$$

$$f + p \leq L \qquad d + k \leq c \tag{7.9b}$$

$$p + a \leq L \qquad k + b \leq c \tag{7.9c}$$

The optimum reachable workspace criterion c = L (Eq. 6.26) is still imposed, as well as Eq. 6.20. Therefore, the above six conditions may be represented by a single equation, where equality represents the limiting case.

$$2a = L = \sqrt{3}\, LH \tag{7.10}$$

Combining Eq. 7.10, Eq. 6.20, and the normalization condition (Eq. 6.1e), LH is uniquely solved to be LH = 0.1614. This leads to a = 0.1400 and L = c = 0.2800. The resulting optimum reachable workspace is a solid circle of radius R = 0.2800, area A = 0.2463, and thus a 20% area reduction from the mathematical reachable workspace optimum for L=0.10. The associated dextrous workspace is null; this fact is supported by Eq. 6.23 and Fig. 6.16a. Therefore, all "N8R9-1" manipulators with a dextrous workspace have the potential for link interference problems.

Chapter 8 Further Topics and Conclusion

8.1 Further Topics

Various topics which have relevance to this dissertation but are not presented in detail are briefly discussed in this section. The subjects in this section are spatial robotic mechanisms, variable geometry trusses, manipulator stiffness, and extra freedom configurations and safety.

8.1.1 Spatial Parallel Robotic Mechanisms

The theory and applications of robotic mechanisms are limited to planar manipulators in this dissertation. The motion of all links may be represented in one plane. As mentioned in Chapter 2, planar robotic mechanisms are made more versatile by the addition of Z-axis travel for the hand. If this is done, the area reachable by the manipulator hand extends to a volume, which enables the manipulator to perform more complicated tasks. However, the stiffness advantage of parallel robotic mechanisms may not apply outside of the plane of mo-

tion. In addition, with a simple Z-axis hand motion, the hand orientation is controlled only about the Z-axis, perpendicular to the plane of motion. A natural extension of the work in this dissertation is spatial in-parallel-actuated robotic mechanisms. This section briefly discusses topics relevant to spatial robotic mechanisms.

Type and number synthesis for spatial robotic mechanisms is performed analogously to that for planar robotic mechanisms, presented in Chapter 2. The Grubler equation (Eq. 2.1) for predicting overall planar degrees-of-freedom is replaced by the Kutzbach equation for predicting overall spatial degrees-of-freedom:

$$F = 6(N-1) - 5J_1 - 4J_2 - 3J_3 - 2J_4 - J_5 \qquad (8.1)$$

where:

F ≡ number of freedoms of the device

N ≡ number of links (including ground)

J_1 ≡ number of 1 DOF joints

J_2 ≡ number of 2 DOF joints

J_3 ≡ number of 3 DOF joints

J_4 ≡ number of 4 DOF joints

J_5 ≡ number of 5 DOF joints

For general spatial tasks, a minimum of six degrees-of-freedom is required to control position and orientation within a fixed reference frame, so spatial manipulators must possess at least six overall degrees-of-freedom. A second alternative is to design a three degree-of-freedom spatial manipulator to achieve the position in space; a hand with three more degrees-of-freedom is then required to provide the general orientation capability. Therefore, F can be either six or three in Eq. 8.1. Assuming only one, two, and three degree-of-freedom joints are used, the Kutzbach equation is rearranged to calculate values of J_1 given N, J_2 , and J_3. Only integer values for J_1 are of practical use. Equation 8.2a represents F=6 and Eq. 8.2b represents F=3.

$$J_1 = \frac{6N - 4J_2 - 3J_3 - 12}{5} \tag{8.2a}$$

$$J_1 = \frac{6N - 4J_2 - 3J_3 - 9}{5} \tag{8.2b}$$

From Eqs. 8.2a and 8.2b, infinitely many combinations produce manipulators of six or three degrees-of-freedom. Due to the presence of two and three degree-of-freedom joints, the possible combinations of configurations are more complicated for the spatial case than the planar case. Therefore, the mobility results given in Tables 8.1a and 8.1b (for F=6 and F=3, respectively) have the following limitations: $J_2 = 0$, $J_3 \leq 12$, and $N \leq 20$. Each entry of Tables 8.1a and 8.1b generally represents several connectivity possibilities. Example spatial robotic mechanisms are presented for F=6 and F=3, in Figs. 8.1a and 8.1b, respectively.

The three degree-of-freedom manipulator pictured in Fig. 8.1b comes from entry 14 of Table 8.1b. The six degree-of-freedom manipulator pictured in Fig. 8.1a is a special mobility case; it is not derived from an entry in Table 8.1a. This device has fourteen links, six one degree-of-freedom joints, and twelve three degree-of-freedom joints. Kutzbach's criterion predicts twelve global degrees-of-freedom for this combination. However, there are six idle degrees-of-freedom, one about each S-S leg. Therefore, a total of six effective degrees-of-freedom exist. The manipulator of Fig. 8.1a is Stewart's Platform (Stewart, 1965), discussed previously in Section 1.2. This device was originally designed to be a flight simulator. It may also be viewed as a spatial parallel robotic mechanism.

From Figs. 8.1a and 8.1b, it is intuitively evident that the stiffness of spatial parallel robotic mechanisms is high relative to spatial serial robots. The load bearing characteristics are similarly greater. However, the potential for link interference is great, which further limits the relatively small workspace compared to serial manipulators. Spatial robotic mechanisms are geometrically complex, and thus the forward and inverse kinematic position problems are generally difficult to solve. Indeed, practical application of such devices may be limited to those configurations that possess simple closed-form solutions to the kinematic position

Table 8.1a Spatial Mobility for F = 6

J_3	N	J_1
0	2	0
0	7	6
0	12	12
0	17	18
1	5	3
1	10	9
1	15	15
1	20	21
2	3	0
2	8	6
2	13	12
2	18	18
3	6	3
3	11	9
3	16	15
4	4	0
4	9	6
4	14	12
4	19	18
5	7	3
5	12	9
5	17	15
6	5	0
6	10	6
6	15	12
6	20	18
7	8	3
7	13	9
7	18	15
8	6	0
8	11	6
8	16	12
9	9	3
9	14	9
9	19	15
10	7	0
10	12	6
10	17	12
11	10	3
11	15	9
11	20	15
12	8	0
12	13	6
12	18	12

Table 8.1b Spatial Mobility for F = 3

J_3	N	J_1
0	4	3
0	9	9
0	14	15
0	19	21
1	2	0
1	7	6
1	12	12
1	17	18
2	5	3
2	10	9
2	15	15
2	20	21
3	3	0
3	8	6
3	13	12
3	18	18
4	6	3
4	11	9
4	16	15
5	4	0
5	9	6
5	14	12
5	19	18
6	7	3
6	12	9
6	17	15
7	5	0
7	10	6
7	15	12
7	20	18
8	8	3
8	13	9
8	18	15
9	6	0
9	11	6
9	16	12
10	9	3
10	14	9
10	19	15
11	7	0
11	12	6
11	17	12
12	10	3
12	15	9
12	20	15

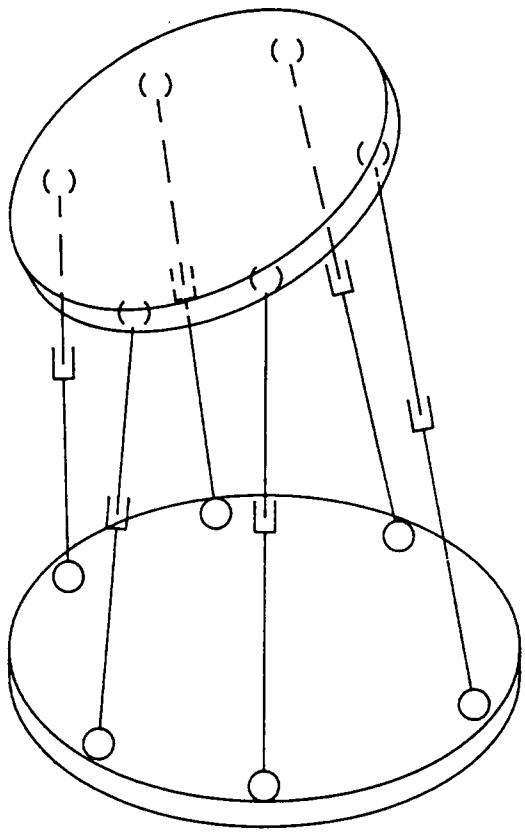

8.1a
Stewart's Platform
("N14P6S12")

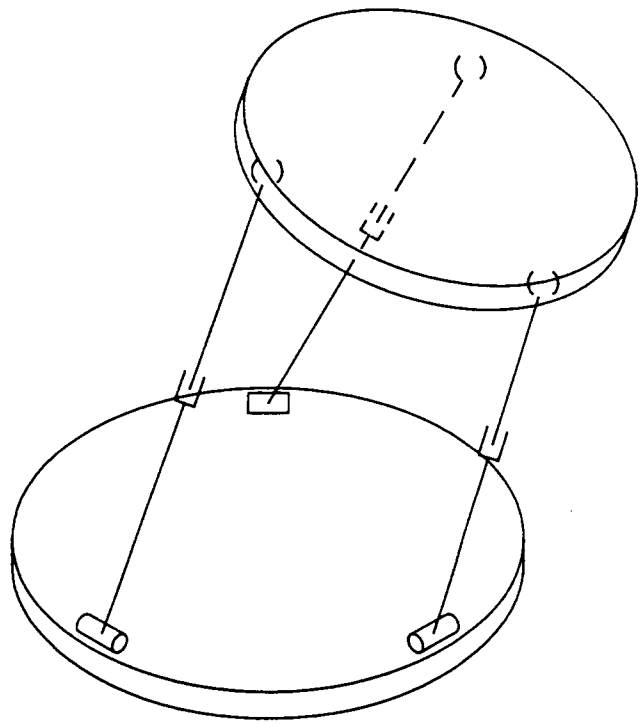

8.1b
"N8R3P3S3"

Figure 8.1
Spatial Parallel Robotic Mechanisms

problems. Such manipulators seem to be in the minority. Further research into spatial robotic mechanisms is warranted in order to realize their capabilities as robotic manipulators.

8.1.2 Variable Geometry Trusses

Variable Geometry Trusses (VGTs) are a family of kinematic structures closely related to the robotic mechanisms discussed in this dissertation. VGTs are either planar or spatial. They are trusses with a number of extensible links; the number of extensible links equals the degree-of-freedom of the VGT. Originally developed as collapsing structures for space applications, VGTs may also be viewed as robotic manipulators.

VGTs may be designed to possess hundreds of degrees-of-freedom. Their kinematic topologies generally consist of identical modules repeated many times. The kinematic position problem of one module may be solved once and then applied to each module in order to achieve the total solution. The position solution of each module may be closed-form or numerical; closed-form solutions are desired.

The joints of a VGT are designed so that all links, including the extensible links, are two-force members. Thus, the load bearing characteristics are excellent. The structural mass is also relatively low. Due to the truss nature of VGTs, the structural stiffness is high. As a robotic manipulator, however, running speeds may be slow. Unlike many parallel manipulators studied on this dissertation, VGTs can reach back to their own base. The snake-like, modular structure makes VGTs an extensive, stiff, serial-like manipulator, suitable for applications such as remote nuclear plant maintenance, plus ocean and space functions.

8.1.3 Parallel Manipulator Stiffness

The stiffness, or resistance to deflection, of parallel robotic mechanisms is one of the primary advantages of this type of manipulator. With high stiffness, the deflections are small and the load bearing capability is large. In addition, the accuracy is better and/or the structural mass is reduced, compared to a serial manipulator. The stiffness of parallel robotic mechanisms may be modelled using the finite element method or an iterative approach with a closed form solution at each step.

Manipulator stiffness is not studied quantitatively in this dissertation. Intuitively, the stiffness of parallel robotic mechanisms is much greater than that of serial configurations. This statement is backed up by a manipulator stiffness study performed by Y.P. Tsang in a class project at Virginia Polytechnic Institute and State University (Tsang, 1984). Comparing normalized stiffnesses for planar manipulators, Tsang found that if the linear deflection of a fully-parallel manipulator under load is 1.0, a parallel-serial configuration's displacement is 3.5, while a serial robot's displacement is 20.0. Similarly, the results for angular deflection are 1.0, 3.0, and 15.0, respectively. Therefore, the fully-parallel manipulator configuration is fifteen to twenty times stiffer than its serial counterpart. Though the study is limited in scope, it dramatically shows the parallel manipulator stiffness advantage. Spatial parallel manipulators may enjoy an even greater stiffness advantage over spatial serial robots.

Further research into the stiffness of various manipulator configurations is warranted. Parallel robotic mechanisms avoid the need for complex control systems for accurate positioning; the necessary stiffness is inherent in the geometry. In order to compare the stiffness of different robotic manipulator configurations, a non-dimensionalized stiffness number must be developed.

The stiffness of parallel robotic mechanisms may be further increased by driving more motors than the existing manipulator degrees-of-freedom. Figure 2.9 shows the three degree-of-freedom "N10R12" robotic mechanism which has four dyads connecting the hand link to the ground link. Three motors at G1, G2, and G3 control the three degrees-of-freedom.

A fourth motor may be added at G4 to provide a preload in the structure. This extra motor would be driven against the other three so that the joint clearances are never slack. Serial manipulators do not have this option for increasing stiffness.

8.1.4 Extra Freedom Configurations and Safety

Planar parallel robotic mechanisms have the potential for a peculiar kinematic defect. Under specific geometric conditions, especially for symmetric manipulators, extra freedom(s) may arise. The result is chaotic motion which cannot be controlled. This condition arises from parallel topology, and thus does not affect serial robots.

Figure 8.2a shows the three degree-of-freedom "N8R9-1" manipulator in a geometric position where there are actually four degrees-of-freedom. The manipulator is symmetric, corresponding links are parallel, and the hand angle is zero. The three links attached to the ground link are positioned by motors. Figure 8.2b shows the manipulator sub-structure when the above three links are fixed. Normally, this sub-chain is a structure ($F=0$). However, due to the parallel nature of the sub-structure, it has one degree-of-freedom: it is a parallelogram four-bar linkage with another parallel, equal link attached. In reality, the links will not line up perfectly parallel, but will be close enough to cause an extra freedom problem.

It is possible that this condition is desired in certain situations. For example, the manipulator of Fig. 8.2a could be driven into the position shown after use in order to fold up into a compact space for storage. However, this problem is generally undesirable and potentially dangerous. It must be guarded against through geometric design and/or robot control.

Another safety concerned should be addressed. In practical robot applications, safety dictates that there should be a warning line to separate humans and objects from the robot's reach. Usually this warning line is based on the effective workspace of the robot hand, projected onto the floor. For parallel manipulators, it is common for moving links to extend outside of the manipulator hand workspace. Therefore, the safety line must be expanded to account for all such possibilities.

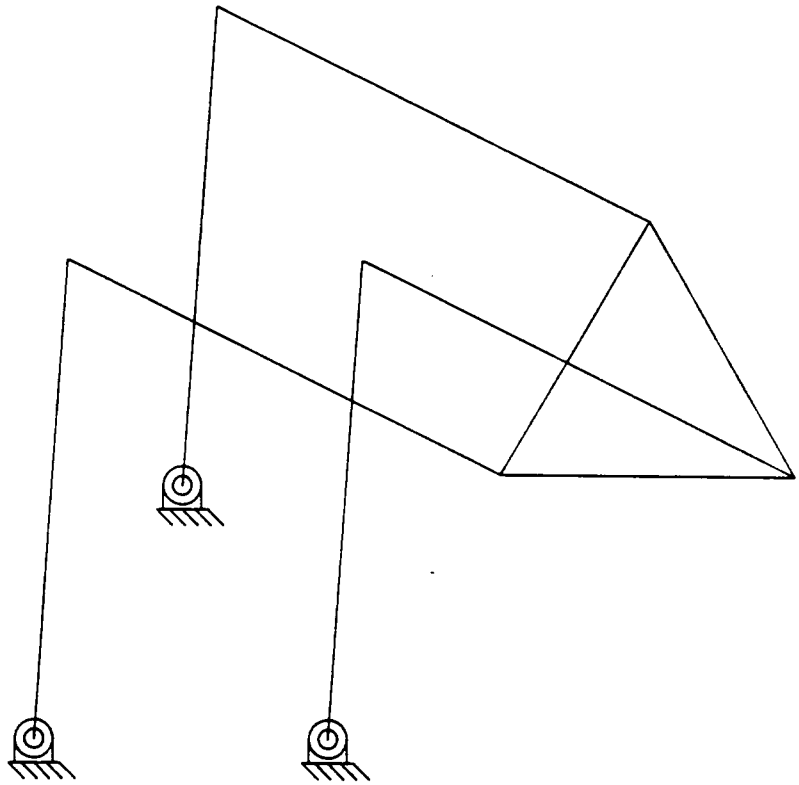

8.2a
"N8R9-1" Manipulator with
Zero Hand Angle

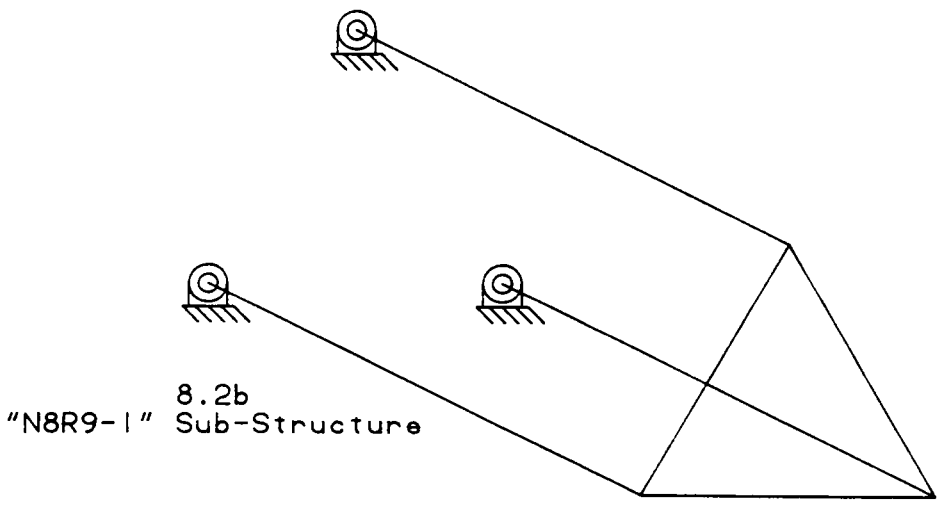

8.2b
"N8R9-1" Sub-Structure

Figure 8.2
Extra Freedom Configuration

8.2 Conclusion

This dissertation presents analysis and configuration comparisons of planar robotic mechanisms. Robotic mechanisms are closed-loop, in-parallel actuated robotic manipulators. They have been proposed and investigated in the robotics field as an alternative to the existing serial industrial robot configuration. The primary advantage of robotic mechanisms is high accuracy, which is provided through manipulator geometry, rather than sensing, control techniques, or composite materials. The high stiffness leads to high load bearing capability. The primary disadvantage of robotic mechanisms is a limited workspace, further reduced by link interference problems.

This section discusses the conclusions and highlights of the foregoing chapters which combine to provide complete kinematic design for planar robotic mechanisms. The individual topics are type and number synthesis, kinematic position solution, velocity and acceleration analysis, kinetostatic analysis, workspace optimization, and link interference avoidance.

Chapter 2 develops type and number synthesis for planar robotic mechanisms. Using Grubler's criterion for planar degrees-of-freedom, combinations of links and one degree-of-freedom joints are calculated for two and three manipulator degrees-of-freedom. Eight potentially useful planar robotic mechanisms are identified for subsequent use in later chapters. There are infinitely many manipulators having two or three planar degrees-of-freedom; the specific manipulators of Chapter 2 are chosen based on relative geometric simplicity.

Chapter 3 presents forward and inverse kinematic position solutions for planar robotic mechanisms. A closed-form algorithm is repeatedly applied to achieve an efficient overall closed-form solution. The forward kinematic problems of three specific manipulators have six solutions, so no closed-form solution exists. However, with the aid of Sylvester's eliminant, the solution is obtained in terms of a sixth degree polynomial. The methods of Chapter 3 are adaptable to other manipulators; as the geometric complexity increases, closed-form solutions may not exist. In general, there are multiple solutions to a given forward or inverse kinematic position problem. This presents a challenge for robot control.

Following the kinematic position solution, forward and inverse velocity and acceleration analysis involves linear systems of equations, as detailed in Chapter 4. Therefore, there is generally a unique solution to the derivative problem. Velocity and acceleration solutions are used in manipulator motion control and dynamics analysis.

Chapter 5 presents a matrix method for kinetostatic analysis. A power requirement comparison is made between three general manipulator configurations: serial, parallel-serial, and fully parallel. Physical manipulator parameters are assumed for comparison purposes only. The workspaces of three specific comparison manipulators are designed to be approximately equal. The result is that the fully parallel manipulator requires about five times more power than the other two configurations. This result is not necessarily a condemnation of parallel robotic mechanisms from a dynamic point of view. The study does not account for robot stiffness; the parallel manipulator links may be sized smaller than the serial robot links and still provide a stiffness advantage. In Chapter 5, the same link cross section was used for all three manipulator configurations. The parallel manipulator encounters more positions near dynamic singularities where a pair of links fold upon each other. Parallel robotic mechanism dynamic characteristics are likely to be better than serial configuration dynamics if robot stiffness is considered and a smaller workspace is sufficient. Parallel robots may be designed with all motors fixed to the ground link, which represents a significant dynamic advantage over serial robots with moving motors.

Workspace determination and optimization is presented in Chapter 6. The first part is a numerical workspace maximization that deals with eight manipulators from Chapter 2. The three manipulators with the largest reachable workspaces are selected for further consideration. Closed-form geometrical methods are developed for reachable and dextrous workspace determination applied to the three robotic mechanisms. Using these methods, workspace area is maximized, based on normalization constraints. The methods of Chapter 6 are extendable to various robotic mechanism configurations. Workspace optimization of planar robotic mechanisms is important to mitigate the effects of reduced workspace compared to serial robots.

The relatively small workspace of a planar robotic mechanism may be further reduced by link interference, covered in Chapter 7. A position-dependent link interference detection method is developed and used to determine the actual workspace of the three optimized manipulator workspaces from Chapter 6 (Chapter 6 ingores link interference). The result is drastically reduced workspaces due to link interference. Therefore, workspace optimization is repeated, with the additional constraint of freedom from link interference. Link interference is a serious problem which must be remedied through geometrical design or robot control.

This dissertation presents a balanced view of the advantages and disadvantages of planar robotic mechanisms compared to serial robots. The overall recommendation is that robotic mechanisms should be pursued as a versatile alternative. This dissertation provides the analytical basis for complete kinematic design of planar robotic mechanisms. Primarily due to excellent stiffness and load bearing characteristics, robotic mechanisms are a promising future alternative to the conventional serial manipulator configuration.

References

Aradayfio, D.D., and Qiao, D., "Kinematic Simulation of Novel Robotic Mechanisms Having Closed Kinematic Chains", ASME Paper 85-DET-81, 1985.

Baker, J.E., "On Mobility and Relative Freedom in Multi-Loop Linkages and Structures", *Mechanism and Machine Theory*, v. 16, n. 6, 1981, pp. 583-597.

Cox, D.J., and Tesar, D., "The Dynamic Modeling and Command Signal Formulation for Parallel Multi-Parameter Robotic Devices", Department of Energy Report, 1981.

Cwiakala, M., "Workspace of a Closed-Loop Manipulator", ASME Paper 86-DET-95, 1986.

Davies, T.H., "Kirchoff's Circulation Law Applied to Multi-Loop Kinematic Chains", *Mechanism and Machine Theory*, v. 16, 1981, pp. 171-183.

Djoldasbekov, U.A., and Slutskii, L.I., "Manipulator with Variable Link Lengths: Kinematics and Possibilities", *Mechanism and Machine Theory*, v. 18, n. 4, 1983, December 1983, pp. 271-274.

Earl, C.F., and Rooney, J., "Some Kinematic Structures for Robot Manipulator Design", *Journal of Mechanisms, Transmissions, and Automation in Design*, v. 105, n. 1, March 1983, pp. 15-22.

Fichter, E.F., and McDowell, E.D., "A Novel Design for a Robot Arm", *Advances in Computer Technology*, v. 1, 1980, pp. 250-256.

Freeman, R.A., and Tesar, D., "The Generalized Coordinate Selection for the Dynamics of Complex Planar Mechanical Systems", *Journal of Mechanical Design*, Trans ASME, v. 104, n. 1, January 1982, pp. 206-217.

Freudenstein, F., and Mayourian, M., "The Development of an Atlas of the Kinematic Structures of Mechanisms", *Journal of Mechanisms, Transmissions, and Automation in Design*, v. 106, n. 4, December 1984, pp. 458-461.

Ganter, M.A., and Uicker, J.J., "Dynamic Collision Detection Using Swept Solids", *Journal of Mechanisms, Transmissions, and Automation in Design*, v. 108, n. 4, December 1986, pp. 549-555.

Gosselin, C., and Angeles, J., "The Optimum Kinematic Design of a Planar Three-Degree-of Freedom Parallel Manipulator", *Journal of Mechanisms, Transmissions, and Automation in Design*, v. 110, n. 1, March 1988, pp. 35-41.

Gosselin, C., and Angeles, J., "The Optimum Kinematic Design of a Spherical Three-Degree-of Freedom Parallel Manipulator", *Proceedings of the 1987 ASME Design Automation Conference*, DE-Vol. 10-2, September 1987, pp. 111-115.

Hunt, K.H., "Structural Kinematics of In-Parallel-Actuated Robot Arms", *Journal of Mechanisms, Transmissions, and Automation in Design*, v. 105, n. 4, December 1983, pp. 705-712.

Hunt, K.H., "Geometry of Robotic Devices", *Mechanical Engineering Transactions of the Institution of Engineers, Australia*, v. ME7, n. 4, November 1982, pp. 213-220.

Keil, M.J., Myklebust, A., and Reinholtz, C.F., "Prediction of Link Interference in Planar Mechanisms", *Proceedings of the 9th Applied Mechanisms Conference*, Kansas City, MO., October 1985.

Kumar, A., and Waldron, K.J., "The Workspace of a Mechanical Manipulator", *Journal of Mechanical Design*, v. 103, n. 3, July 1981, pp. 665-672.

Mabie, H.H, and Reinholtz, C.F., *Mechanisms and Dynamics of Machinery, Fourth Edition*, John Wiley & Sons, New York, 1987, pp. 413-418.

Mohamed, M.G., "Structural Kinematics of Partially-Parallel Robotic Mechanisms", *Proceedings of the 1987 ASME Design Automation Conference*, DE-Vol. 10-2, September 1987, pp. 31-35.

Mohamed, M.G., and Duffy, J., "A Direct Determination of the Instantaneous Kinematics of Fully Parallel Robot Manipulators", *Journal of Mechanisms, Transmissions, and Automation in Design*, v. 107, n. 2, June 1985, pp. 226-229.

Mruthyunjaya, T.S., "A Computerized Methodology for Structural Synthesis of Kinematic Chains: Part 1 - Formulation; Part 2 - Application to Several Fully or Partially Known Cases; Part 3 - Application to the New Case of 10-link, 3DOF Chains", *Mechanism and Machine Theory*, v. 19, n. 6, 1984, pp. 487-530.

Myklebust, A. and Tesar, D. "Five Position Synthesis of Six-Link Mechanisms Coordinating up to Four Motion Parameters", *Communications of the Third World Congress for the Theory of machines and Mechanisms*, Kupari, Yugoslavia, Sept. 13-20, 1971, pp. 387-424.

Powell, I., "The Kinematic Analysis and Simulation of the Parallel Topology Manipulator", *The Marconi Review*, v. 45, n. 226, 3rd Quarter 1982, pp. 121-138.

Sandor, G.N., Yang, S.P., Xu, L.J., and De, P., "Spatial Kinematic Synthesis of Adaptive Hard Automation Modules: An RS-SRR-SS Adjustable Spatial Motion Generator", *Journal of Mechanisms, Transmissions, and Automation in Design*, v. 108, n. 3, September 1986, pp. 292-299.

Sandor, G.N., and Erdman, A.G., *Advanced Mechanism Design: Analysis and Synthesis, Volume 2*, Prentice-Hall, Inc., Englewood Cliffs, NJ, 1984, pp. 202-204.

Selfridge, R.G., "The Reachable Workspace of a Manipulator", *Mechanism and Machine Theory*,v. 18, n. 2, 1983, pp. 131-137.

Shigley, J.E. and Uicker, J.J., *Theory of Machines and Mechanisms*, McGraw-Hill Book Company, New York, 1980.

Stewart, D., "A Platform with 6 Degrees of Freedom", *Proceedings of the Institute of Mechanical Engineers*, v. 180, Part 1, n. 15, 1965-66, pp. 371-386.

Stoughton, R., and Kokkinis, T., "Some Properties of a New Kinematic Structure for Robot Manipulators", *Proceedings of the 1987 ASME Design Automation Conference*, DE-Vol. 10-2, September 1987, pp. 73-79.

Sugimoto, K., "Kinematic and Dynamic Analysis of Parallel Manipulators by means of Motor Algebra", ASME Paper 86-DET-139, 1986.

Sugimoto, K., and Duffy, J., "Determination of Extreme Distances of a Robot Hand - Part 1: A General Theory", *Journal of Mechanical Design*, v. 103, n. 3, July 1981, pp. 631-636.

Sugimoto, K., and Duffy, J., "Determination of Extreme Distances of a Robot Hand - Part 2: Robot Arms With Special Geometry", *Journal of Mechanical Design*, v. 103, n. 3, October 1981, pp. 776-783.

Sumpter, B., and Soni, A.H., "Simulation Algorithm of Oklahoma Crawdad Robot", *Proceedings of the 9th Applied Mechanisms Conference*, Kansas City, MO., October 1985, pp. VI.1-VI.3.

Tsai, Y.C., and Soni, A.H., "Workspace Synthesis of 3R, 4R, 5R, and 6R Robots", *Mechanism and Machine Theory*, v. 20, n. 6, 1985, pp. 555-563.

Tsang, Y.P., "Computation for the Rigidity Ratio of Three Structural Types of Manipulators", Project for ME 5110, Advanced Kinematics, Virginia Polytechnic Institute & State University, Dr. C.F. Reinholtz, Instructor, Fall, 1984.

Waldron, K.J., "The Constraint Analysis of Mechanisms", *Journal of Mechanisms*, v. 1, 1966, pp. 101-114.

Weng, T., Sandor, G.N., Xu, Y., and Kohli, D., "On the Workspace of Closed-Loop Manipulators with Ground-Mounted Rotary-Linear Actuators and Finite Size Platform", *Proceedings of the 1987 ASME Design Automation Conference*, DE-Vol. 10-2, September 1987, pp. 55-61.

Williams, R.L., and Reinholtz, C.F., "Forward Dynamic Analysis and Power Requirement Comparison of Parallel Robotic Mechanisms", *Proceedings of the 20th Biennial Mechanisms Conference*, Design Engineering Division of ASME, Kissimmee, Fla., Sept. 1988.

Williams, R.L., and Reinholtz, C.F., "Closed-Form Workspace Determination and Optimization for Parallel Robotic Mechanisms", *Proceedings of the 20th Biennial Mechanisms Conference*, Design Engineering Division of ASME, Kissimmee, Fla., Sept. 1988.

Williams, R.L., and Reinholtz, C.F., "Planar Robotic Mechanisms, Part I: Forward and Inverse Kinematic Simulation", *Proceedings of the 1987 Applied Mechanisms Conference*, Volume 1, Session 3b, December 1987.

Williams, R.L., and Reinholtz, C.F., "Planar Robotic Mechanisms, Part II: Workspace Optimization", *Proceedings of the 1987 Applied Mechanisms Conference*, Volume 1, Session 3b, December 1987.

Yan, H.S., and Chen, J.J., "Creative Design of a Wheel Damping Mechanism", *Mechanism and Machine Theory*, v. 20, n. 6, 1985, pp. 597-600.

Yang, D.C.H., and Lee, T.W., "Feasibility Study of a Platform Type of Robotic Manipulator from a Kinematic Viewpoint", *Journal of Mechanisms, Transmissions, and Automation in Design*, v. 106, n. 2, June 1984, pp. 191-198.

Young, L., and Duffy, J., "A Theory for the Articulation of Planar Robots: Part I - Kinematic Analysis for the Flexure and the Parallel Operation of Robots", *Journal of Mechanisms, Transmissions, and Automation in Design*, v. 109, n. 1, March 1987, pp. 29-36.

Young, L., and Duffy, J., "A Theory for the Articulation of Planar Robots: Part II - Motion Planning Procedure for Interference Avoidance", *Journal of Mechanisms, Transmissions, and Automation in Design*, v. 109, n. 1, March 1987, pp. 37-41.

Appendix A. Newton-Raphson Method

The numerical Newton-Raphson predictor-corrector method may be used to solve the position analysis problem of planar robotic mechanisms. This section presents the Newton-Raphson solution technique applied to the forward kinematics problem of the "N8R9-1" manipulator, pictured in Fig. 2.5. The ternary link of this manipulator is assumed equilateral.

The numerical Newton-Raphson method attempts to satisfy the loop closure equations by iteration, given an initial guess for the solution. Convergence is not guaranteed; it is dependent on the initial guess. The input parameters of the "N8R9-1" manipulator are θ_1, θ_2, and θ_3; the output parameters are x_H, y_H, and θ_H. There are four unknown intermediate parameters, the angles ϕ_1, ϕ_2, ϕ_3, and ϕ_4. The angle ϕ_2 is equal to the hand orientation angle θ_H. Because there are four unknowns, two vector loop equations are required.

$$ae^{i\theta_1} + be^{i\phi_1} + ce^{i\phi_2} + de^{i\phi_3} - fe^{i\theta_2} = \underline{G}_2 - \underline{G}_1 \qquad (A.1a)$$

$$ae^{i\theta_1} + be^{i\phi_1} + ce^{i(\phi_2+\frac{\pi}{3})} + ke^{i\phi_4} - pe^{i\theta_3} = \underline{G}_3 - \underline{G}_1 \qquad (A.1b)$$

The Newton-Raphson iterative method is based on the first order Taylor series expansions of Eqs. A.1a and A.1b, which follow.

$$ae^{i\theta_1} + be^{i\phi_1} + ibe^{i\phi_1}\delta_1 + ce^{i\phi_2} + ice^{i\phi_2}\delta_2 + de^{i\phi_3} + ide^{i\phi_3}\delta_3$$

$$-fe^{i\theta_2} = \underline{G}_2 - \underline{G}_1 \qquad (A.2a)$$

$$ae^{i\theta_1} + be^{i\phi_1} + ibe^{i\phi_1}\delta_1 + ce^{i(\phi_2+\frac{\pi}{3})} + ice^{i(\phi_2+\frac{\pi}{3})}\delta_2 + ke^{i\phi_4} + ike^{i\phi_4}\delta_4$$

$$-pe^{i\theta_3} = \underline{G}_3 - \underline{G}_1 \qquad (A.2b)$$

where:

$$\delta_i \equiv \delta\phi_i \qquad i = 1, 2, 3, 4 \qquad (A.2c)$$

Equations A.2a and A.2b are separated into real and imaginary components using Euler's identity. The result is four scalar equations of the form given in Eq. A.3. This linear system of equations results from collecting variation terms on the left and known terms on the right.

$$[J]\{\delta\} = \{GR\} - \{IN\} - \{PV\} \qquad (A.3)$$

Equation A.3 is a general form, applicable to various manipulators. The vector $\{GR\}$ represents the constant ground vector, $\{IN\}$ is the input vector which depends on the input parameters θ_i, and $\{PV\}$ is the position vector which is a function of the previous intermediate parameters ϕ_i. The matrix $[J]$ is the Jacobian matrix. The terms for Eq. A.3 are as follows.

$$[J] = \begin{bmatrix} -b\sin\phi_1 & -c\sin\phi_2 & -d\sin\phi_3 & 0 \\ b\cos\phi_1 & c\cos\phi_2 & d\cos\phi_3 & 0 \\ -b\sin\phi_1 & -c\sin(\phi_2+\frac{\pi}{3}) & 0 & -k\sin\phi_4 \\ b\cos\phi_1 & c\cos(\phi_2+\frac{\pi}{3}) & 0 & k\cos\phi_4 \end{bmatrix} \qquad (A.3a)$$

$$\{\delta\} = \begin{bmatrix} \delta\phi_1 \\ \delta\phi_2 \\ \delta\phi_3 \\ \delta\phi_4 \end{bmatrix} \qquad (A.3b)$$

$$\{GR\} = \begin{bmatrix} G_{2x} \\ G_{2y} \\ G_{3x} \\ G_{3y} \end{bmatrix} \tag{A.3c}$$

$$\{IN\} = \begin{bmatrix} a\cos\theta_1 - f\cos\theta_2 \\ a\sin\theta_1 - f\sin\theta_2 \\ a\cos\theta_1 - p\cos\theta_3 \\ a\sin\theta_1 - p\sin\theta_3 \end{bmatrix} \tag{A.3d}$$

$$\{PV\} = \begin{bmatrix} b\cos\phi_1 + c\cos\phi_2 + d\cos\phi_3 \\ b\sin\phi_1 + c\sin\phi_2 + d\sin\phi_3 \\ b\cos\phi_1 + c\cos(\phi_2 + \frac{\pi}{3}) + k\cos\phi_4 \\ b\sin\phi_1 + c\sin(\phi_2 + \frac{\pi}{3}) + k\sin\phi_4 \end{bmatrix} \tag{A.3e}$$

Convergence to the solution is achieved when Eq. A.4 is satisfied, where ε is the chosen tolerance.

$$|\delta_{max}| \leq \varepsilon \tag{A.4}$$

When convergence is obtained the forward kinematics problem is solved, because the output parameters may be found from the manipulator geometry.

$$x_H = a\cos\theta_1 + b\cos\phi_1 + LH\cos(\theta_H + \frac{\pi}{6}) \tag{A.5a}$$

$$y_H = a\sin\theta_1 + b\sin\phi_1 + LH\sin(\theta_H + \frac{\pi}{6}) \tag{A.5b}$$

$$\theta_H = \phi_2 \tag{A.5c}$$

The inverse kinematics problem may be solved in a similar manner using the Newton-Raphson numerical method. In this case, three vector loop closure equations are written, from the hand to a fixed pivot for each of the three legs of the manipulator. These equations are solved independently, following a procedure similar to that described above.

In general, there are multiple solutions to the kinematic position analysis problem of planar robotic mechanisms. The Newton-Raphson technique yields only one of the possible solutions, depending on the initial guess. Closed-form solutions should be used whenever available, as detailed in Chapter 3.

Appendix B. Forward Kinematics Coefficients

The polynomial coefficients for the forward kinematic solution of the "N8R9-1", "N8R6P3-4", and "N10R12" manipulators are given in this section. One polynomial, Eq. 3.27, solves the forward kinematic position problems for these three manipulators, as discussed in Section 3.3.3.

The S_i coefficients of Eq. 3.27 are given first. This polynomial is in terms of the tangent half-angle of θ_2. All S_i coefficients depend on X_i coefficients, given next.

$$S_1 = -X_1 + X_4 - X_7 + X_9 \tag{B.1a}$$

$$S_2 = -2X_6 + 2X_8 + 2X_2 \tag{B.1b}$$

$$S_3 = 3X_1 - X_4 - X_7 + 3X_9 - 4X_3 + 4X_5 \tag{B.1c}$$

$$S_4 = 4X_8 - 4X_2 \tag{B.1d}$$

$$S_5 = -3X_1 - X_4 + X_7 + 3X_9 + 4X_3 + 4X_5 \tag{B.1e}$$

$$S_6 = 2X_6 + 2X_8 + 2X_2 \tag{B.1f}$$

$$S_7 = X_1 + X_4 + X_7 + X_9 \tag{B.1g}$$

The X_i terms are the coefficients of the trigonometric polynomial, Eq. 3.26.

$$X_1 = 2(H_{22}H_{10} - H_{24}H_1 - H_{26}H_4) \tag{B.2a}$$

$$X_2 = 2(H_{22}H_{11} - H_{23}H_{10} - H_{26}H_6 - H_{25}H_1) \tag{B.2b}$$

$$X_3 = -2(H_{23}H_{11} + H_{26}H_5) \tag{B.2c}$$

$$X_4 = H_{21}H_{10} + 2H_{22}H_{12} - H_{28}H_1 - 2H_{24}H_2 - H_{27}H_4 -$$

$$2H_{26}H_7 + 8H_{26}H_{24} - 2(H_{15}^2 - H_{18}^2) \tag{B.2d}$$

$$X_5 = -2H_{23}H_{13} - H_{27}H_5 - 2(H_{16}^2 - H_{19}^2) \tag{B.2e}$$

$$X_6 = H_{21}H_{11} - 2H_{23}H_{12} + 2H_{22}H_{13} - 2H_{25}H_2 - H_{27}H_6 -$$

$$2H_{26}H_8 + 8H_{26}H_{25} - 4(H_{15}H_{16} - H_{18}H_{19}) \tag{B.2f}$$

$$X_7 = H_{21}H_{12} + 2.H_{22}H_{14} - H_{28}H_2 - 2H_{24}H_3 - H_{27}H_7 - 2H_{26}H_9 +$$

$$4(H_{27}H_{24} + H_{26}H_{28}) - 4(H_{15}H_{17} - H_{18}H_{20}) \tag{B.2g}$$

$$X_8 = H_{21}H_{13} - 2H_{23}H_{14} - 2H_{25}H_3 - H_{27}H_8 + 4H_{27}H_{25} - 4(H_{16}H_{17} - H_{19}H_{20}) \tag{B.2h}$$

$$X_9 = H_{21}H_{14} - H_{28}H_3 - H_{27}H_9 + 2H_{27}H_{28} - 2(H_{17}^2 - H_{20}^2) \tag{B.2i}$$

The X_i terms depend on H_i terms, which are given below. The H_i terms are functions of the fixed parameters of the "N8R9-1" sub-structure pictured in Fig. 3.2b, either directly or through Eqs. 3.22c, 3.23c, 3.23e, and 3.23f.

$$H_1 = 4(r_1 r_2)^2 \tag{B.3a}$$

$$H_2 = -4R_1 r_1 r_2 \tag{B.3b}$$

$$H_3 = R_1^2 \tag{B.3c}$$

$$H_4 = 4RR^2 \tag{B.3d}$$

$$H_5 = 4RI^2 \tag{B.3e}$$

$$H_6 = 8RR(RI) \tag{B.3f}$$

$$H_7 = -4R_2RR \tag{B.3g}$$

$$H_8 = -4R_2RI \tag{B.3h}$$

$$H_9 = R_2^2 \tag{B.3i}$$

$$H_{10} = 4RRr_1r_2 \tag{B.3j}$$

$$H_{11} = 4RIr_1r_2 \tag{B.3k}$$

$$H_{12} = -2(R_2r_1r_2 + R_1RR) \tag{B.3l}$$

$$H_{13} = -2R_1RI \tag{B.3m}$$

$$H_{14} = R_1R_2 \tag{B.3n}$$

$$H_{15} = -r_3r_6(r_1r_2 \cos\alpha + RR \cos\alpha + RI \sin\alpha) \tag{B.3o}$$

$$H_{16} = -r_3r_6(r_1r_2 \sin\alpha + RI \cos\alpha - RR \sin\alpha) \tag{B.3p}$$

$$H_{17} = r_3r_6((r_1^2 + r_2^2) \cos\alpha + r_1r_8 \cos(\theta_8 - \alpha)) \tag{B.3q}$$

$$H_{18} = r_3r_6(r_1r_2 \sin\alpha - RI \cos\alpha + RR \sin\alpha) \tag{B.3r}$$

$$H_{19} = r_3r_6(-r_1r_2 \cos\alpha + RR \cos\alpha + RI \sin\alpha) \tag{B.3s}$$

$$H_{20} = r_3r_6(-(r_1^2 + r_2^2) \sin\alpha + r_1r_8 \sin(\theta_8 - \alpha)) \tag{B.3t}$$

$$H_{21} = 2r_3r_6((r_1^2 + r_2^2)\cos\alpha + r_1r_8\cos(\theta_8 - \alpha)) \qquad (B.3u)$$

$$H_{22} = -r_2r_3r_6(2r_1\cos\alpha + r_8\cos(\alpha - \theta_8)) \qquad (B.3v)$$

$$H_{23} = -r_2r_3r_6r_8\sin(\alpha - \theta_8) \qquad (B.3w)$$

$$H_{24} = -RRr_6^2 \qquad (B.3x)$$

$$H_{25} = -RIr_6^2 \qquad (B.3y)$$

$$H_{26} = -r_1r_2r_3^2 \qquad (B.3z)$$

$$H_{27} = r_3^2(r_1^2 + r_2^2) \qquad (B.3aa)$$

$$H_{28} = r_6^2(r_1^2 + r_2^2 + r_8^2 + 2r_1r_8\cos\theta_8) \qquad (B.3bb)$$

Appendix C. graPHIGS Animation Programs

C.1 "N6R6" Forward Kinematics Animation

The following FORTRAN program, "N6R6ANMT", animates the "N6R6" manipulator using the forward kinematics solution. Valuators 1, 2, and 3 are used to read in values for the manipulator actuators, θ_1 , θ_2, and θ_3, over the range -2π to 2π. This program is run on an IBM 5080 terminal.

```
C
C     THE PURPOSE OF THIS PROGRAM IS TO ANIMATE THE 3-DOF PLANAR
C  "N6R6" MANIPULATOR.  VALUATORS 1-3 ARE USED TO VARY TH1 - 3.
C  THIS IS FORWARD KINEMATIC SIMULATION; graPHIGS CALLS ARE MADE.
C
C     BOB WILLIAMS          1/6/88
C
      PROGRAM N6R6ANMT
C
      COMMON /FIXPAR/A,B,C,D,H,L,PI
      COMMON /ANGLES/TH1,TH2,TH3,XY1,XY2,XYH,XYC,XY
      COMMON /SAVE/TH1S,TH2S,TH3S
      COMMON /ASSSSS/ASSEM
C
      REAL A, B, C, D, H, L, PI, XY1(6), XY2(4), XYH(4), XYC(6), XY(4),
     $     COLORS(18), WINDOW(4), VUPORT(4), CSIZE(3),
     $     AREA1(6), TWOPI
      INTEGER ASIZE(3), CLASS, DEVICE, DCHOI, DATAC(35), IWSID,
     $        VIEW1, CHOICE, ERRIND, PRFORM, LNGTHM, LNGTHT
```

```
      CHARACTER*8 ERFILE, WSTYPE, CONNID
      CHARACTER*16 DIALS
      CHARACTER*41 MSG1
      LOGICAL ASSEM
C
C  ADJUST DIAL SENSITIVITY
C
      WRITE(12) 1,0,0,8
      REWIND(12)
      READ(12) DIALS
C
C  DATA INITIALIZATION
C
      DATA ERFILE/'ERROR   '/, WSTYPE/'5080    '/, CONNID/'IBM5080 '/
     $    IWSID/1/, VIEW1/1/, PRFORM/2/, LNGTHM/41/, LNGTHT/24/
     $    MSG1/'PLEASE USE LIGHTED CHOICE KEY TO EXIT'/,
     $    VUPORT /0.,1.,0.,1./
      DATA DCHOI/140/,DATAC/32,0,0,   1,1,1,1,
     $                       1,1,1,1,1,1,1,
     $                       1,1,1,1,1,1,1,
     $                       1,1,1,1,1,1,1,
     $                       1,1,1,1,1,1,1,
     $                        1,1,1,2/
      DATA COLORS/ 0., 0., 1.,
C2 WHITE
     $          1., 1., 1.,
C3 RED
     $          1., 0., 0.,
C4 GREEN
     $          0., .3, 0.,
C5 BLUE
     $          0., 0., 1.,
C6 BLACK
     $          0., 0., 0. /
C
      PI = ARCOS(-1.0)
      TWOPI = 2. * PI
C
C  INPUT LENGTHS, FIXED PIVOTS, INITIAL HAND LOCATION, RANGE
C
      READ (21,*) RANGE
      READ (21,*) A, B, C, D, H, L
      READ (21,*) TH1S, TH2S, TH3S
      XY(1) = 0.0
      XY(2) = 0.0
      XY(3) = L
      XY(4) = 0.0
C
C  UNCHANGING XY TERMS
C
      XY1(1) = 0.0
      XY1(2) = 0.0
      XY2(1) = L
      XY2(2) = 0.0
C
C  SET WINDOW
C
```

```
      WINDOW(1) = -RANGE/2.
      WINDOW(2) =  RANGE/2.
      WINDOW(3) = -RANGE/2.
      WINDOW(4) =  RANGE/2.
C
C   CALCULATE MAXIMUM WORKSPACE CIRCLE
C
C     CALL CIRCLE(3.0,0.0,0.0)
C
C   OPEN GRAPHIGS AND WORKSTATION, COLOR STATEMENTS
C
      CALL GPOPPH(ERFILE,0)
      CALL GPOPWS(IWSID,CONNID,WSTYPE)
      CALL GPCML(IWSID,1)
      CALL GPCR(IWSID,1,6,COLORS)
C
C   OBTAIN ACTUAL DISPLAY SURFACE SIZE, USED FOR
C   CALCULATION OF ECHO AREAS.
C
      CALL GPQADS(IWSID,ERRIND,1,CSIZE,ASIZE)
      IF (ERRIND .NE. 0) THEN
         PRINT *, 'ERRIND NOT EQUAL TO ZERO'
         STOP
      ENDIF
C
C   DRAW THE INITIAL ROBOT STRUCTURE; 100 IS RESET FOR NON-ASSEMBLY
C
100   ASSEM = .TRUE.
      TH1 = TH1S
      TH2 = TH2S
      TH3 = TH3S
      CALL DRAW
C
C   ASSOCIATE STRUCTURE ONE TO VIEW ONE
C
      CALL GPARV(IWSID,VIEW1,1,1)
      CALL GPVMP2(IWSID,VIEW1,WINDOW,VUPORT)
      CALL GPVCH(IWSID,VIEW1,2,2,2,2,4,2,2,2)
      CALL GPUPWS(IWSID,PRFORM)
      CALL GPDRV(IWSID,VIEW1,1)
C
C   INITIALIZE VALUATOR DEVICE; ASK FOR AN INPUT
C   THE ECHO AREA IS THE ENTIRE DISPLAY SURFACE.
C
      AREA1(1) = 0.0
      AREA1(2) = CSIZE(1)
      AREA1(3) = 0.5 * CSIZE(2) + 0.12
      AREA1(4) = CSIZE(2)
      AREA1(5) = 0.0
      AREA1(6) = CSIZE(3)
C
      CALL GPVLMO(IWSID,1,1,2)
      CALL GPINVL(IWSID,1,TH1S,4,AREA1,-TWOPI,TWOPI,16,DIALS)
      CALL GPVLMO(IWSID,1,3,2)
      AREA1(3) = AREA1(3) - .005
      CALL GPVLMO(IWSID,2,1,2)
      CALL GPINVL(IWSID,2,TH2S,4,AREA1,-TWOPI,TWOPI,16,DIALS)
```

```
      CALL GPVLMO(IWSID,2,3,2)
      AREA1(3) = AREA1(3) - .005
      CALL GPVLMO(IWSID,3,1,2)
      CALL GPINVL(IWSID,3,TH3S,4,AREA1,-TWOPI,TWOPI,16,DIALS)
      CALL GPVLMO(IWSID,3,3,2)
      AREA1(3) = AREA1(3) - .005
C
C     INITIALIZE CHOICE DEVICE
C
      CALL GPCHMO(IWSID,1,1,2)
      CALL GPINCH(IWSID,1,1,2,AREA1,DCHOI,DATAC)
      CALL GPCHMO(IWSID,1,3,2)
C
C     REQUEST PF KEY HIT; DISPLAY MESSAGE REQUESTING INPUT
C
      CALL GPMSG(IWSID,LNGTHM,MSG1)
C
C     EMPTY STRUCTURE
C
102   CALL GPEST(1)
      TIME = 20.0
      CALL GPAWEV(TIME,J,CLASS,DEVICE)
C
C     CHECK FOR EXIT - CHOICE = 32
C
      IF(CLASS .EQ. 4) THEN
         CALL GPGTCH(CHOICE)
         IF(CHOICE.EQ.32) GOTO 999
      ELSE
         IF(DEVICE.EQ.1) CALL GPGTVL(TH1)
         IF(DEVICE.EQ.2) CALL GPGTVL(TH2)
         IF(DEVICE.EQ.3) CALL GPGTVL(TH3)
      ENDIF
C
C     DRAW NEW STRUCTURE; RESET (100) IF NON-ASSEMBLY
C
      CALL DRAW
      IF (ASSEM) THEN
         TH1S = TH1
         TH2S = TH2
         TH3S = TH3
C
C     ASSOCIATE NEW STRUCTURE TO VIEW ONE
C
         CALL GPARV(IWSID,VIEW1,1,1)
         CALL GPVMP2(IWSID,VIEW1,WINDOW,VUPORT)
         CALL GPVCH(IWSID,VIEW1,2,2,2,2,4,2,2,2)
         CALL GPUPWS(IWSID,PRFORM)
         CALL GPDRV(IWSID,VIEW1,1)
         CALL GPDAST
         GOTO 102
      ELSE
         GOTO 100
      ENDIF
C
999   CALL GPMSG(IWSID,LNGTHT,TMSG)
```

```
      CALL GPCLPH
C
      STOP
      END
C
C  SUBROUTINE DRAW
C
C  THIS SUBROUTINE DRAWS THE ROBOT
C
      SUBROUTINE DRAW
C
      COMMON /FIXPAR/A,B,C,D,H,L,PI
      COMMON /ANGLES/TH1,TH2,TH3,XY1,XY2,XYH,XYC,XY
      COMMON /ASSSSS/ASSEM
      COMMON /SAVE/TH1S,TH2S,TH3S
C
      REAL A, B, C, D, H, L, PI, XY1(6), XY2(4), XYH(4), XYC(6), XY(4)
      LOGICAL ASSEM
C
C  OPEN STRUCTURE
C
      CALL GPOPST(1)
C
C  CALCULATE COORDINATES OF REVOLUTE JOINTS
C
      CALL COORD
C
C  DRAW ROBOT, IF ASSEMBLES
C
      IF (ASSEM) THEN
          CALL GPPLCI(2)
          CALL GPPL2(3,2,XY1)
          CALL GPPL2(2,2,XY2)
          CALL GPPL2(2,2,XYH)
          CALL GPMT(4)
          CALL GPPMCI(2)
          CALL GPPM2(2,2,XY)
          CALL GPIS(2)
          CALL GPICI(2)
          CALL GPPG2(1,3,2,XYC)
C          CALL GPPL2(61,2,CIRC)
      ENDIF
C
C  CLOSE STRUCTURE
C
      CALL GPCLST
C
      RETURN
      END
C
C  SUBROUTINE COORD
C
C  THIS SUBROUTINE CALCULATES THE REVOLUTE JOINT LOCATIONS
C
      SUBROUTINE COORD
C
      COMMON /FIXPAR/A,B,C,D,H,L,PI
```

```
      COMMON /ANGLES/TH1,TH2,TH3,XY1,XY2,XYH,XYC,XY
      COMMON /ASSSSS/ASSEM
      COMMON /SAVE/TH1S,TH2S,TH3S
C
      REAL A, B, C, D, H, L, PI, XY1(6), XY2(4), XYH(4), XYC(6), XY(4)
      LOGICAL ASSEM
C
      ASSEM = .TRUE.
C
C     CALCULATE POINTS F1 AND F2
C
      F1X = A*COS(TH1)
      F1Y = A*SIN(TH1)
      F2X = D*COS(TH2) + L
      F2Y = D*SIN(TH2)
C
C     CALCULATE POINT F3 USING SOLVPT - 2 SOLUTIONS
C
      CALL SOLVPT(B,C,F1X,F1Y,F2X,F2Y,PHI11,PHI12)
      IF (ASSEM) THEN
         F3X1 = F1X + B*COS(PHI11)
         F3Y1 = F1Y + B*SIN(PHI11)
         F3X2 = F1X + B*COS(PHI12)
         F3Y2 = F1Y + B*SIN(PHI12)
      F3X = F3X1
      F3Y = F3Y1
C
C     CALCULATE PHI2 AND F4 - 2 SOLUTIONS
C
         PHI21 = ATAN2((F2Y-F3Y1),(F2X-F3X1))
            F4X1 = F3X1 + C*COS(PHI21+(PI/3.))
            F4Y1 = F3Y1 + C*SIN(PHI21+(PI/3.))
         PHI22 = ATAN2((F2Y-F3Y2),(F2X-F3X2))
            F4X2 = F3X2 + C*COS(PHI22+(PI/3.))
            F4Y2 = F3Y2 + C*SIN(PHI22+(PI/3.))
      F4X = F4X1
      F4Y = F4Y1
C
C     CALCULATE (XH,YH) - 2 SOLUTIONS
C
         PSI = PI/3. - PHI21
            THH = TH3 - PSI
            XH = F4X1 + H*COS(THH)
            YH = F4Y1 + H*SIN(THH)
C        PSI = PI/3. - PHI22
C           THH = TH3 - PSI
C           XH = F4X2 + H*COS(THH)
C           YH = F4Y2 + H*SIN(THH)
      ENDIF
C
C
C     ASSIGN XY ARRAYS FOR GRAPHIGS
C
      XY1(3) = F1X
      XY1(4) = F1Y
      XY1(5) = F3X
      XY1(6) = F3Y
```

```
      XY2(3) = F2X
      XY2(4) = F2Y
      XYH(1) = F4X
      XYH(2) = F4Y
      XYH(3) = XH
      XYH(4) = YH
      XYC(1) = F2X
      XYC(2) = F2Y
      XYC(3) = F3X
      XYC(4) = F3Y
      XYC(5) = F4X
      XYC(6) = F4Y
C
      RETURN
      END
C
C  SUBROUTINE SOLVPT
C
      SUBROUTINE SOLVPT(R1,R2,X,Y,XX,YY,TH1,TH2)
C
      COMMON /ASSSSS/ASSEM
C
      REAL X, Y, XX, YY, R1, R2, AA, BB, CC, R, THETA, PI,
     $     T1, T2, TH1, TH2
      LOGICAL ASSEM
C
      PI = ACOS(-1.0)
C
      R = SQRT((XX-X)**2 + (YY-Y)**2)
      THETA = ATAN2((YY-Y),(XX-X))
      AA = R2**2 - R**2 - R1**2 - 2.*R*R1*COS(THETA)
      BB = 4.*R*R1*SIN(THETA)
      CC = R2**2 - R**2 - R1**2 + 2.*R*R1*COS(THETA)
      DISCR = BB**2 - 4.*AA*CC
      IF (DISCR .LT. 0.) THEN
         ASSEM = .FALSE.
      ELSE
         T1 = (-BB + SQRT(DISCR))/(2.*AA)
         T2 = (-BB - SQRT(DISCR))/(2.*AA)
         TH1 = 2.*ATAN(T1)
         TH2 = 2.*ATAN(T2)
      ENDIF
C
      RETURN
      END
C
C  SUBROUTINE CIRCLE
C
      SUBROUTINE CIRCLE(RMAX,XC,YC)
C
      COMMON /CIRCE/CIRC
C
      REAL CIRC(122), RMAX, TH, DTH, XC, YC, PI
      INTEGER N
C
      PI = ARCOS(-1.0)
C
```

```
      N = 60
      DTH = 2.*PI/N
      TH = 0.0
      DO 200 I = 1,N+1
         CIRC(2*I-1) = XC + RMAX*COS(TH)
         CIRC(2*I) = YC + RMAX*SIN(TH)
         TH = TH + DTH
200   CONTINUE
C
      RETURN
      END
```

C.2 "N6R6" Inverse Kinematics Animation

This section presents the modifications necessary to convert program "N6R6ANMT" of Appendix C.1 to animate the inverse kinematics solution. Valuators 1, 2, and 3 are used to enter values for the manipulator hand location, x_H , y_H, and θ_H, over the workspace range.

One major change is required: Subroutine COORD must be changed so that the inverse kinematics solutions is utilized, rather than the forward solution as in Appendix C.1. In this section, a new Subroutine COORD is presented for the inverse kinematic position solution. Prior to this, six lines dealing with input data must be changed in the main program. The valuators must be initialized to read in x_H , y_H, and θ_H values, instead of θ_1 , θ_2, and θ_3. The following six lines are substituted for "N6R6ANMT" program line numbers 105, 106, 107, 129, 133, and 137. Line number 105 directly follows FORTRAN statement label 100. The new Subroutine COORD follows these six lines.

```
      XH = XHS
      YH = YHS
      THH = THHS
      CALL GPINVL(IWSID,1,XHS,4,AREA1,-1.00,1.00,16,DIALS)
      CALL GPINVL(IWSID,2,YHS,4,AREA1,-1.00,1.00,16,DIALS)
      CALL GPINVL(IWSID,3,THHS,4,AREA1,-TWOPI,TWOPI,16,DIALS)


C
C  SUBROUTINE COORD
C
C  THIS SUBROUTINE CALCULATES THE REVOLUTE JOINT LOCATIONS
C
      SUBROUTINE COORD
C
      COMMON /FIXPAR/A,B,C,D,H,L,PI
      COMMON /ANGLES/XH,YH,THH,XY1,XY2,XYH,XYC,XY
      COMMON /CIRCE/CIRC
      COMMON /VARBLS/X, Y, XX, YY
      COMMON /ASSSSS/ASSEM
      COMMON /SAVE/TH1S,TH2S,XHS,YHS,THHS
C
      REAL A, B, C, D, H, L, PI, XY1(6), XY2(4), XYH(4), XYC(6), XY(4),
     $     XX(2), YY(2), X(2), Y(2)
      LOGICAL ASSEM
C
```

```
      PI = ARCOS(-1.0)
C
C  CALCULATE TWO VALUES FOR THETA2
C
      F4X = XH - H*COS(THH)
      F4Y = YH - H*SIN(THH)
      XX(2) = F4X
      YY(2) = F4Y
      CALL SOLPT(D,C,2,TH21,TH22)
      IF (ASSEM) THEN
C
C  CHOOSE TH2 CLOSER TO PREVIOUS ANGLE
C
        IF (ABS(TH21-TH2S) .LT. ABS(TH22-TH2S)) THEN
           TH2 = TH21
        ELSE
           TH2 = TH22
        ENDIF
        TH2S = TH2
C
C  FOR PROPER THETA2, FIND 2 THETA1'S
C
          F2X = L + D*COS(TH2)
          F2Y = D*SIN(TH2)
          PHI = ATAN2((F4Y-F2Y),(F4X-F2X))
          F3X = F2X + C*COS(PHI+(PI/3.))
          F3Y = F2Y + C*SIN(PHI+(PI/3.))
          XX(1) = F3X
          YY(1) = F3Y
          CALL SOLPT(A,B,1,TH11,TH12)
          IF (ASSEM) THEN
C
C  CHOOSE TH1 CLOSER TO PREVIOUS ANGLE
C
            IF (ABS(TH11-TH1S) .LT. ABS(TH12-TH1S)) THEN
               TH1 = TH11
            ELSE
               TH1 = TH12
            ENDIF
            TH1S = TH1
C
C  FOR PROPER THETA1, CALCULATE POINT F1
C
             F1X = A*COS(TH1)
             F1Y = A*SIN(TH1)
         ENDIF
      ENDIF
C
C  ASSIGN XY ARRAYS FOR GRAPHIGS
C
      XY1(3) = F1X
      XY1(4) = F1Y
      XY1(5) = F3X
      XY1(6) = F3Y
      XY2(3) = F2X
      XY2(4) = F2Y
      XYH(1) = F4X
```

```
      XYH(2) = F4Y
      XYH(3) = XH
      XYH(4) = YH
      XYC(1) = F2X
      XYC(2) = F2Y
      XYC(3) = F3X
      XYC(4) = F3Y
      XYC(5) = F4X
      XYC(6) = F4Y
C
      RETURN
      END
```

The vita has been removed from the scanned document